Assessing cross-shore coastal erosion processes in Bạc Liêu, Vietnam

Sam de Wit

Delft University of Technology

TU Delft

Assessing cross-shore coastal erosion processes in Bạc Liêu, Vietnam

by

Sam de Wit

to obtain the degree of Master of Science
at the Delft University of Technology,

Student number:	4956028	
Project duration:	September 1, 2024 – April, 2025	
Thesis committee:	dr. D. S. Van Maren,	TU Delft, daily supervisor
	Prof. dr. ir. Z. B. Wang,	TU Delft
Additional supervisors:	dr. M. Van Der Wegen	Deltares
	dr. S. H. Trương	Thuy Loi University

Cover: Eroding mangrove forest near the waterline in Bạc Liêu, Vietnam

TU Delft

Preface

This thesis is the final step in obtaining my Civil Engineering Master's degree. Over the last eight months, I've focused on coastal erosion in the Mekong Delta, a topic that has fascinated me ever since I first visited Vietnam in 2023. With this work, I hope to provide a meaningful contribution to the ongoing efforts to protect the Mekong Delta's ecosystems and inhabitants.

However, this would not have been possible without the help of a few people. I'd like to start by thanking my daily supervisor, Bas, for guiding me through this process and for all the critical discussions that shaped my research. I'm also grateful to Mick for his invaluable support with the modeling, and to Zheng Bing for his contributions and feedback. A special thanks goes out to Sơn (and his project DTDL.CN-51/23), Linh, Tùng, Hùng, Trung and all their colleagues involved in the Mangrove Living Lab for their guidance during my stay in Vietnam and for showing me around their wonderful country. Finally, I would like to thank my friends and family for their constant support throughout this journey.

Sam de Wit
Amsterdam, May 2025

Summary

As part of the Mangrove Living Lab project, this research examines how multiple drivers influence coastal erosion in Bạc Liêu, Vietnam. Currently, observed erosion in this region cannot be explained by natural sediment redistribution, and literature suggests that tidal flows are more cross-shore dominated in Bạc Liêu compared to adjacent provinces. Consequently, four key anthropogenic drivers that primarily act in the cross-shore direction are explored: (1) land subsidence due to increased groundwater extraction, (2) reduced sediment availability, (3) foreshore degradation leading to higher waves, both induced by fluvial sediment deficit, and (4) the construction of sea dikes and fishpond dams in the intertidal zone, resulting in tidal flow restriction, wave reflection and coastal squeeze.

Two main methods are applied: a cross-shore elevation level analysis to assess spatial differences in subsidence and sediment supply, and a numerical model to assess the influence of each driver individually and combined. The elevation analysis revealed that subsidence varies spatially along the coast. Moreover, historic satellite images show that a site without subsidence has been accreting in the past, while a site experiencing subsidence remained stable during the same period. After 2004, they both began eroding. This suggests that differences in subsidence rates largely explain spatial variations in current coastline positions, while the erosion itself is likely driven by additional drivers. However, the limited spatial and temporal coverage of elevation transects highlights the need for more extensive data collection. Numerical modeling indicates that reduced wave heights and increased suspended sediment greatly reduce erosion rates, and can even overshadow the effect of subsidence when combined. This demonstrates that historic and ongoing fluvial deficit is likely the main driver of the current erosion. The role of intertidal structures remains inconclusive due to model limitations and differing theoretical interpretations. Refining the current model or developing more advanced alternatives will help improve understanding of these coastal erosion processes. This is needed to support the development of integrated solutions that protect both the communities and ecosystems of Bạc Liêu.

Contents

1

Introduction

1.1. The Mekong Delta

The Vietnamese Mekong River Delta (hereafter: Mekong Delta) is located in the southern part of the country and covers a vast triangular area of 39700 km^2 [58]. It started forming about 3500 years ago when coastal currents redistributed the sediment supply from the Mekong river to the southwest, creating the Cà Mau peninsula [55]. Today, the Mekong delta stretches from the border with Cambodia in the northwest to Ho Chi Minh City in the northeast and Cà Mau province in the south. In Cambodia, the Mekong River divides into two main branches: the Mekong (Tiền River) and Bassac (Hậu River). With complex multi-channel systems, these rivers end in estuaries that reach the South China Sea on the eastern coast of the Mekong Delta (Figure 1.1).

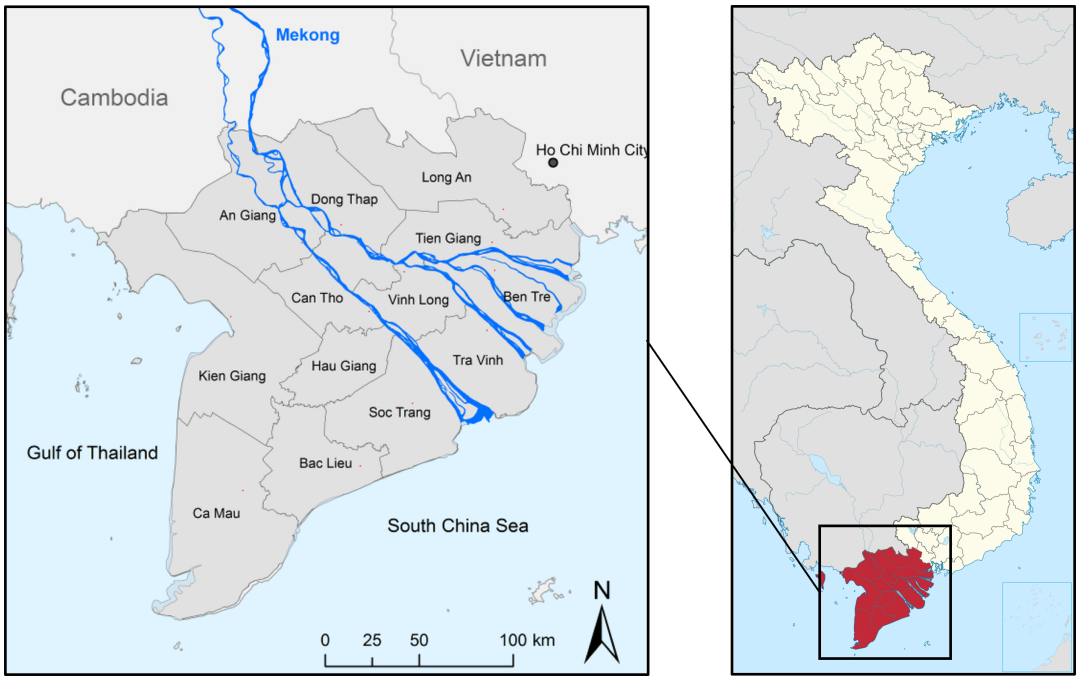

Figure 1.1: The Mekong Delta, Vietnam [27]

In 2018, the Mekong Delta had a population of 17.43 million people and represented 12% of Vietnam's gross domestic product [43]. Furthermore, 70.97% of the water surface area for aquaculture and 47.86% of the planted area for cereal production in Vietnam are located in the Mekong Delta [43]. Additionally, the region is home to at least 247 bird species, 924 fish species, and hundreds of plant

species [10]. The combination of the vast area of agriculture and aquaculture, and the large biodiversity make the Mekong Delta an important region in Vietnam.

The Mekong Delta is a relatively flat region with an average elevation level of 0.82 meters [41], making it prone to flooding, especially with the threat of rising sea levels [22] and land subsidence [39]. Additionally, more than half of the 600km long shoreline has been retreating due to coastal erosion with rates of up to $20m/y$ [3]. To protect the Mekong Delta and its inhabitants from these threats, coastal protection and an in-depth understanding of the system and driving processes are paramount.

1.2. Mangrove Living Lab

This research is part of the Mangrove Living Lab, a collaborative project from TU Delft, Thuy Loi University (TLU, Hanoi, Vietnam), Hanoi University of Natural Resources and Environment (HUNRE , Hanoi, Vietnam) and researchers from the Southern Institute of Water Resources and Planning (SIWRP, Ho Chi Minh-city, Vietnam). The project's main goals are "to gain better insight and knowledge through conducting of in-field measurement campaigns, and to demonstrate and showcase various lessons learned and potential (nature-based) solutions for coastal management in Vietnam" [34].

1.3. Problem definition

This section describes the main problem this report addresses. First, based on previous research, a research gap is identified, after which the scope and objectives of this research are explained.

1.3.1. Previous research

Many researchers [3][9][35][44][48] have investigated the mechanisms that drive coastal erosion in the Mekong Delta. These drivers can be classified into two categories: anthropogenic and natural drivers. Examples of anthropogenic drivers are subsidence due to groundwater extraction [39], mangrove squeeze and tidal flow restriction due to the construction of sea dikes [48][66] and loss of fluvial sediment supply due to sand mining and the construction of upstream hydro power dams [3]. Natural drivers are the natural redistribution of sediment along the coast due to currents driven by tides, waves, wind, and density differences.

Using a 3D hydro-morphodynamic numerical model, Marchesiello et al. (2019)[35] conclude that most of the observed erosion and accretion patterns [3] in the Mekong delta can be explained by natural redistribution of sediment and direct deposition of sediment near the river mouths. They argue that their model gives a good representation of the observed erosion trends, except for a few locations. One of these locations is the coast of Bạc Liêu province. At this location, erosion is observed while their model predicts accretion (Figure 1.2), implying that external, potential anthropogenic drivers are causing the erosion.

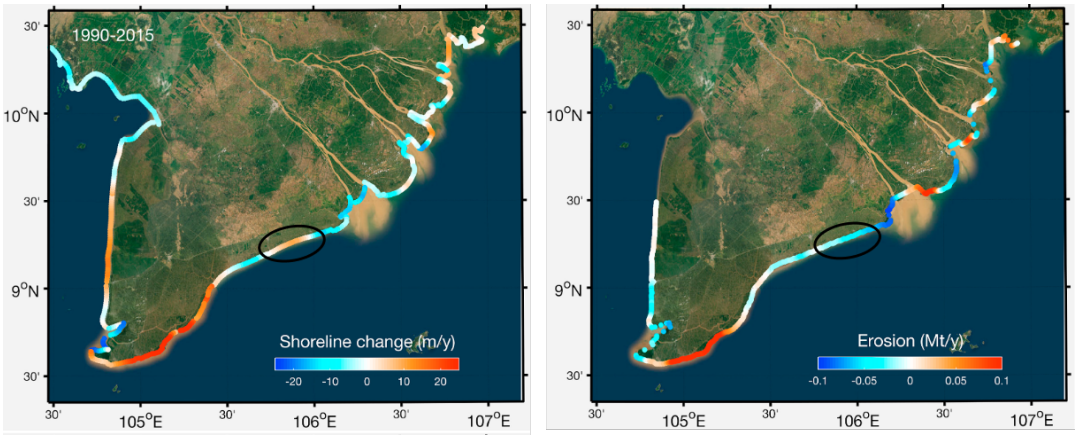

Figure 1.2: Observed (left) [3] vs modeled (right) [35] erosion (red) and accretion (blue) patterns in the Mekong delta. At the coast of Bạc Liêu province (black circle) erosion is observed while accretion is expected based on the natural redistribution of the sediment.

Based on work of Besset et al. (2019) [4], Marchesiello et al. (2019)[35] state that the erosion observed in Bạc Liêu is not likely attributed to mangrove loss. Furthermore, their one-month simulations of the river supplying low and high sediment concentrations to the system, suggest that a reduction in fluvial sediment is also not likely to have a direct influence on erosion rates in Bạc Liêu. Therefore, they hypothesize that relatively high rates of man-induced subsidence explain the observed erosion in Bạc Liêu.

Minderhoud et al. (2017)[39] researched this subsidence and concluded that over the past 25 years, as groundwater extraction increased to meet the rising demand for freshwater, the coast of Bạc Liêu has been subsiding at an average rate of 1.5 cm/year. However, during field work in Bạc Liêu, erosion cliffs of more than one meter were observed at the mangrove fringe. Moreover, Van Bijsterveld et al. (2023)[60] found that mangroves are naturally resilient against subsidence by vertical accretion keeping the coast stable if the sediment supply is sufficient. These findings suggests that subsidence does not fully explain the observed erosion in Bạc Liêu and that other, additional processes are likely in play.

The construction of sea dikes and dams to protect fishponds, can contribute to erosion by reducing the width of the mangrove forest [48]. This reduces the capability of mangroves to attenuate waves and trap sediment. Additionally, the construction of earthen dams and sea dikes in the intertidal zone, reduces the tidal prism, possibly decreasing sedimentation rates inside the mangrove forest [66]. Furthermore, while fluvial sediment supply deficit might not directly influence erosion rates, its long-term consequences could lead to large-scale foreshore degradation, which in turn affects sediment availability and wave dissipation over the mudflat. Additionally, the formation of the erosion cliffs can lead to wave reflection at the cliff, resulting in even more erosion [66]. Using a depth-averaged numerical model of the South China Sea, Phan et al. (2019) [47] demonstrated that radial tidal currents cause tidal flows to be more perpendicular to the coast of Bạc Liêu compared to other provinces.

These findings suggest that erosion and formation of erosion cliffs in Bạc Liêu results from a combination of drivers predominantly working in cross-shore direction including subsidence, construction of structures in the intertidal zone, and a reduction of fluvial sediment supply. While these mechanisms have been individually described and sometimes quantified, their contribution to shoreline erosion has not yet been integrally quantified in a model-based study accounting for all these potential mechanisms on a specific coastal section.

1.3.2. Scope and objectives

This research focuses on the coast of Bạc Liêu and the primary mechanisms driving coastal erosion. Man-induced subsidence, sediment deficit and the construction of sea dikes have been theorized to contribute to the erosion.

The main objective is to asses how each driver influences cross-shore erosion processes in Bạc Liêu. A numerical model will be used to simulate multiple scenarios and qualify the effects of the different drivers. Additionally, qualitative analysis on elevation levels inside the mangrove forests will assess the relative importance of subsidence and sediment availability across different sections of the coastline. Field observations from a one-week field campaign and historical data will provide further insights into past and present coastal changes and processes driving the erosion of the coast of Bạc Liêu.

1.4. Research questions

The main question this research attempts to answer is:

How do different erosion drivers influence cross-shore sediment transport processes and erosion rates along the coast of Bạc Liêu, Vietnam?

In order to answer the above research question, four sub-questions are defined:

- *How have historic changes in land use and foreshore morphology influenced key erosion drivers?*
- *What are the individual effects of subsidence, sediment deficits, and sea dike construction on cross-shore sediment transport and erosion rates?*
- *What are the combined effects of subsidence, sediment deficits, and sea dike construction on cross-shore sediment transport and erosion rates?*

- *What factors explain spatial variations in erosion along the Bạc Liêu coast?*

1.5. Outline

After the introduction this report consists of five chapters. Chapter 2 provides the context of this study by an extensive literature review about hydrodynamic in the Mekong Delta, sediment transport processes and erosion drivers. Additionally, the current and historic state of the Bạc Liêu coast are examined. Next, chapter 3 describes the methods used to answer the research question. The results are presented in chapter 4 and critically discussed in chapter 5. Finally, conclusions are drawn in chapter 6.

2

Literature review

2.1. Hydrodynamics of the Mekong delta

Sediment transport processes in the Mekong coastal zone near Bạc Liêu are controlled by (the seasonal variation of) waves, tides and residual currents. These aspects are explored in the following sections.

2.1.1. Waves

The coastal region of the Mekong Delta is facing a (sub-)tropical climate which is governed by the monsoon. The rainy season in the Mekong Delta lasts from May till October/November, when the Indian monsoon governs the local weather, bringing rain with a monthly mean precipitation of 8 – 10 mm/day [29]. During this season low energy waves with an average offshore wave height of $0.5m$ [48] reach the shore from a South-West direction. The dry season lasts from November till April, during which high energy waves with an average offshore wave height of $0.8m$ [48] reach the shore from the North-East [16]. By using a numerical model, Phan (2020) [46] found that the coast of Bạc Liêu experiences lower waves compared to the adjacent provinces on the east side of the Mekong delta.

2.1.2. Tides

The Mekong delta is historically classified as a tide dominant delta. Especially on the east side, near the coast of Sóc Trăng and Bạc Liêu, the tides dominate the sediment transport [13]. The tides in the east coast of the Mekong delta are mixed, but mainly semi-diurnal, whereas the tide in the major part of the South China Sea is mainly diurnal. It has been theorized by Phan et al. (2019) [47] that this anomaly is caused by shoaling and resonance of the M_2 semi-diurnal component.

Phan et al. (2019) [47] modeled the currents induced by the tides and hypothesize that the tidal flow direction appears more perpendicular near the coast of Bạc Liêu than in other provinces (Figure 2.1). They state that the tidal amplitude is amplified nearshore due to shoaling and resonance, while the offshore amplitude remains low due to the formation of a standing tidal wave caused by reflection at the Malaysian coast. This contrast, in combination with basin geometry and the shallow, sloping topography, creates convex hydraulic gradients that lead to radial tidal currents on the Mekong deltaic shelf. This leads to the assumption that cross-shore sediment transport processes may have a greater impact on erosion in Bạc Liêu compared to other provinces. It must be noted that Marchesiello et al. (2019) [35] also modeled tidal currents, but no radial currents, or stronger cross-shore currents near Bạc Liêu, where observed in their work. This may be due to the smaller scale of their model and the choice for open boundaries, neglecting the formation of a standing tidal wave as hypothesized by Phan et al. (2019) [47].

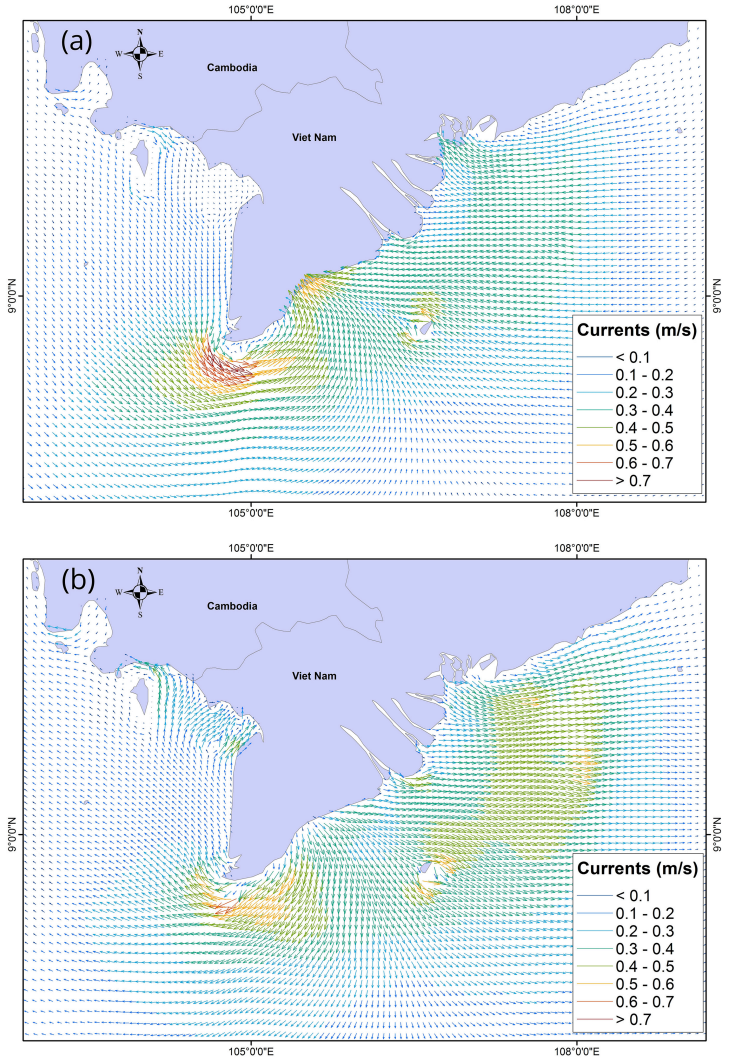

Figure 2.1: Modeled tidal currents in the Mekong delta during flood (a) and ebb (b). The figure shows a rather perpendicular tidal flow direction towards the Bạc Liêu coast [47].

2.1.3. Residual Currents

The flow velocities induced by the tides are in the order of a few decimeters per second. However, seasonally varying long shore currents induced by the winds, are of a higher order, and therefore mostly overshadow the currents induced by the tides, especially during the dry season. Marchesiello et al. (2019) [35] and Phan (2020) [46] both modeled the residual currents, and found that due to the stronger waves and wind speeds during the North East monsoon (dry season), a net long shore current towards the Southwest is present. However, due to the lower waves and perpendicular oriented tidal flow, this longshore, residual current is weaker near Bạc Liêu [46].

2.2. Mudflat sediment dynamics

Having established the dominant hydrodynamic processes in the Mekong Delta, this section explores how these processes interact with sediment dynamics on mudflats.

Intertidal flats are areas that dry and flood during a tidal cycle. They exist in tide dominated, estuarine and deltaic systems, like the Mekong Delta. Due to the relatively low energy conditions and tide dominance of the system, small particles have a chance to settle near the coast, causing the flats to consist mostly of mud. The coarser, sandy sediments occur further offshore. Between the upper part of the intertidal zone to the supratidal zone, vegetation like salt marshes and mangroves (in tropical and subtropical areas) occur [7].

The shape of a tide dominated mudflat is typically a convex-up shape which becomes more concave-up if waves have a relatively higher influence [28]. It can be divided in two areas: the topset is the area near shore with a gentle slope and the foreset is the zone farther seaward with a steeper slope. The transition between both zones is the rollover point [64]. Figure 2.2 shows an arbitrary example of a stable, tide dominated mudflat with mangroves. The following subsections explain how cross- and long shore currents transport the sediment and how mangroves play a role in these processes.

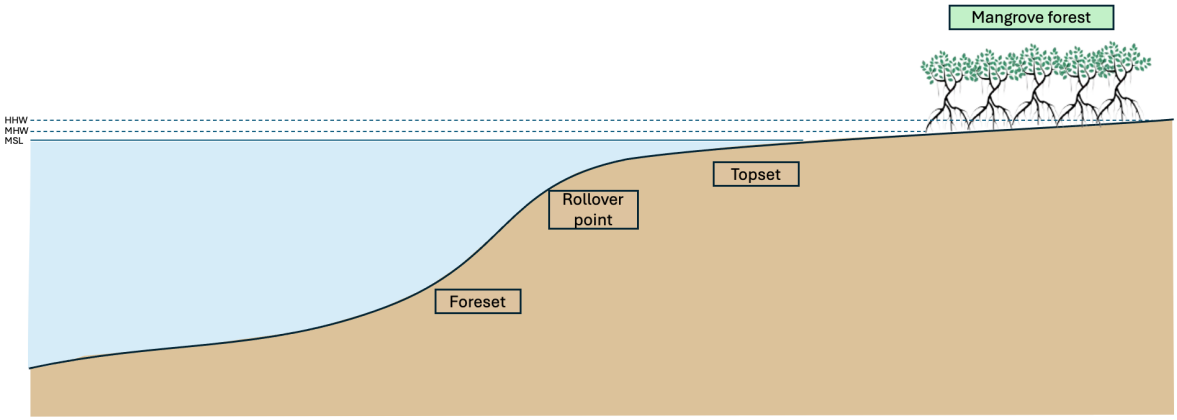

Figure 2.2: Schematization of a stable mudflat

2.2.1. Cross-shore sediment transport

The convex-up shape of the mudflat causes waves to attenuate as they approach the shore, creating a spatial variation in hydrodynamic energy in the cross-shore direction. As the water is shallower and energy is lower, sediment particles can settle more easily, and low shear stresses result in only limited sediment resuspension. In contrast, in offshore, high-energy areas, less sediment settles and more sediment is resuspended.

Waves contribute to this process as they stir up the sediment offshore during low tide, mobilizing sediment to be transported onshore. Therefore, when the tide rises and water is flowing in landward direction, suspended sediment is flowing towards the coast, where it can easily settle. This results in higher bed levels towards the coast. On the other hand, waves also contribute to erosion as they reach the shore [67].

Therefore, the direction of the net cross-shore sediment transport depends on the relative influence of waves and tides. Ultimately, tide-dominant low energy conditions lead to a net transport of sediment in landward direction [18] [51]. This hypothesis has been verified for the east coast of the Mekong delta by Phan et al. (2019) [47]. Additionally, the wave energy determines the level of the equilibrium profile.

2.2.2. Long-shore sediment transport

A long-shore current is a current that flows parallel to the shoreline and depth contours. Its direction and velocity are primarily influenced by tides and wave breaking in the surf zone [7]. Subsection 2.1.3 explains how wind, waves and tides cause a residual current in southwest direction. As a result, the dominant net long-shore current along the east coast of the Mekong Delta flows in a southwesterly direction, theoretically providing favorable conditions for redistributing sediment from the river mouths to the shores of Bạc Liêu and Cà Mau [35]. However, long-shore transport rates differ along the coast and depend on the magnitude of the breaking wave height and its incident angle. Phan (2020) [46]

modeled residual currents (2.1.3) and subsequent sediment transport rates and found that the lowest longshore sediment transport rate along the east coast of the Mekong delta is near Bạc Liêu, due to its shallower bathymetry leading to a smaller breaking wave height compared to adjacent provinces.

Given this lower wave energy and the more perpendicular orientation of tidal currents (subsection 2.1.2), cross-shore currents are assumed to play a more significant role in sediment transport along the coast of Bạc Liêu compared to other provinces in the Mekong Delta.

2.2.3. Mangroves

Mangrove forests are complex ecosystems that play a vital role in maintaining healthy coastal environments in (sub)tropical regions. They provide habitats for diverse plant and animal species, stabilize shorelines and store carbon. Moreover, since mangroves thrive in the intertidal zone, they play an important role in the near-shore sediment dynamics on a mudflat. Mangroves typically grow between the mean high water (MHW) and high high water (HHW) line. This means that during HHW, the roots, trunks, and sometimes even canopies, are submerged under water, leading to wave dissipation [26]

Field measurements on wave attenuation by mangroves are only limitedly available [37]. As an alternative, numerical [6] [33] [48] and empirical [38] models have been used to predict wave attenuation in mangrove forests. The numerical model by Vo-Luong et al. (2008) [33] showed that short waves will dissipate by $50 - 70\%$ in the first $20m$ of a mangrove forest. Phan et al. (2014) [48] showed that after $300 - 400m$ the the long-wave energy is only 10% compared to the the seaward edge of the mangroves. The empirical model from Mendez et al. (2003) [38] also shows a relation between the presence of vegetation and wave height reduction (Figure 2.3).

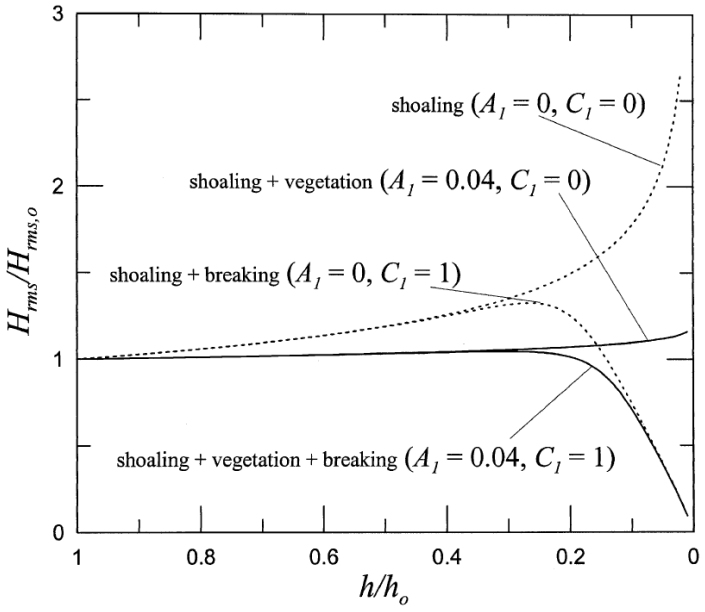

Figure 2.3: Non-dimensional root-mean-square wave height evolution over a plane sloping beach for different theories [38]

In Figure 2.3 C_1 denotes a breaking parameter. A_1 is essentially the submerged frontal area of the mangroves multiplied by the drag coefficient.

$$A_1 = 2C_D b_v N \alpha 3\pi \tag{2.1}$$

Where:

C_D = Depth-averaged drag coefficient$(-)$
b_v = Plant area per unit height of each vegetation stand normal to flow direction(m)
N = Number of vegetation stands per unit horizontal area$(-)$
α = Dimensionless scaling factor representing the proportion of water depth occupied by vegetation$(-)$

Apart from attenuating waves, mangroves also generate drag forces, which reduce flow velocities [36]. Together, these two factors promote sediment deposition within mangrove ecosystems leading to vertical accretion, especially near the fringe. The low waves and flow velocities also cause less sediment to be resuspended [21]. Additionally, the roots of the mangroves can also directly trap sediment, making it harder for the sediment to get resuspended. Lastly, biomass from the mangroves itself also contributes to vertical accretion and sediment trapping [11]. Therefore, if mangroves receive enough sediment they can adapt and keep up with sea level rise and subsidence [52]. According to a study by Van Bijsterveld et al. (2023) [60], mangrove trees can survive RSLR and sedimentation rates by growing new or extending their pneumatophore rootmats. Figure 2.4 shows the hypothetical response of a mangrove forest to RSLR combined with sediment availability.

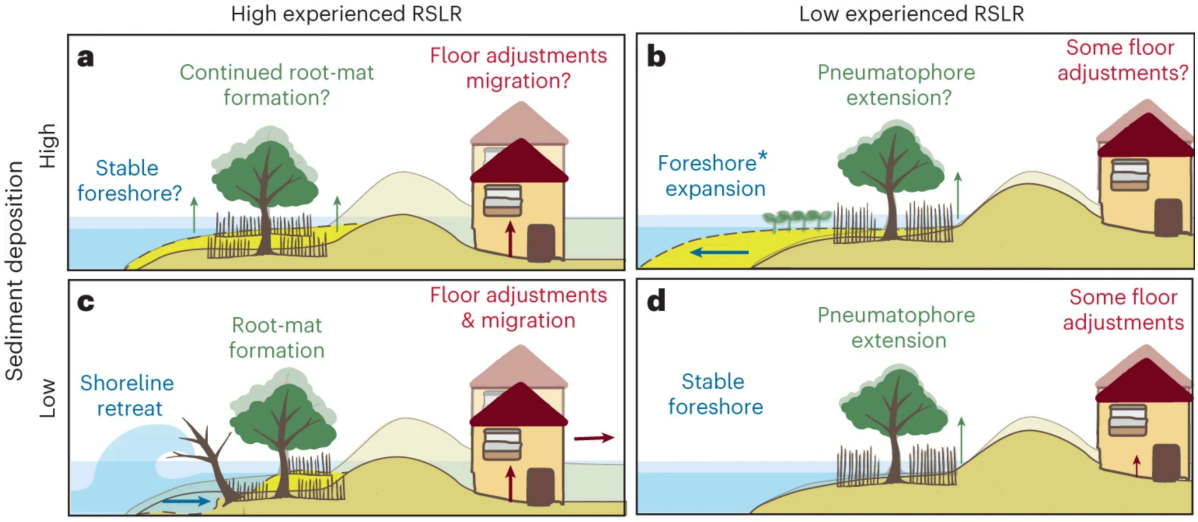

Figure 2.4: Four hypothetical situations for a mangrove forest responding to RSLR and sediment availability. Pre-subsidence profiles are shown as transparent lines, with sunken profiles as solid lines. Translucent water indicates sea-level rise, while dashed lines represent sedimentation (yellow) or erosion (transparent in c). **a** shows a stable vegetated foreshore with sediment matching RSLR. **b** shows expanding foreshores under low RSLR and high sediment supply. **c** shows that high RSLR and low sediment availability causes erosion and mangrove retreat, forcing adaptation or migration. **d** shows limited sediment supply together with low RSLR leads to pneumatophore extension [60].

2.3. Drivers of coastal erosion

Coastal erosion severely impacts the residents of the Mekong Delta, not only increasing vulnerability to flooding but also leading to economic decline and social unrest due to the loss of land [17]. Building on the understanding of sediment dynamics discussed in the previous section, this section examines the natural and anthropogenic drivers that influence sediment transport processes and potentially contribute to coastal erosion in Bạc Liêu.

2.3.1. Natural redistribution of sediment

Deltas are generally unstable hydro-morphodynamic systems which retreat and progradate in seasonal and multi-decadal cycles [67]. This means that under the influence of waves, tides, wind and river plumes, some areas will naturally erode, while others will naturally accrete. From their study, Marchesiello et al. (2019) [35] conclude that this natural redistribution by long shore currents is the main contributor to the observed erosion and accretion patterns in the Mekong delta, and that other driving factors are only influencing the system on a local scale. However, based on Figure 1.2 and the theory explained in subsection 2.2.2, it is assumed that natural redistribution through longshore sediment transport has a small effect on the erosion rates in Bạc Liêu.

2.3.2. Land subsidence and sea level rise

Due to over-exploitation of groundwater, the land in the Mekong delta has been subsiding heavily over the last decades [15]. It started in the 1960s with a limited number of wells, but nowadays more than a

million wells are being used for domestic, industrial, and agricultural purposes [63], leading to average subsidence rates of $0.5cm/y$ between 1991 and 2010 growing to $1.5cm/y$ after 2011 [39]. Minderhoud et al. (2017) [39] has modeled the subsidence (rates) in the Mekong delta (Figure 2.5), and demonstrated that subsidence rates in Bạc Liêu are relatively high, making it likely to be contributing to the observed erosion.

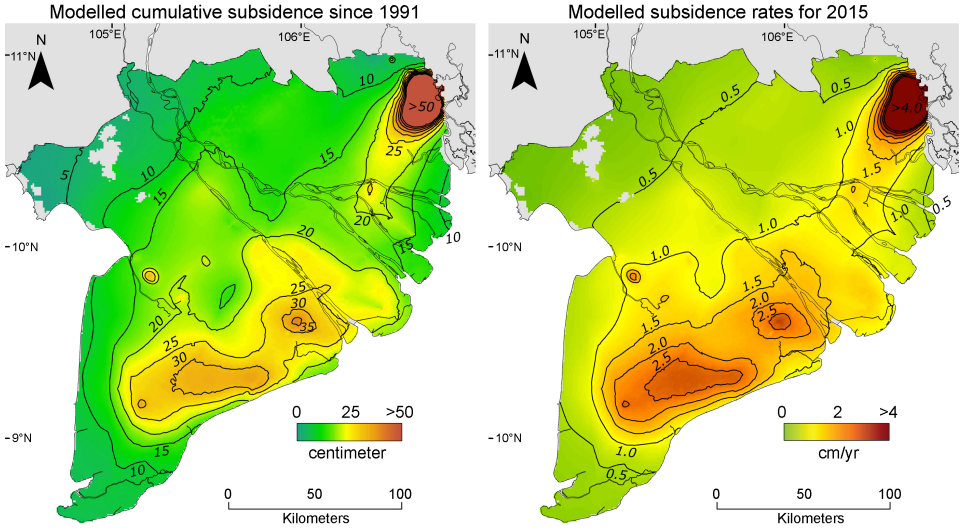

Figure 2.5: Modeled subsidence (left) between 1991 and 2005 and subsidence rates for 2015 (right) in the Mekong delta. The figure shows relatively high subsidence (rates) near the coast of Bạc Liêu. [39]

Furthermore, due to global warming, sea levels are likely rising at an average global rate of at least $0.32cm/y$ [53]. The effect of land subsidence in combination with sea level rise is called relative sea level rise (RSLR) and its contribution to coastal erosion depends on the slope of the coast. For example: a slope of 0.1% together with a RSLR of $1.5cm/y$ leads to a shoreline retreat of $15m/y$, which is already quite substantial. Furthermore, as RSLR leads to higher water levels, waves feel less friction from the bottom, leading to higher waves reaching the shore, which can lead to more erosion (subsection 2.2.1).

2.3.3. Fluvial sediment supply deficit

River sediments are the primary driver of pro-gradation of the Mekong Delta. A recent model-based study by Tanh et al. (2025) [57] states that the Mekong River currently delivers an amount of 22.8 Mt of sediment to the sea. However, sediment loads have been substantially higher in the past. Since the late 1990s, the construction of 89 hydroelectric dams [23] has resulted in significant sediment trapping in upstream reservoirs, reducing the sediment supply to the coastal system. In addition, approximately $55Mt$ of sediment is mined out of the river each year to be used as construction material [8]. These factors combined, possibly aggravated by a climate change-induced discharge reduction [12], are expected to cause a reduction of sediment reaching the coastal system in 2050 of up to 95% compared to the period 2000 - 2010 [62].

Tamura et al. (2020) [56] argues, however, that these recent activities are not the only contributors to the sediment deficit and that historic processes also play a significant role. During French colonization, from 1858, the Mekong delta has been intensely modified through the construction of multiple canals to improve navigability and agricultural irrigation [5]. Floodwaters were directed through the canals to overflow into rice fields, depositing fertile sediment. This process, combined with sediment accumulation in the canals, intercepted and stored muddy sediment within the delta plain that would have otherwise been transported to the coast [27].

Naturally, as less sediment is available for coastal redistribution, less suspended sediment has the chance to reach the shore. Furthermore, long term sediment deficit has led to an ongoing shrinkage of the subaqueous delta [30] [56]. This causes higher waves to reach the shore, potentially leading to more shoreline erosion.

2.3.4. Loss of mangroves

As explained in subsection 2.2.3, mangroves stimulate sediment deposition by attenuating waves and enforcing drag. Therefore, mangrove loss would imply a reduction in sediment deposition rates. Phan et al. (2014) [48] hypothesized an inverse linear relationship between mangrove width and erosion rates. Such relationships are not valid everywhere in the delta, as suggested by Besset et al. (2019) [4]. Nonetheless, both studies do agree that mangrove removal contributes to the aggravation of shoreline erosion. Over the past 50 years, the mangrove forests in the Mekong delta have decreased significantly in size. In 1973, the total area of mangrove forests in the Mekong Delta was 185,800 ha, of which only 102,160 was left in 2020 [49]. Driving factors are wood cutting to make place for aquaculture, agriculture and urban development. Additionally, coastal erosion itself and 'mangrove squeeze' (subsection 2.3.5) have contributed to the large-scale mangrove deforestation [2], making mangrove loss both a driver and a result of coastal erosion.

2.3.5. Impermeable structures in the intertidal zone

Subsection 2.2.1 described how, in an low energy, convex-up mudflat, cross-shore sediment transport leads to net deposition towards the coast, with mangroves enhancing sediment accumulation (subsection 2.2.3). However, these processes are disrupted when hard structures are constructed in the intertidal zone, primarily to protect aquaculture farms and coastal villages. This subsection discusses the resulting processes and their impact on coastal erosion based on the work of Winterwerp et al. (2013) [66].

- **Mangrove squeeze**: When sea levels rise, land subsides or the foreshore erodes, coastal ecosystems, like mangrove forests, have the tendency to migrate in landward direction [19]. However, when hard structures are built, mangroves are 'squeezed' between the structure and shoreline, reducing the width of the forests and consequently its positive effect on wave attenuation and sediment deposition rates [48].
- **Tidal flow restriction**: The construction of hard, impermeable structures within the intertidal zone, also has an effect on the tidal flow, as less water can flow into the intertidal system. Since tides transport sediment in landward direction (subsection 2.2.1), this causes a reduction in onshore sediment supply. Winterwerp et al. (2013) [66] calculated that building a dike between the mean high water line and high high water spring line can reduce sediment import by 10% for every tidal cycle.
- **Wave reflection**: When incoming waves reach a structure, wave reflection will occur. This creates standing waves that can be up to two times as large as the original incoming wave [20]. Since bed shear stress scales with the square of the wave height, erosive forces increase by a factor of 2–4. Due to the irregular nature of incoming waves, they quickly become uncorrelated, limiting the area of influence. For shorter waves (2–4 s), this corresponds to a length scale of 10–25 m seaward of the dam or dike, while for longer swell waves, the influence can extend to a few hundred meters seaward of the dike [66].

To summarize, the construction of impermeable structures in the intertidal zone can reduce sediment import by tides and increase sediment export by waves. Although these differences are small, the gross sediment fluxes are very large, so even a small effect could notably impact the net sediment flux. The negative effects of tidal flow restriction and wave reflection are schematized in Figure 2.6. However, contrary to the ideas of Winterwerp et al. (2013) [66], Zhong & Hu (2021) [68] argue that the reduction of tidal flow could also lead to a reduction of imposed shear stresses. Therefore, they say that the construction of a dike can, in some cases, also have an accreting effect seaward of the dike.

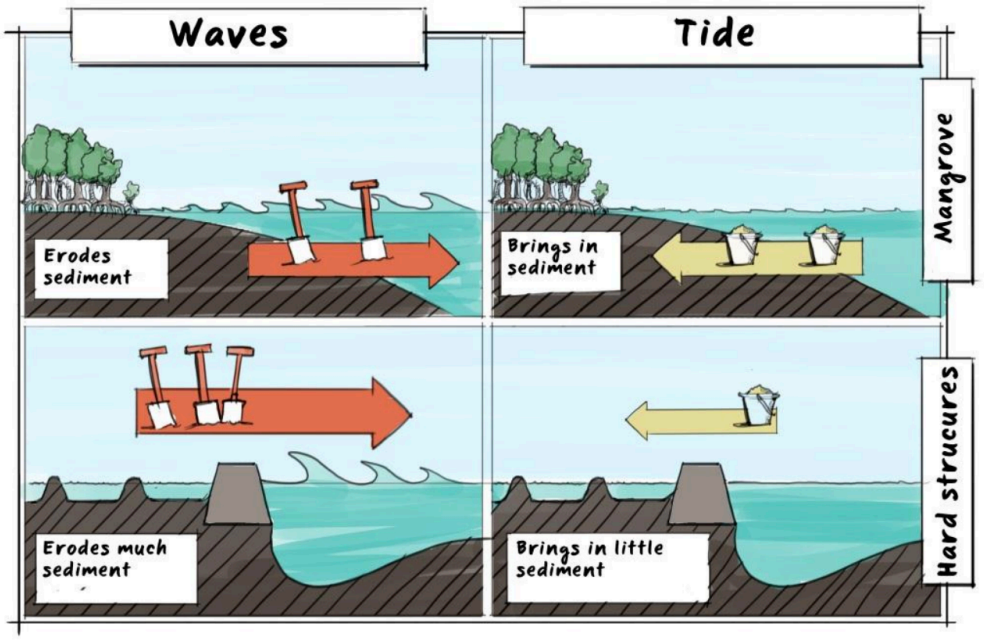

Figure 2.6: Schematization of the effects of the tides and waves, both for a situation with mangroves and hard structures [65].

2.3.6. Erosion feedback loop

The previous subsections described how different natural and anthropogenic drivers can lead to shoreline erosion of the Mekong delta. Due to this erosion, the shape of the cross-shore profile can change from a convex-up to a concave-up bed profile (Figure 2.7). As mangroves thrive on convex-up profiles, this change is unfavorable for mangrove growth.

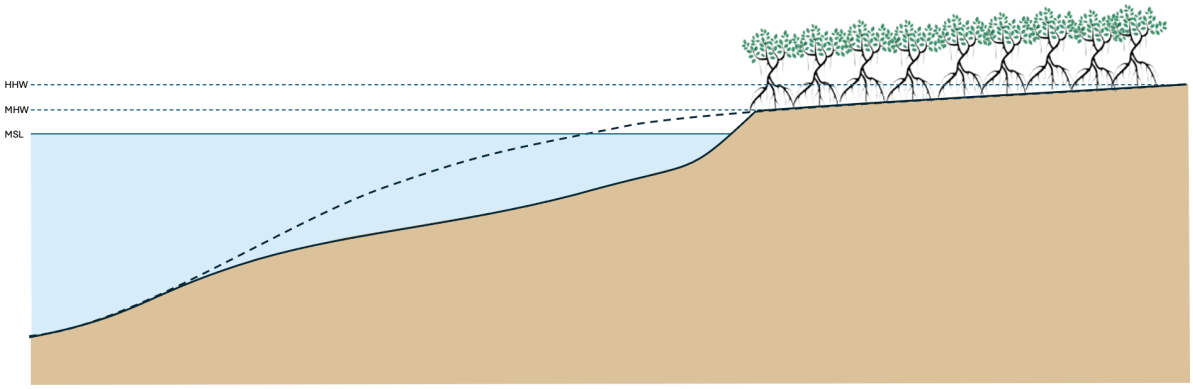

Figure 2.7: Schematization of a mudflat transforming from a convex-up (dashed line) to a concave-up (solid line) profile

Winterwerp et al. (2013) [66] describes how this change in the cross-shore bed profile can initiate a

positive feedback loop: As the shape of the bed profile changes from convex-up to concave-up, water depths increase. This causes larger waves to reach the shore and reflect, inducing more erosion, leading to higher water depths, leading to less wave attenuation, etc. Simultaneously, the concave-up bed profile provides unfavorable conditions for mangroves to grow and, as they erode, they get squeezed between the shore line and structures as described in subsection 2.3.5. This decreases the width of the mangrove forests, leading to more erosion, leading to less favorable conditions for mangroves to grow, etc. Figure 2.8 shows these feedback loops and the other relations between processes driving coastal erosion in the Mekong delta.

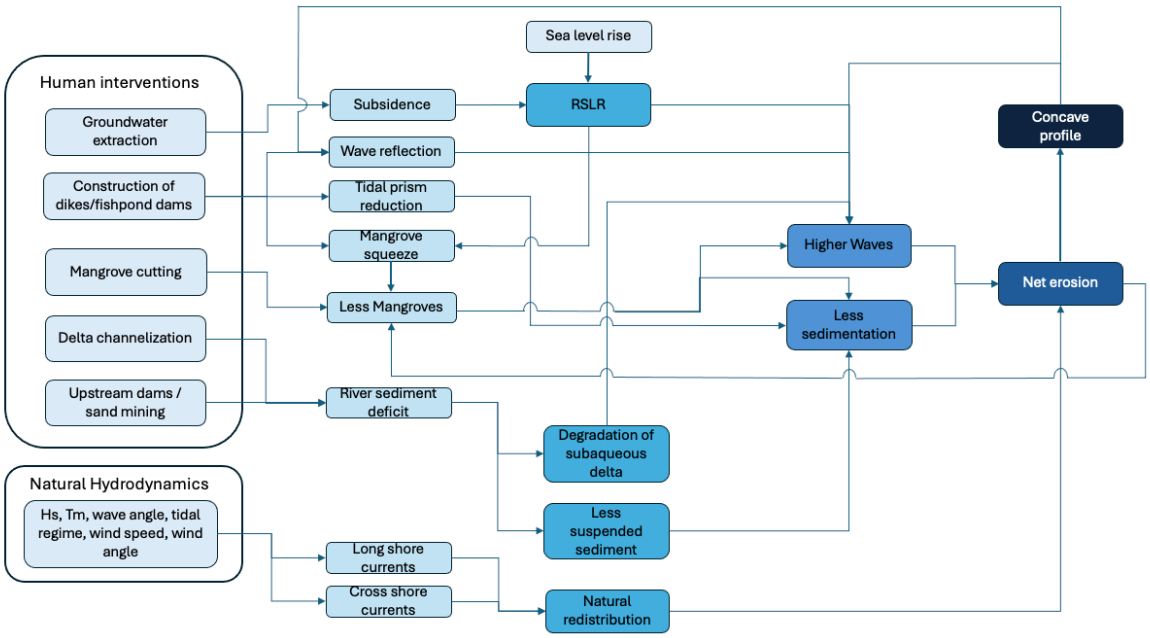

Figure 2.8: Theoretical relations and feedback effects of processes driving coastal erosion.

2.4. The Bạc Liêu coast: historic vs current state

This section examines the current and historic state of the coastal system, as well as the different types of land use and land use changes within and behind the mangrove forests. Based on literature and observations made during a one-week field trip in December 2024, local phenomena and historic changes are linked to the processes and erosion drivers discussed in the previous chapters.

2.4.1. Land use

The land use in Bạc Liêu has changed significantly over the last decades. In the early 1990's the main agricultural production was rice cultivation. This was done extensively, but heavily reliant on seasonal hydrological regimes. However, between 1990 and 2010, the region underwent significant changes in both the area and structure of its farming systems. By the late 1990's, driven by the high financial returns from aquaculture, particularly shrimp farming, a substantial portion of rice-growing areas had been converted to shrimp cultivation [45]. From 2000 till 2010 this trend continued, due to the financial benefits and salt intrusion making the land less favorable for rice cultivation [46]. In 2015, the total land coverage for aquaculture in Bạc Liêu was between 40,000 [46] and 130,000 hectares [50], making it the main contributor to Bạc Liêu's economy, with a total yearly seafood production of roughly 300,000 tons, yielding over 29 trillion Vietnamese Dong [50].

Figure 2.9 illustrates the land use change in Bạc Liêu between 2000 and 2010. The figure shows that next to a shift from rice farming to aquaculture, the remaining rice farms intensified, switching from a single to a double or a triple rice farming system. These land use changes caused a higher demand for freshwater leading to more ground water extraction [40], ultimately leading to more subsidence [39], of which the potential effects on erosion are explained in subsection 2.3.2.

Apart from turning old rice farms into aquaculture, the aquaculture also started to exist within mangrove forests. This so called 'mangrove integrated farming' is less extensive and uses less groundwater. It is is driven by both environmental and economic factors [25].

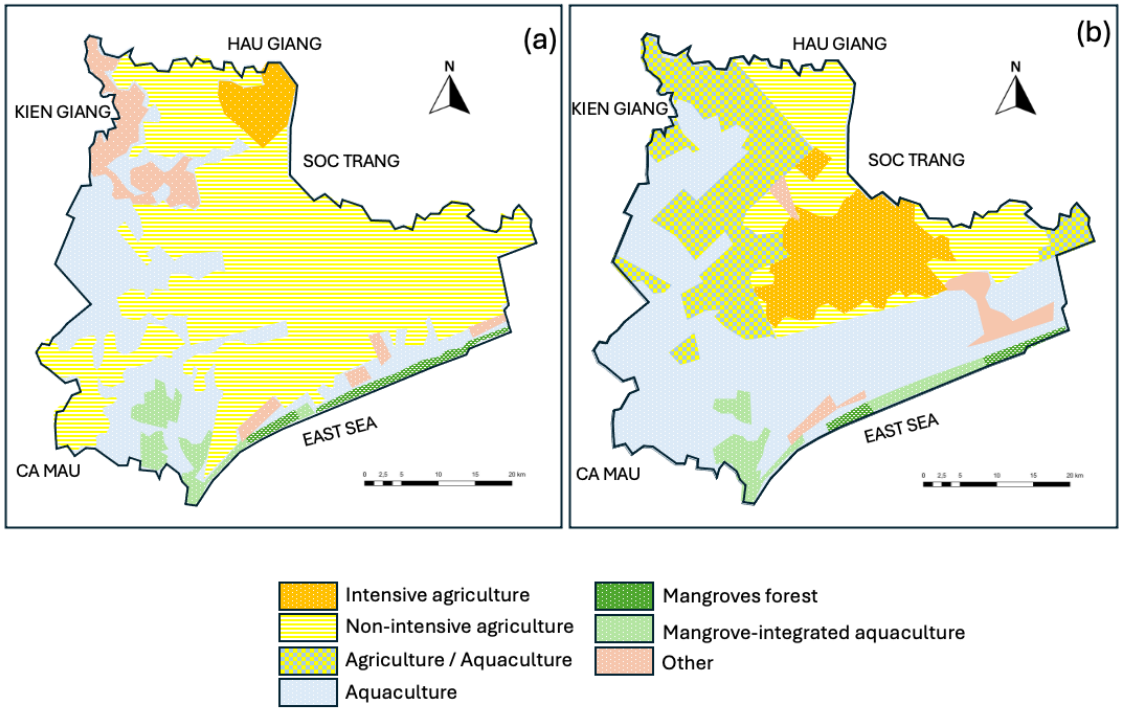

Figure 2.9: Land use in Bạc Liêu in 2000 (a) and 2010 (b) showing a large shift from rice cultivation to shrimp farming, and mangrove forest to mangrove integrated shrimp farming (Adjusted from Pham et al., 2015 [45]).

In order to protect their farms, mangrove integrated farmers build small earthen dikes between the natural mangroves and their fishponds (Figure 2.11). The extensive farms and adjacent villages are protected by a bigger sea dike separating the mangrove forest from the land. The potential effects of these structures on erosion rates are explained in subsection 2.3.5. Figure 2.10 shows a satellite image of a coastal section of Bạc Liêu, with the dikes and mangrove sections indicated in different shades and colors.

Figure 2.10: Overview of coastal land use in Bạc Liêu. The sea (light blue) borders the natural mangrove forest (light green) which is separated from the mangrove integrated fishponds (dark green) with an earthen dike (brown line). The fishponds are separated from the hinterland with a concrete dike (black line). In the hinterland, many extensive fish farms can be observed.

Figure 2.11: Earthen dike separating natural mangroves from mangrove integrated fishponds

2.4.2. Subaqueous delta

The subaqueous part of the Mekong delta is relatively young and formed approximately 1000 years ago [54]. It has a thickness of approximately $15m$ [31] and, along the coast of Bạc Liêu, consists mostly of mud and muddy sand [59]. Based on high resolution Chirp sonar profiles from 2006/2007 [31] and data from the Southern Institute of Water Resources and Planning (SIWRP), for which the collection date and method are unspecified, the subaqueous delta in front of the Bạc Liêu coast reaches a water

depth of approximately $20m$ below MSL at a cross-shore distance of approximately $20km$. The map is shown in appendix A.1

On the other hand, historic bathymetry maps from the British admiralty from 1881, show a maximum depth of approximately $6.5m$ below MSL at an offshore distance of more than $20km$ from the present-day coast of Bạc Liêu. A section of the map is shown in appendix A.2. Although the old admiralty map was made with a lower resolution and with less advanced measurement instruments, the great difference in water depth between the historic and present state, suggests that a large scale degradation of the subaqueous delta has taken place over the last century. This idea is further examined by Liu et al. (2017) [30]. They found that the Mekong delta has a relatively shallow rollover point compared to other large delta's, and that the topset at the area in front of the Bạc Liêu coast is very poorly developed, both implying that the subaqueous part of the mudflat is eroding.

This subaqueous degradation is most likely driven by changes in long shore sediment transport, either caused by fluvial sediment supply deficit or changes in local oceanographic regime [56]. While these processes are beyond the scope of this research, their apparent influence on the shape of the subaqueous delta and the resulting changes in cross-shore sediment transport are hypothesized to potentially impact coastal erosion rates in Bạc Liêu, as discussed in subsection 2.3.3.

2.4.3. Coastline

Over the last 4,500 years, the Mekong Delta's coastline has migrated about 200 km seawards, driven by high rates of fine sediment deposition and rapid compaction, leading to the formation of the Cà Mau peninsula [42]. However, a study by Anthony et al. (2015) [3] showed that this accretion has slowed down and that large parts of the Mekong Delta's coastline are now retreating. When zooming in to the coast of Bạc Liêu (Figure 2.12), it becomes clear that some parts of the shoreline only have a very narrow strip of natural mangroves (left), while other regions still have a relatively wide strip of mangroves (right). There is no general consensus on why these local differences occur on such a small scale, yet.

In order to prevent coastal erosion, the Bạc Liêu government has built different interventions near the coastline such as pile rock breakwaters and bamboo fences. Some structures seem to be successful, while others are failing.

Figure 2.12: Coastal section in Bạc Liêu shows local differences in current state of the natural mangrove forest.

2.5. Conclusion

The Mekong delta's tides, combined with its monsoon dependent wave regime, create a complex coastal sediment transport system. While tides dominate sediment transport on the east coast, residual longshore currents driven by waves transport sediment from the river mouths in a southwestward direction. Based on a numerical model by Marchesiello et al. (2019) [35], this littoral drift should promote sedimentation and accretion along the coast of Bạc Liêu. However, studies by Anthony et al. (2015)

[3] and Luijendijk et al. (2018) [32] show that the coast is, in fact, eroding. Additionally, Phan (2019) [47] suggests that tidal currents are more perpendicular to the coast in Bạc Liêu, compared to adjacent provinces. This leads to the assumption that cross-shore sediment transport processes play a key role in the mechanisms driving coastal erosion in Bạc Liêu.

Drivers like land subsidence, sediment deficit, subaqueous delta degradation and the construction of impermeable structures in the inter tidal zone have been hypothesized to cause coastal erosion in the Mekong Delta, but a detailed understanding of their specific effects on individual coastal sections remains limited. Furthermore, limited research has been conducted on how these drivers interact and possibly strengthen each other.

The Bạc Liêu coast serves as an interesting study area to investigate erosion processes because of the wide range in potential drivers and land use. Land subsidence due to groundwater extraction and coastal squeeze and tidal flow restriction due to the construction of dikes and fishpond dams are all closely linked to the regions' aquaculture and agriculture industries. Sediment deficit and large scale subaqueous delta degradation are driven by upstream human activities. All these theoretical drivers could potentially play a role in the observed erosion patterns in Bạc Liêu. Most importantly, the high economic and societal value of the land and its inhabitants, combined with previously failed efforts to combat coastal erosion, make a deeper understanding of the underlying processes crucial.

3

Methods

In order to gain a further understanding of the processes driving coastal erosion in Bạc Liêu and answer the research question(s), this study uses both numerical modeling and a qualitative analysis of cross-shore bathymetry profiles within the mangrove forests. A one-week field campaign was conducted to collect data that supports building the model and to perform the qualitative analysis. The model is used to simulate the effects of the construction of sea dikes, subsidence and sediment deficit on erosion rates and bed level change.

3.1. Analysis of elevation levels in mangrove forests

According to the theory explained in subsection 2.2.3, mangrove forests are able to adapt to RSLR depending on the rate of RSLR, sediment availability and sedimentation rates. Additionally, the field observations discussed in subsection 2.4.1 show that a large part of the mangrove forest is used as fishponds and is excluded from the coastal system through an earthen dike. Consequently, no sediment transport takes place in this area. Therefore, by assuming that subsidence rates in the natural mangrove forests and fishponds are equal, differences in elevation levels can be used to make conclusions about sediment availability and RSLR rates.

Elevation levels are collected using a Trimble R8s RTK GNSS device along a cross-shore transect. Correct measurements start at the concrete dike, through the mangrove integrated fishponds, over the earthen dike, up until the end of the natural mangrove forest at an interval of $5 - 10m$. Data from nine transects has been collected over the last 2 years (Figure 3.1).

Figure 3.1: Nine test locations in Bạc Liêu

By analyzing the bed level data, different patterns in elevation differences between natural mangrove forests and fishpond areas can be identified. The elevation comparison can help determine whether sediment accretion is keeping pace with RSLR or whether additional processes, such as sediment deficits or hydrodynamic changes, are influencing erosion patterns.

A higher elevation in the fishponds compared to the natural mangrove forest may indicate that RSLR is not the only factor playing a role in the erosion, and that external factors are likely playing a role as well. While on the other hand, a lower fishpond area than the natural mangrove area at a stable coast, suggests that sediment accretion is sufficient to compensate for RSLR. These interpretations will be further explored in Figure 4.1.2, where the specific cases are analyzed

Additionally, historic satellite images from 1986 till 2022 (Appendix E) are used to calculate average erosion and accretion rates, which are used and to further explain observed patterns in elevation levels

3.2. Numerical model

To further examine the effect of specific erosion drivers, a numerical model that is capable of simulating hydrodynamics and morphodynamic responses is used. The main objective is to simulate the long-term morphodynamic response to (the absence of) four erosion drivers: the construction of sea dikes and fishpond dams, subsidence, an decreased suspended sediment conncentration and degradation of the subaqueous delta.

3.2.1. Model choice and limitations

Mflat [61] is a 1D line model that is suitable for simulating hydrodynamic processes and morphodynamic responses on mudflats. It is an open-source MATLAB code that is able to model both cross-shore tidal hydrodynamics, along with a stationary wave model on a 1D-, cross-shore, high resolution grid.

In order to derive solutions effectively and relatively fast, Mflat applies a simplification of the shallow water equations, neglecting the cross-shore momentum equation and, thus, inertia and friction effects. This is justified under the assumption that cross-shore velocities remain low.

Mflat computes sediment transport by using an advection-diffusion equation, and bed level changes result from sediment transport changes and gradients. However, Mflat does not include flocculation and consolidation processes, influencing settling and erosion properties of the sediment, which can impact the mudflat morphodynamics.

Wave action is governed by a stationary wave energy balance. Wind input, wave breaking, and dissipation by friction collectively shape the gradient of wave energy across the mudflat. Mflat does not include a function describing wave reflection. As a result, its direct effect on erosion (subsection 2.3.5) and feedback effects (subsection 2.3.6) are neglected. Additionally, it includes a vegetation model which can accurately calculate the effect of mangroves on wave dissipation and critical shear stress.

Despite its simplicities, Mflat reasonably quantifies processes relevant for erosion in Bạc Liêu in an effective way. To minimize errors and obtain a representation that closely reflects real-world conditions, the model needs to be set up with realistic parameters and have proper calibration.

3.2.2. Model set up & calibration

This section summarizes the model set up and calibration procedure. A more detailed description is given in Appendix B

Bathymetry

Mflat calculates sediment transport and resulting bed level changes on an initial cross-shore bathymetry profile. This initial profile is based on a combination of bathymetry measurements both in the mangrove forest and fishponds (Living lab, 2023) and the subaqueous delta (SIWRP, n.d.). The data from transect 23-66 (Figure 3.1) has been chosen to represent the mangrove forest and fishponds, as the effects of different erosion drivers will be more apparent on an initially wider forest. The used profile has a length of $3.5km$ and is shown in Appendix B.1.

Hydrodynamics

The waves in the model are represented by two parameters: The root mean squared wave height (H_{rms}) and the peak period (T_p). Using a 20 year time series from Copernicus satellite program [14] average values for H_{rms} and T_p are obtained for both the dry season and wet season at a location $35km$ offshore. As the domain of the model is only $3.5km$, the transformation of the waves first needs to be calculated over a larger domain, which is shown in appendix B.1. The wave transformation procedure and its results are explained in appendix B.2.1.

The parameters governing the tides in the model are the amplitude, phase and frequency of the different tidal constituents. There are over eighty tidal constituents governing the tides of the coast of Bạc Liêu, of which M_2, S_2, N_2, K_2, P_1, O_1, K_1 and S_a are most dominant [24][47]. It is assumed that using these eight tidal constituents gives a sufficient representation of the tidal regime. A correction factor A_0 is applied to match high water peaks with reality (Appendix B.3.2).

Since winds in Bạc Liêu are mostly in longshore direction, wind effects are neglected. This assumption is further motivated in Appendix B.2.2

Mangrove characteristics

Mflat has an extensive vegetation module, including the growth and spreading of seedlings as well as the dissipative properties and sediment entrapment of grown plants. For the purpose of this research, plants are modeled as fully grown at the beginning of the simulation. The height, diameter and density of mangrove trees are used to calculate wave dissipation and are based on basic measurements during fieldwork in 2023. The sediment entrapment capabilities of the mangroves are represented by locally increasing the critical shear stress by a factor K_c. The derivation of this factor is given in Appendix B.3.

Sediment characteristics and calibration

Sediment parameters determine the ability of particles to move. The most important parameters are the fall velocity, the critical shear stress, an erosion parameter and the suspended sediment concentration on the domain boundary (SSC). Using data from the Medium Resolution Imaging Spectrometer (MERIS), Marchesiello et al. (2019) [35] calculated an SSC of approximately $0.5g/l$. The other sediment parameter values are not known for Bạc Liêu and, together with a few numerical parameters, need to be calibrated.

Historic satellite images show that the coast at transect 23-66 is eroding with a rate of approximately $16.67m/y$ for the last eighteen years (Appendix E). This research assumes that the profile has not reached equilibrium yet, and will keep eroding with the same rate. Additionally, it is assumed that the foreshore will undergo some erosion and that the elevation of the mangroves stays constant. These phenomena need to be reflected in the reference model. The whole calibration process is discussed in Appendix B.3

Figure 3.2 shows a schematization of the model with its parameters. Used values can be found in Appendix B.4

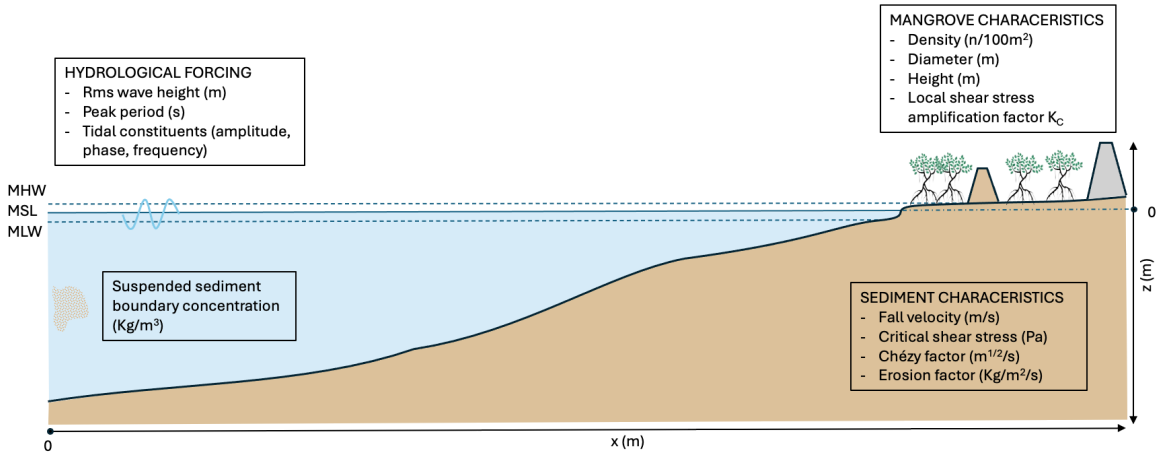

Figure 3.2: Schematization of the used numerical model with important physical parameters indicated

3.2.3. Model scenarios

This section outlines the different scenarios simulated to assess the effects of various erosion drivers.

Reference simulation

First, following the calibration process, a reference simulation over 16 morphological years is conducted. In this reference simulation, the erosion drivers assumed for the current situation at transect 23-66 are applied. These include a suspended sediment concentration of $0.5g/l$, the presence of dikes and fishpond dams, current bathymetry and associated wave heights, and no subsidence (subsection 4.1.2). Next, scenarios are simulated to assess the effect of different erosion drivers over the same period.

Subsidence

As discussed in subsection 2.3.2, large parts of Bạc Liêu are subsiding. Based on the model of Minderhoud et al. (2017) [39], subsidence is introduced in the model by lowering the bed level at a rate of $1.5cm/year$ over the entire profile. This should increase wave heights reaching the shore, and lower the bed level over the entire profile, therefore increasing horizontal erosion rates (subsection 2.3.2). According to the theory of subsection 2.2.3, if sufficient sediment is transported towards the coast, natural mangroves should be able to trap this sediment and accrete vertically at the same rate. To prevent water from reaching the fishponds once the ground has subsided, the fishpond dam is raised with $0.4m$.

Removal of fishpond dams

Subsection 2.4.1 discussed that dikes and fishpond dams were constructed within the mangrove zone to protect mangrove integrated aquaculture farms and villages. Prior to the construction of dikes and fishpond dams, the mangrove forest likely extended uninterrupted for multiple kilometers. By removing these barriers, tidal flow is restored, wave reflection is absent, and mangroves are not squeezed. Therefore, based on the theory discussed in subsection 2.3.5, it is expected that removing the dikes will decrease the horizontal erosion rate compared to the reference situation. This scenario is simulated using an extended profile without dikes, as presented in appendix C.1.

Suspended sediment concentration

As discussed in subsection 2.3.3, historic delta channelization and the construction of upstream hydropower dams have caused less sediment to reach the coastal system. This sediment deficit has likely reduced the suspended sediment concentration. To assess the impact of this change, a scenario with increased SSC is simulated. It is assumed that the historic SSC is $0.7g/l$. It must be noted that this value is not derived from measurements, as historic sediment data is lacking. Instead, it is a hypothesized increase above the present day value to asses how a moderate increase in SSC can influence long-term morphodynamic outcomes. It is expected that increasing SSC will reduce the horizontal erosion rate compared to the reference.

Historic foreshore

Based on the findings of subsection 2.4.2, the historic foreshore was likely at a higher elevation than it is today. As the water depth is shallower across the profile, wave heights are expected to be lower across the entire profile. To simulate this, boundary wave heights are recalculated on an elevated profile (section C.2). It is expected that the lower wave heights will reduce the horizontal erosion rate. Furthermore, because wave heights are recalculated based on a shallower historic foreshore, applying these waves to the current foreshore is expected to reduce the depth of the current foreshore.

Combinations

While the individual driver simulations provide insight into the isolated impacts of each driver, they also result in unrealistic scenarios, as different drivers are likely playing a role at the same time. By combining different scenarios, a more accurate understanding of the real-world interactions between these drivers is obtained. Table 3.1 shows used values and bathymetry for all modeled scenario.

	Subsidence rate (cm/year)	**Bathymetry**	**Boundary SSC (g/l)**	**Root-mean-squared wave height at boundary per season (m)**
Reference	0	Figure B.3	0.5	0.3 (dry), 0.23 (wet)
Subsidence	1.5	Figure B.3	0.5	0.3 (dry), 0.23 (wet)
No dikes	0	Figure C.1	0.5	0.3 (dry), 0.23 (wet)
Increased SSC	0	Figure B.3	0.7	0.3 (dry), 0.23 (wet)
Historic foreshore	0	Figure B.3	0.5	0.22 (dry), 0.19 (wet)
Subsidence + No dikes	1.5	Figure C.1	0.5	0.3 (dry), 0.23 (wet)
Subsidence + Increased SSC	1.5	Figure B.3	0.7	0.3 (dry), 0.23 (wet)
Subsidence + Historic foreshore	1.5	Figure B.3	0.5	0.22 (dry), 0.19 (wet)
No dikes + Increased SSC	0	Figure C.1	0.7	0.3 (dry), 0.23 (wet)
No dikes + Historic foreshore	0	Figure C.1	0.5	0.22 (dry), 0.19 (wet)
Increased SSC + Historic foreshore	0	Figure B.3	0.7	0.22 (dry), 0.19 (wet)
Subsidence + No dikes + Increased SSC	1.5	Figure C.1	0.7	0.3 (dry), 0.23 (wet)
Subsidence + No dikes + Historic foreshore	1.5	Figure C.1	0.5	0.22 (dry), 0.19 (wet)
Subsidence + Increased SSC + Historic foreshore	1.5	Figure B.3	0.7	0.22 (dry), 0.19 (wet)
No dikes + Increased SSC + Historic foreshore	0	Figure C.1	0.7	0.22 (dry), 0.19 (wet)
Subsidence + No dikes + Increased SSC + Historic foreshore	1.5	Figure C.1	0.7	0.22 (dry), 0.19 (wet)

Table 3.1: Used bathymetry and values for subsidence rate, boundary SSC and boundary root-mean-squared wave heights for all modeled scenarios.

4

Results

This chapter provides the results of the study. First, the measured cross-sections are presented and analyzed, highlighting patterns and their implications for coastal erosion and mangrove dynamics. Next, the results of the numerical model are examined, further assessing the impact of different drivers on erosion rates.

4.1. Mangrove cross-sections analysis

This section presents the measured cross-sections and highlights the insights drawn from them.

A total of nine datasets were collected. However, only two complete transects from a 2023 field campaign covered the entire profile (starting at the dike, through the fishponds and natural mangroves and ending at the cliff). The remaining seven transects were either incomplete or likely contained measurement errors, limiting their usefulness for the analysis. The complete transects are discussed in this section, the incomplete transects are discussed in Appendix D. Of these seven transects, it must be noted that none strongly confirmed or contradicted the outcomes of this research.

Of the two complete transects, one location has a very narrow strip of natural mangroves (transect 23-45) and one location a wide strip of natural mangroves (transect 23-66).

4.1.1. Transect 23-45

Figure 4.1 shows the cross-section of transect 23-45. The figure reveales that the fishponds lie partially below MHW. Since mangroves typically begin growing from MHW (subsection 2.2.3), and fishponds are excluded from the sediment transport system (subsection 2.4.1), the lower bed level likely results from subsidence. Additionally, the figure shows that a part of the natural mangroves is at a higher elevation than a large part of the fishponds. Assuming that both areas subside with the same rate, this higher elevation is most likely attributed to the vertical accretion of the natural mangroves.

This idea is further examined by comparing the maximum height difference with the modeled subsidence rates of Minderhoud et al. (2017) [39]. Figure 2.5 shows a cumulative subsidence of around $25cm$ between 1991 and 2015 and a predicted subsidence rate of around $1.5cm/y$ from 2015 onward at the Bạc Liêu coast. This suggests that the total subsidence in 2024 should be approximately $38.5cm$. Figure 4.1 indicates that the lowest level inside the fishponds is at $MSL + 0.74m$, while MHW and the highest point of the natural mangroves, are at $MSL + 1.1m$, resulting in a $36cm$ difference. These findings suggest that a part of the natural mangroves accrete at a rate similar to subsidence, indicating some sediment deposition (See section 5.2 for further discussion). However, historic satellite images (Appendix E) show that the coast is eroding, meaning that sediment deposition is not high enough to keep the coast stable. The observed situation corresponds with situation c in Figure 2.4.

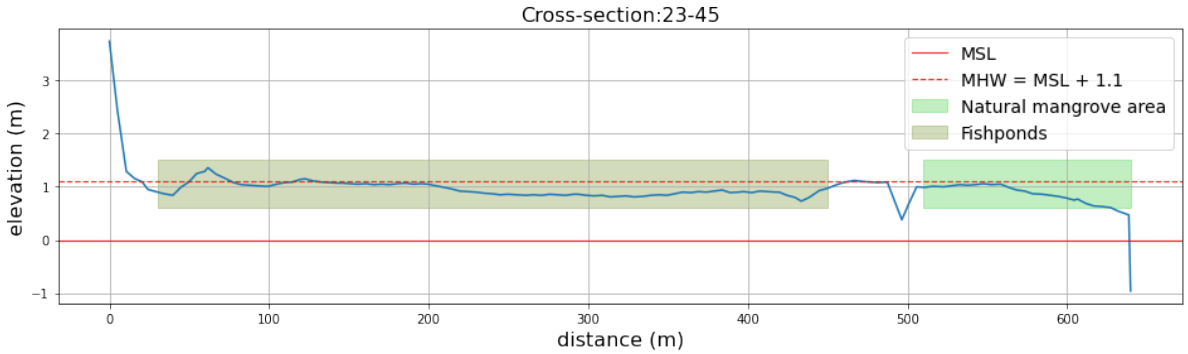

Figure 4.1: Cross-section profile of a location with severe erosion. Mean sea level and mean high water are indicated with red lines. The shaded areas correspond to the location of the fishponds (dark green) and natural mangroves (light green)

4.1.2. Transect 23-66

Figure 4.2 presents the cross-section of transect 23-66. The figure shows that both the fishponds and natural mangroves, are approximately at MHW. Since the fishponds are disconnected from the sediment transport system, and therefore cannot vertically accrete, it follows that subsidence is absent or limited in this area, and does not substantially affect the erosion at this coastal section.

Subsection 2.2.3 explained that if a coastal section experiences little to no RSLR and receives enough sediment, the coast should be stable or accreting. However, historic satellite images (Appendix E) show ongoing erosion, implying that other drivers limit sediment deposition rates.

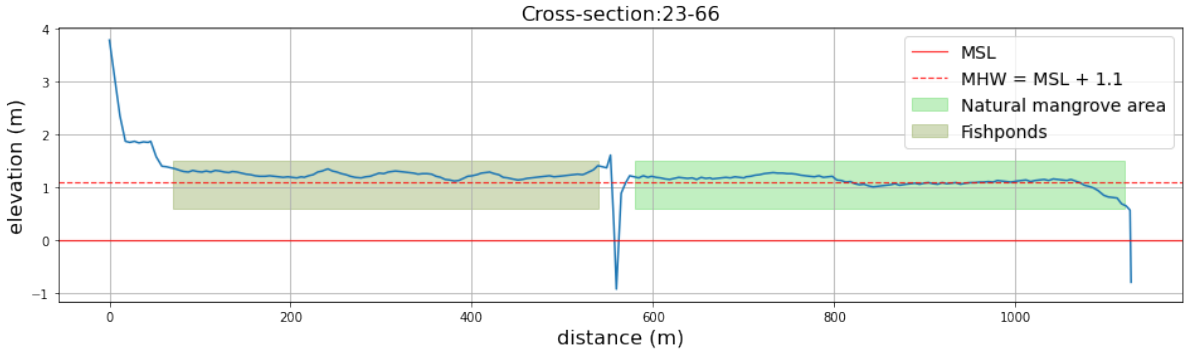

Figure 4.2: Cross-section profile of a location with moderate erosion and a wide natural mangrove strip. Mean sea level and mean high water are indicated with red lines. The shaded area's correspond to the location of the fishponds (dark green) and natural mangroves (light green).

4.1.3. Spatial variations and erosion rates

Transect 23-66 and 23-45 are approximately $5km$ apart, but show notable differences in their current state. Transect 23-66 has a wide strip of natural mangroves, while transect 23-45 is almost completely eroded. The historical coastline evolution at transect 23-45 (Appendix E) shows that between 1986 and 2004 the coastline remained relatively stable, while from 2004 onward, the coast began eroding with an average rate of approximately $10m/y$. On the other hand, transect 23-66 accreted several hundred meters between 1986 and 2004 before it began to erode at an average rate of approximately $16.7m/y$.

These observations, along with the findings from the previous subsections, imply that transect 23-45 changed from a system with a stable shore line, experiencing RSLR but with large sediment deposition (situation a in Figure 2.4) to an eroding system experiencing RSLR and low deposition rates (situation c in Figure 2.4). Simultaneously, transect 23-66 transitioned from an accreting system with little to no subsidence (situation b in Figure 2.4), to an eroding system. This suggests that sediment deposition rates must have declined at both transects after 2004 and that an increased subsidence rate is not the main driver causing this shift.

4.2. Numerical model

This section presents the outcomes of the numerical model. First, the reference model, derived from the calibration process (Appendix B.3), is introduced. Next, the results from scenario simulations are discussed. All scenarios, including the reference simulation, were simulated for 244 12-hour tidal cycles, multiplied by a morphological factor of 50, resulting in over 16 morphological years.

4.2.1. Reference model

The bed profile evolution of the reference model is shown in Figure 4.3. It reasonably corresponds real-world phenomena expected at transect 23-66, at least in terms of horizontal erosion rates for which data is available. The computed horizontal erosion rate is 16.7m/year (Table 4.1), which reasonably corresponds to the observed erosion rate over the past 20 years (Appendix E). Additionally, the natural mangrove area remains vertically stable, with no significant accretion or erosion, aligning with the findings in subsection 4.1.2. Lastly, the model predicts foreshore erosion which is likely exaggerated but no data is available to verify this. This foreshore erosion is expected based on the theory discussed in subsection 2.3.6. A detailed description of the reference model is provided in Appendix B.3.

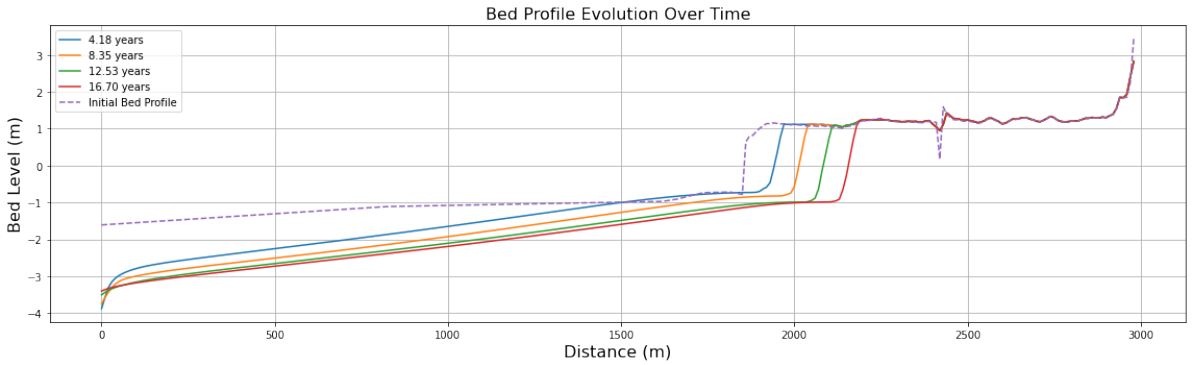

Figure 4.3: Bed profile evolution of the reference model for sixteen morphological years

4.2.2. Individual impact of erosion drivers

This subsection presents the results of simulations examining the individual effects of drivers of erosion such as subsidence, removal of dikes and fishpond dams, increased SSC and a shallower foreshore (hence lower waves).

Subsidence

Figure 4.4 shows the bed profile evolution for the scenario with a subsidence rate of $1.5cm/year$ over the entire profile. As predicted in subsection 2.3.2, the profile experiences an increased horizontal erosion rate compared to the reference scenario (Figure 4.9, Table 4.1). However, contrary to the expectations based on subsection 2.2.3, the remaining mangrove area does not remain vertically stable. Instead, it lowers at an average rate of $1.3cm/year$ (Figure 4.5). This vertical bed profile evolution is slightly lower than the subsidence rate, suggesting some deposition occurs. However, the deposition rates are insufficient to offset the imposed subsidence. Possible reasons for this and implications on the interpretation of this result are discussed in subsection 5.3.2.

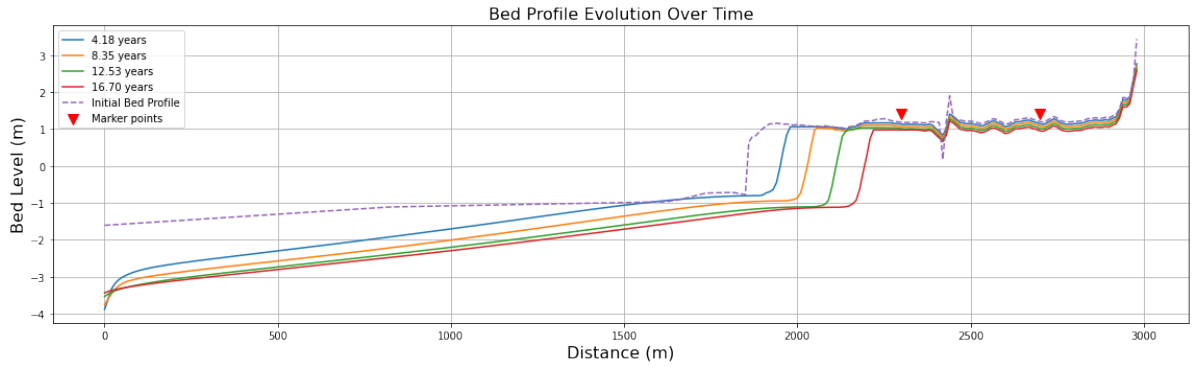

Figure 4.4: Bed profile evolution of a simulation with a subsidence rate of $1.5cm/year$

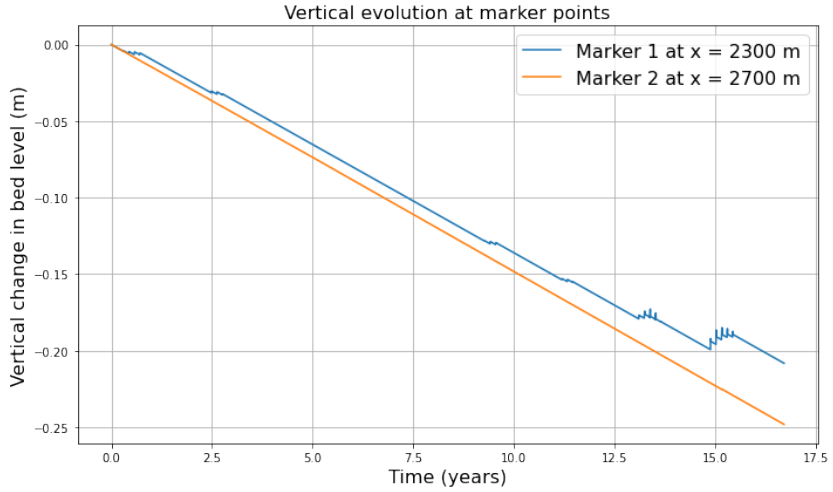

Figure 4.5: Bed level evolution inside the natural mangrove area (marker 1) and fishponds (marker 2)

Removal of dikes and fishpond dams

Figure 4.6 shows the bed profile evolution for the scenario with no dikes and an extended mangrove forest. The profile indicates a similar foreshore elevation horizontal erosion rate. In fact, Figure 4.9 suggests that horizontal erosion intensifies when the dikes are removed. These findings are inconsistent with the conceptual relations described in subsection 2.3.5 and Figure 2.8 as it is expected that removing dikes would lead to a decrease of horizontal erosion rates. Possible reasons and implications on the interpretation of this result are discussed in subsection 5.3.3.

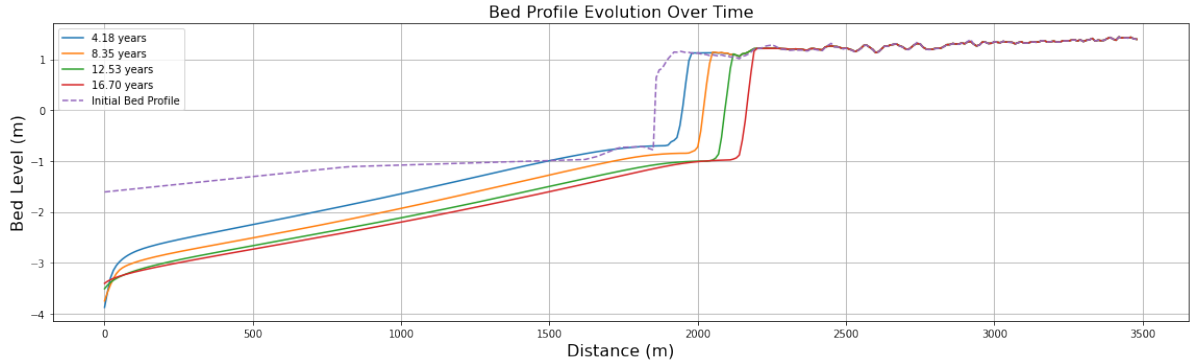

Figure 4.6: Bed profile evolution of a simulation with no dikes and extended mangrove forest

Increased SSC

Figure 4.7 shows the bed profile evolution for the scenario with increased SSC. The profile indicates a higher foreshore elevation and a lower horizontal erosion rate (Figure 4.9). This is consistent with the conceptual relations described in Figure 2.8, which suggest that higher suspended sediment concentration allows for more sediment to settle. Furthermore, because the foreshore erodes less in this scenario and even accretes near the foot of the cliff, lower waves reach the shore, causing reduced erosion.

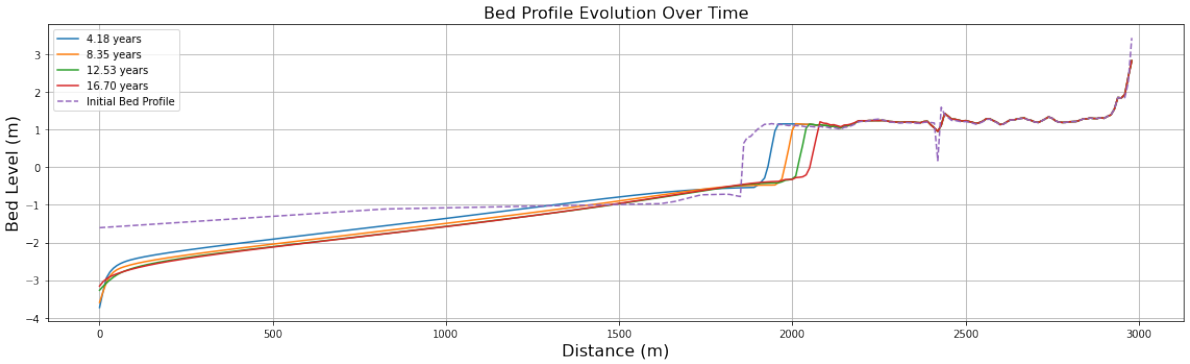

Figure 4.7: Bed profile evolution of a simulation with increased SSC

Historic foreshore

Figure 4.8 shows the bed profile evolution of the situation with reduced wave heights, due to a less deep historic foreshore. It shows a higher foreshore, and a reduced horizontal erosion rate compared to the reference situation (Figure 4.9). This is expected and consistent with the conceptual relations shown in Figure 2.8 and the theory explained in subsection 2.2.1.

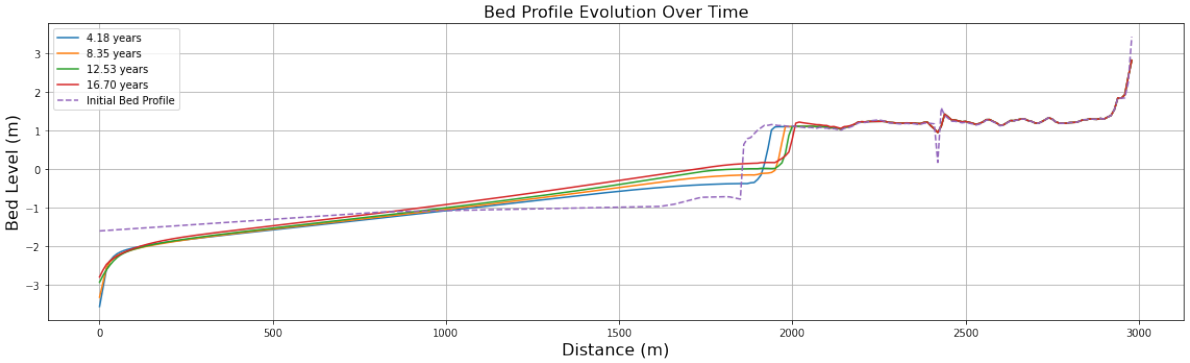

Figure 4.8: Bed profile evolution of a simulation with reduced wave heights.

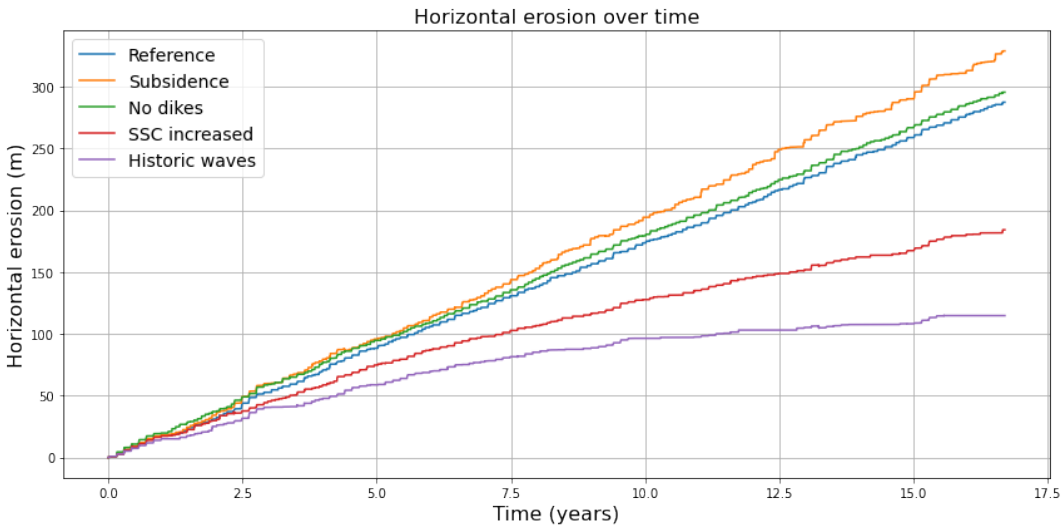

Figure 4.9: Comparison of simulated horizontal erosion rates at the cliff for five different scenarios. Numerical values for the average erosion rates are shown in Table 4.1

The results indicate that the profile is sensitive to all drivers, showing an increase in horizontal erosion rate when dikes are removed or subsidence is introduced and a decrease when the suspended sediment concentration is increased or lower wave heights are imposed at the boundary. This aligns with the hypothesis that observed erosion in Bạc Liêu is driven by a combination of drivers, rather than just one. Excluding the dike removal scenario, all simulations show expected behavior based on the conceptual relations presented in Figure 2.8.

Figure 4.9 shows that the model is most sensitive to wave height reduction. In this scenario, the horizontal erosion rate reduces to 3m/year for the last 3.5 years (Table 4.1). This suggests that the historic degradation of the subaqueous delta has had the most influence on current erosion rates.

4.2.3. Combinations

This section presents the most interesting findings from the simulations made with combined (absence of) drivers. The bed profile evolution of all possible combinations are presented in Appendix F.

4.2.4. Historic scenario

The results from section 4.1 and Appendix E strongly suggest that transect 23-66 changed from an accreting system to an eroding system, without experiencing subsidence. Therefore, the cause of this shift is likely due to a decrease in SSC, increase of incoming wave energy and/or the construction of dikes and fishpond dams. In a historic scenario, no drivers are present and therefore the bed profile evolution is simulated without these drivers (Figure F.9).

Figure 4.10 shows the horizontal erosion with different combinations of drivers. The most notable observation is that simulations with dikes removed always yield to a higher erosion rate. This is unexpected and further discussed in subsection 5.3.3. Furthermore, it shows that when both historic wave heights and higher SSC are combined, the coast becomes nearly stable, with only a horizontal erosion rate of 1.3m/year for the last 3.5 years (Table 4.1). The bed profile evolution of this combination (Figure F.6) even shows some vertical accretion in the natural mangrove forest. This supports the hypothesis that the historic degradation of the subaqueous delta and reduced sediment availability due to long term sediment deficits (subsection 2.3.3) have had a large impact on the coasts stability.

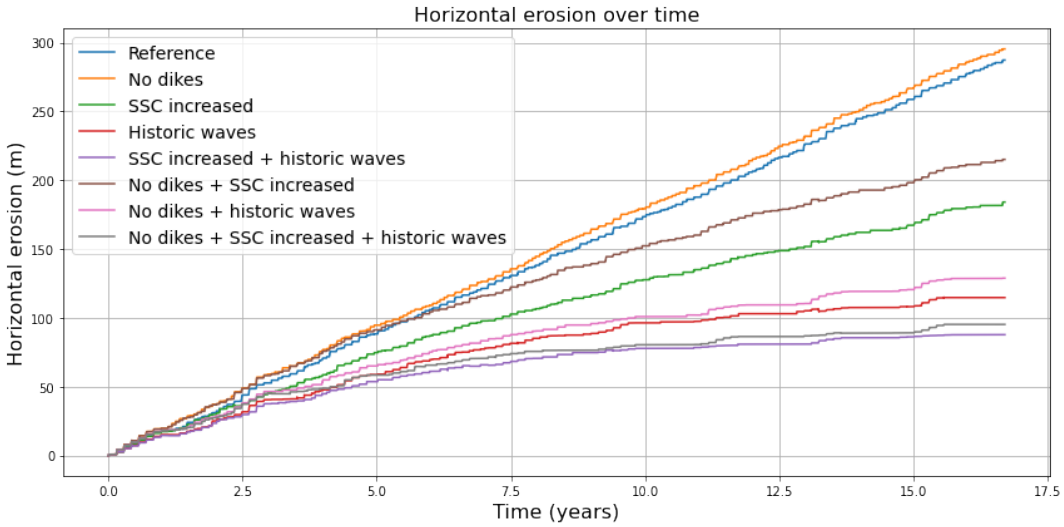

Figure 4.10: Comparison of simulated horizontal erosion rates at the cliff for scenarios with increased SSC, reduced wave heights and without dikes combined. Numerical values for the average erosion rates are shown in Table 4.1

4.2.5. Sediment deficit vs subsidence

Next, simulations are made with subsidence, increased SSC and reduced wave heights. The resulting horizontal erosion rates (Figure 4.11) demonstrate that when subsidence is introduced, erosion rates increase across all scenarios. However, for the scenarios with historic wave heights, this increase is limited and still stays well below the current reference scenario. This implies that the effect of subsidence on the erosion of the coast is limited if sediment supply is sufficient, which is in line with the theory discussed in subsection 2.2.3.

Additionally, it must be noted that in the scenario with subsidence, historic wave heights and increased SSC (Figure F.10), the cliff starts to smooth out. This could indicate that the profile is evolving to a new equilibrium profile without cliff.

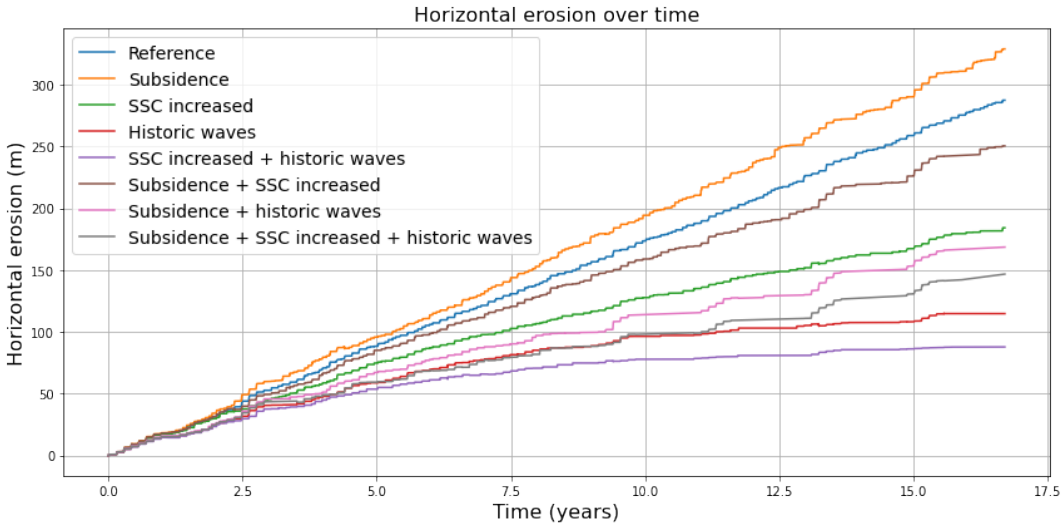

Figure 4.11: Comparison of simulated horizontal erosion rates at the cliff for scenarios with subsidence, increased SSC and reduced wave heights. Numerical values for the average erosion rates are shown in Table 4.1

Simulation	Average erosion rate (m/yr)	Last 3.5 years (m/yr)
Reference	16.7	16.6
Subsidence	19.7	19.2
No dikes	17.7	17.1
Increased SSC	11	8.6
Historic foreshore	6.9	3
Subsidence + No dikes	20.3	20.4
Subsidence + Increased SSC	15	13
Subsidence + Historic foreshore	10.1	8.6
No dikes + Increased SSC	12.9	8.9
No dikes + Historic foreshore	7.7	3.9
Increased SSC + Historic foreshore	5.3	1.3
Subsidence + No dikes + Increased SSC	15.6	13.5
Subsidence + No dikes + Historic foreshore	10.3	9.7
Subsidence + Increased SSC + Historic Waves	8.8	8.1
No dikes + Increased SSC + Historic foreshore	5.7	2.3
Subsidence + No dikes + Increased SSC + Historic foreshore	10	10.8

Table 4.1: Average horizontal erosion rates over 16 morphological years for each scenario

5

Discussion

5.1. Main drivers of coastal erosion

The results presented in Chapter 4 suggest that erosion along the Bạc Liêu coast is not caused by a single dominant process, but by the interaction of several erosion drivers. The observed elevation levels in the cross-sections (section 4.1) point to spatially varying subsidence, and the numerical model results (section 4.2) confirm that other drivers —such as foreshore shape, sediment availability, and coastal infrastructure— also play a decisive role in shaping current erosion rates. This contradicts the conclusion by Marchesiello et al. (2019), who suggested that subsidence is the main driver of erosion in Bạc Liêu. Instead, it is argued that differences in subsidence rates have played a crucial role in historic accretion patterns along the coast, while the consequences of long-term sediment deficits (reduced SSC and degradation of the foreshore) are likely the main drivers of the ongoing erosion along the whole coast. The role of dike construction remains uncertain due to unexpected modeling results and a lack of academic consensus (subsection 5.3.3).

Additionally, findings from the historic coastline evolution (Appendix E) show that erosion/accretion maps like those of Anthony et al. (2015) [3] and Luijendijk et al. (2018) [32] should be interpreted with caution, as they cover the cumulative erosion/accretion over a period during which the Bạc Liêu coast changed from an accreting or stable to an eroding system. Therefore, they may incorrectly classify parts of the Bạc Liêu coast as accreting regions.

These findings highlight the complexity of erosion patterns and reinforce the need to critically evaluate both field data and model outcomes. The following sections assess the reliability of the results, discuss key methodological assumptions, and identify opportunities for future research.

5.2. Discussion of field data and mangrove cross-section analysis

The elevation profiles from transects 23-45 and 23-66 form a key part of this study's argument regarding the role of subsidence and sediment deposition. The results of section 4.1 suggest that local differences in subsidence rates have caused a difference in historic accretion of the coast, while erosion at both transects is likely driven by (a combination of) other drivers.

However, while the differences in elevation between fishponds and natural mangrove forests were interpreted as indicators of sediment deposition and subsidence effects, several uncertainties arise with this approach.

5.2.1. Limited spatial coverage

The qualitative analysis of elevation levels within mangrove forests (section 4.1) demonstrates the potential of RTK GNSS data. However, of the nine collected cross-sections, only two covered the full profile, while others were incomplete or potentially contained measurement errors. This limits spatial coverage and the ability to generalize conclusions across the entire Bạc Liêu coastline.

Additionally, while the two complete transects may be good case studies and show erosion patterns and elevation levels that can be explained by existing theory, without validation against additional nearby cross-sections, elevation levels may also be influenced by other factors than sedimentation and subsidence. For example, the results from subsection 4.1.2 imply no subsidence since the fishpond is approximately at MHW. However, this could also be influenced by local management practices such as fishpond filling and other historic land modifications, not accounted for in this study. While this is considered unlikely, it introduces uncertainty regarding the claim that no subsidence is taking place at transect 23-66, and therefore weakens the conclusion that erosion must be driven by another driver than subsidence.

5.2.2. Dynamic erosion processes

Another source of uncertainty in this analysis is the fact that measurements were taken at a single point in time, while coastal erosion and sedimentation are dynamic processes influenced by seasonal variations and storm events. Capturing data at a single time point does not account for these temporal fluctuations. Consequently, the results from section 4.1 might have been different if the measurements were made in another season or after an extreme event, potentially leading to different elevation levels and other interpretations regarding vertical accretion rates.

For example, the results from subsection 4.1.1 suggest that part of the natural mangrove zone has vertically accreted at a rate comparable to local subsidence. However, the observed high elevation levels could also reflect recent short-term sediment deposition rather than gradual accretion keeping pace with relative sea-level rise.

Moreover, since the measurements were conducted at the end of the wet season, it is possible that the sediment contributing to the higher profile may not be retained in the long term, as increased wave energy during the dry season could redistribute this material.

Although these uncertainties do not discredit the overall conclusions of the transect analysis, repeated measurements over time would offer better insight into temporal dynamics, and limit the chance of assessing misleading snapshots.

5.2.3. Uniform subsidence assumption

One of the key assumptions for this analysis is that subsidence rates have been, and continue to be equal for the fishponds and adjacent natural mangroves. However, this assumption oversimplifies reality as figure 2.5 shows that subsidence rates are spatially non-uniform and decrease in seaward direction. Moreover, the results from section 4.1 demonstrate that two transects, only $5km$ apart, have different subsidence rates. This variability suggests that the assumption of uniform subsidence may not hold, meaning that fishpond areas could have experienced higher subsidence rates compared to the natural mangroves.

This introduces uncertainty in the interpretation of the results in section 4.1. For example, if the fishponds of transect 23-45 have subsided faster than the natural mangroves, the observed elevation difference could primarily be the result of this difference rather than vertical accretion. This raises the question whether the observed elevation differences can reliably be attributed to gradual sedimentation. This, just like ignoring seasonal fluctuations, introduces uncertainty to the dynamics behind the observed elevation differences at transect 23-45. However, it does not influence the overall statement that transect 23-45 has experienced more subsidence than transect 23-66.

5.2.4. Interpretation and relevance

Although the identified limitations bring uncertainty to the results, section 4.1 demonstrates the potential of using RTK GNSS data to qualitatively assess the presence of subsidence and sediment deficits. The uncertainties and limitations described above do not strongly discredit the statement that the difference in fishpond elevations at transect 23-45 and transect 23-66 is likely due to a difference in subsidence. Additionally, the historic coastline evolution shows that both transects began eroding after 2004. These findings contradict the hypothesis of Marchesiello et al. (2019) [35] that subsidence is the main driver of coastal erosion in Bạc Liêu. Instead, it suggests that reduced SSC, subaqueous delta degradation and/or dike construction also play a notable role in the erosion after 2004, while the difference in subsidence rates likely explains the difference in observed accretion rates before 2004.

The limitations identified in the previous subsections highlight several opportunities for future research that could help validate this statement and strengthen the understanding of erosion processes along the Bạc Liêu coast

5.2.5. Future research directions

First and foremost, additional data should be collected. This includes complete cross-shore transects at multiple locations, covering areas with varying historic erosion and accretion patterns. This would allow for validation of the findings presented in section 4.1 and enable more general conclusions to be drawn about the influence of subsidence and sedimentation along the Bạc Liêu coast.

Additionally, measurements should be repeated at the same locations over consistent time intervals. This would allow for the analysis of temporal variability and help capture the influence of short-term factors such as storm events, seasonal sediment dynamics, and longer-term trends related to RSLR or sediment deficit.

Lastly, instead of qualitatively comparing elevation levels of the fishponds and natural mangroves, more exact measurements of subsidence and bed level change could be carried out. This could be done by deploying long-term water loggers in the natural mangrove forest or installing fixed sediment monitoring poles, similar to the approach applied by Van Bijsterveldt et al. (2023) [60] in a different study area.

5.3. Discussion of the numerical model

The results presented in section 4.2 provide useful insights in the behavior of the system in the presence or absence of different erosion drivers. However, the simplifications and assumptions made in the numerical model, introduce uncertainty to the interpretation of these results.

5.3.1. Validity of boundary conditions and tidal constituents

The most important boundary conditions governing the morphodynamic responses in the model are the wave characteristics and SSC. Used values are mostly based on data, but with their implementation in Mflat certain issues arise that influence the results.

For the waves, the boundary values were determined by running a larger model (Appendix B.2.1) and calculating the wave heights for the boundary of the smaller model. This wave transformation process was done at one fixed tidal level, while in the small model, the obtained values are imposed at the boundary for the whole simulation with fluctuating water levels. This results in unrealistically high waves at the boundary of the model during low tide. Consequently, waves tend to break almost immediately at the boundary during low tide, leading to an overestimation of wave-induced bed shear stresses and erosion rates.

Moreover, the simulations with historic wave heights were made with the current bathymetry, while the wave height values were obtained with wave transformation on an elevated foreshore without cliff. This inevitably alters the way the waves behave, and as a result, waves reaching the cliff in this scenario are not the same as they would have been on the actual historic bathymetry. Therefore, the wave heights near the cliff (and thus the horizontal erosion rates) should be interpreted with caution. They do not represent a true back-in-time simulation, because the nearshore bathymetry is mismatched with the imposed wave climate. Instead, the outcomes illustrate a relative comparison of the erosion rate with a less energetic wave forcing.

Another limitation of the wave height derivation is the simplification to seasonal average values. This neglects inter-seasonal variability and storm events, which influence the morphodynamic evolution. Even though this has been accounted for by calibrating the model to observed erosion rates, ignoring these effects makes the model biased towards the mean, and limits the insights it provides about all relevant erosion processes.

Just as the waves, the SSC is also imposed as a constant boundary condition, this is a simplification of reality as the SSC is seasonally governed by longshore currents (section 5.4). Moreover, the choice of SSC for the historic situation is based on an assumption rather than data. The results show that the SSC reduction from $0.7g/l$ to $0.5g/l$ due to ongoing sediment deficit has had large impacts on erosion rates and the stability of the foreshore. However, there is no evidence that this reduction is indeed

this large. If SSC was historically lower than the assumed $0.7g/l$, its effects would have been less pronounced and erosion rates would be higher. On the other hand, if the historic concentration was higher than $0.7g/l$, erosion rates would be even lower.

Lastly, the eight tidal constituents used as input in the model do not lead to an accurate representation of the observed water levels (Figure B.10). This is due to a discrepancy between how the amplitude and phase values are obtained and the way Mflat interprets these. Namely, the phases calculated by Phan et al. (2019) [47] and Hu et al. (2001) are local phases while Mflat uses standardized equilibrium phases. As discussed in appendix B.3, the main implication of the phase difference is the overestimation of sediment deposition in the mangrove area, due to high high water peaks. This is compensated in the calibration by introducing a correction factor A_0.

5.3.2. Calibration trade-offs and overfitting

Introducing A_0 reduces both the high and low water levels, thereby decreasing the frequency and depth of inundation across the entire profile. Figure B.10 shows that the imposed maximum water level peaks align with observed peaks, but the number of peaks exceeding $1m$ are less than reality. As a result, the mangrove forest is inundated less frequently than in reality. This reduction in inundation decreases the amount of sediment reaching the mangroves at high tide, limiting the model's ability to reproduce vertical accretion in scenarios with gradual subsidence, as expected based on the theory in subsection 2.2.3.

Therefore, the simulations with subsidence likely underestimate the bed level in the natural mangrove area, and consequently overestimate water flowing inside. Consequently wave action at the cliff is underestimated, resulting in an underestimate of the horizontal erosion rate at the cliff for simulations with subsidence.

Another notable artifact of the model is the low bed level of large parts of the foreshore. While foreshore erosion is expected, the modeled rates appear unrealistically high. Due to the lack of validation data, it cannot be ruled out that the low foreshore bed levels result from calibration trade-offs.

As explained in subsection 3.2.1, Mflat does not include wave reflection, limiting the model's capacity to simulate cliff toe erosion. However, as this was considered an important feature of the phenomenological calibration, erosion at the toe was forced by applying more erosive sediment settings across the entire profile, which also led to an exaggeration of foreshore erosion. Additionally, to reproduce cliff toe erosion and horizontal erosion rates close to observed values, wave friction parameter f_w was fixed to a low value to allow more wave energy to reach the cliff. This, however, also increased wave energy over the rest of the foreshore, further exaggerating foreshore erosion.

A final, more fundamental limitation of the calibration process is the risk of overfitting. The model was tuned to reproduce expected phenomena on a specific transect. The focus was laid on matching a horizontal erosion rate of approximately $16.67m/year$ while keeping the mangroves vertically stable and allowing for erosion at the toe of the cliff. Achieving this required iterative tuning of different parameters. While this produced plausible results, it may have done so for the wrong reasons.

As the model was calibrated to produce one single outcome, tuning the parameters likely compensated for general Mflat limitations, such as neglecting the momentum balance and simplifying sediment transport processes (subsection 3.2.1). This improves the results for this specific case, rather than actually fitting the parameters to realistically describe the underlying physical processes. Therefore, the current parameter configurations might not lead to realistic results in situations other than the reference case. This limits the general applicability of the model and introduces uncertainty to the scenario results presented in section 4.2.

5.3.3. No dike model

The results show an increase in the horizontal erosion rate when the fishpond dams are removed and the land is modeled as one large natural mangrove forest without dikes. According to the theory discussed in subsection 2.3.5, this outcome is unexpected, and can likely be attributed to a combination of calibration trade-offs, general Mflat limitations, and alternative physical interpretations.

First, because Mflat does not account for wave reflection at the fishpond dams, local erosive forces in

the scenarios with dikes are underestimated. As a result, removing the dike does not change anything in this regard. Furthermore, because of the introduction of A_0, tidal flow and consequent gross sediment fluxes are underestimated in the model, so removing the dike only marginally affects net sediment fluxes. This limits any beneficial effect that dike removal might otherwise have on erosion rates.

Additionally, due to the constant fall velocity of $0.1mm/s$, sediment settles rapidly in shallow mangrove waters, preventing sediment from reaching deep into the mangrove forest. However, in reality, smaller particles with even lower fall velocity will stay in suspension longer and travel deeper into the forest. The result is that the model underestimates how far the sediment is transported into the mangrove forest, therefore limiting the positive effect of dike removal. Moreover, the absence of consolidation in the model may also lead to an overestimation of erosion rates in the no-dike scenario. In reality, sediment behind the dike is likely to be more consolidated (increased τ_{cr}) and therefore more resistant to erosion when first re-exposed to tidal flow. By treating all sediment as equally erodible, the model neglects this resistance, potentially exaggerating the response to dike removal.

Apart from these model limitations, the resulting increased horizontal erosion rate in the no-dike scenario could also be explained with an alternative physical interpretation: removing the dike increases tidal flow and bed shear stresses across the entire profile, which consequently enhances sediment suspension and leads to net erosion of the profile. While this interpretation contrasts with the findings of Winterwerp et al. (2013) [67], similar effects have been observed along Chinese coastlines [68], suggesting that dike removal can, under certain conditions, increase erosive forces.

Therefore, given the model limitations, parameter assumptions, and differing theoretical interpretations, the effect of dike removal remains inconclusive.

5.3.4. Interpretation and relevance

The results from subsection 4.2.2 indicate that increased SSC and lower wave heights imposed at the boundary strongly decrease the horizontal erosion rates, especially when combined. Although the numerical values of these parameters are uncertain and might not perfectly reflect historic real-world conditions, the model does show the sensitivity of the system to these historic changes. This aligns with the results of the transect analysis, as it shows that changes in wave climate and SSC due to historic sediment deficit likely played a substantial role in the change from an accreting or stable system to an eroding system after 2004.

Furthermore, it is found that the role subsidence has on horizontal erosion rates is highly limited when SSC is increased and wave heights are reduced (Figure 4.11). This finding aligns with the work of Van Bijsterveld et al. (2023) [60]. Therefore, it is argued that the model is effective in qualitatively assessing the relative influence of three out of four drivers. However, due to the limitations and uncertainties, numerical outcomes should be used with caution.

5.3.5. Future research directions

Although the model provides insights into the effect the erosion drivers have on erosion rates at the Bạc Liêu coast, future research could enhance the model by addressing the limitations discussed in the previous subsections.

The most valuable improvement to the current model would be recalculating the tidal constituent phases as equilibrium phases instead of local phases. This would enhance the accuracy of water level representation and eliminate the use of A_0. Consequently, it is expected the effects of various erosion drivers would be represented more accurately, as the model would better capture the amount of water flowing into and out of the mangrove zone. In particular, subsidence effects and the impacts of removing dikes and fishpond dams would be better reflected, as these effects are more subtle and rely more strongly on inundation time than the increase of SSC.

Next, the model could be further improved by implementing dynamic boundary conditions. Doing so would enhance the model's capability to account for seasonal fluctuations of SSC, and storm events, providing greater insight into the effects of various erosion drivers on erosion patterns and sediment dynamics at shorter time scales. Additionally introducing a secondary sediment fraction with lower fall velocity and critical shear stress would better capture the horizontal spread of sediment into the mangrove forest and potentially yield more realistic outcomes for the scenarios with subsidence or

without dikes.

Finally, the current model could be improved by validating it against real-world data, such as flow velocity measurements, bathymetric surveys, and other cross-sections. This would increase the model's reliability, allowing for more predictive capabilities and quantitative analysis.

5.4. Longshore currents

A more fundamental limitation of this study is the exclusive focus on cross-shore sediment transport and erosion processes, with the influence of longshore currents largely neglected. This assumption is partly justified based on theoretical work from Phan et al. (2019) [47], who hypothesized that tidal currents are more perpendicular to the coast in Bạc Liêu compared to other provinces. Furthermore, Marchesiello et al. (2019) [35] suggested that erosion patterns in Bạc Liêu are likely driven by local man-induced erosion drivers, predominantly affecting cross-shore sediment transport.

This assumption allows for a more manageable analysis of different erosion drivers and model set-up. However, it must be noted that the Bạc Liêu coast is subject to a complex hydrodynamic regime, where cross- and longshore processes interact.

5.4.1. Implications on results

By neglecting longshore sediment transport, this study assumes that erosion and accretion patterns are governed by local cross-shore processes and that longshore processes only determine the boundary conditions. This introduces certain uncertainties to the interpretation of the results from chapter 4.

For example, the results from subsection 4.1.3 suggest that the differences in historic erosion and accretion rates between transect 23-45 and 23-66 are likely due to differences in subsidence rates. However, this could also be (partly) explained by longshore sediment transport gradients, which are not captured in this analysis.

Additionally, the suspended sediment concentration is modeled as a constant boundary condition, whereas in reality, sediment availability naturally varies both spatially and temporally as a result of longshore transport dynamics. Therefore, by neglecting longshore contributions, the model does not capture potential sediment influxes or deficits from adjacent coastal sections, potentially resulting in an oversimplified sediment budget and underestimating variability in erosion and accretion rates over time.

5.4.2. Future research directions

To address the limitations presented in the previous subsections, future research should include longshore currents into both the field analysis and numerical modeling.

Although the hypothesis that radial tidal currents causing perpendicular flows towards the Bạc Liêu coast [47] is strongly motivated, flow velocity measurements should be made to validate whether the flow velocities are indeed more perpendicular near the coast of Bạc Liêu compared to other provinces.

Additionally, future research could focus on developing a more advanced 2- or 3D model, capturing all hydrodynamic processes governing the erosion in Bạc Liêu.

6

Conclusion

This chapter synthesizes the key insights and outcomes of this research. It revisits the main research question and summarizes the findings for each sub-question. Additionally, recommendations for the Mangrove Living Lab project are presented.

6.1. Main findings

The main goal of this research was to assess how different erosion drivers influence cross-shore sediment transport processes and erosion rates along the coast of Bạc Liêu. To address this goal, four sub-questions were defined.

The first sub-question explored how historic shifts in land use and foreshore morphology have influenced key erosion drivers. A literature analysis revealed that after 1990 agriculture intensified or transitioned to aquaculture. This has led to more groundwater extraction and consequent subsidence. Additionally, field observations showed that the construction of a sea dike and fishpond dams within the mangroves has disconnected a large part of the mangrove forest from the tidal system. This reduced the tidal prism and hindered landward mangrove migration, resulting in mangrove squeeze. Finally, based on a historic map and literature it was found that long-term river sediment supply deficits have deepened the subaqueous delta, allowing larger waves to reach the shore and reducing sediment availability for redistribution.

The second sub-question focused on the individual effects of subsidence, sediment deficits, and sea dike construction on horizontal erosion rates. Using a numerical model, each driver was individually simulated and compared with a reference simulation that represented the current and expected state of the coast. The simulations showed that introducing the assumed historic values for the wave heights and SSC reduced the horizontal erosion rate the most, thereby implying that historic and ongoing sediment deficits accelerate erosion at the coast of Bạc Liêu. Furthermore, the introduction of subsidence caused the coast to erode faster, indicating that subsidence also contributes to erosion in some parts of the Bạc Liêu coast. A scenario without dikes was also modeled but resulted in inconclusive results.

The third sub-question investigated the possible combinations of different drivers. The numerical model showed that a combination of reduced wave heights and increased SSC almost completely stops the horizontal erosion and overshadowed the impact of subsidence. Additionally, an analysis on elevation levels inside the mangroves indicated that some parts of the coast experience more subsidence than others, while the observed erosion rates are similar. This further suggests that a combination of higher waves and reduced sediment availability caused by fluvial sediment deficits is the main driver of erosion in Bạc Liêu.

The final sub-question assessed the spatial variations in erosion along the coast of Bạc Liêu. From the elevation analysis, two locations were considered: one location with a narrow strip of natural mangroves experiencing large subsidence rates (23-45) and one with a wide strip without subsidence (23-66). Historic satellite images showed that the coastline at location 23-45 remained at a stable position between

1986 and 2004, while the coastline at location 23-66 migrated over 600 meters in seaward direction during the same period. After 2004, both locations started to erode. Therefore, this historic difference in accretion, likely driven by spatially varying subsidence, explains the large variations in coastline positions along the Bạc Liêu coast, rather than present-day erosion alone.

Overall, this study demonstrates that coastal erosion in Bạc Liêu is driven by a complex, spatially varying interplay between different drivers. In particular, historic and ongoing fluvial sediment supply deficits have caused large-scale degradation of the delta, increasing wave energy at the shoreline and reducing sediment availability along the entire coast. Additionally, spatially varying subsidence associated with groundwater extraction can locally amplify erosion and has limited coastal accretion in the past, resulting in pronounced differences in current coastline positions. Finally, although the construction of sea dikes and fishpond dams in the intertidal zone appears to further contribute to erosion, the extent of this impact could not be conclusively determined due to the numerical model's limitations and differing theoretical interpretations.

6.2. Recommendations for the Mangrove Living Lab

This study has improved the understanding of how subsidence and the effects of fluvial sediment deficit interact to drive erosion along the Bạc Liêu coast, yet it also highlights certain limitations. To address these gaps and help validate current findings, future Mangrove Living Lab field campaigns could focus on expanding spatial and temporal coverage of complete elevation transects, implementing more robust subsidence monitoring methods, and conducting flow velocity measurements. Additionally, improving the current numerical model or developing more advanced models will help gain better insight and knowledge of coastal erosion processes in Bạc Liêu. Finally, the role of dike construction needs to be further examined in order to get a complete picture of all governing processes.

6.3. Final remarks

This study represents a first attempt to systematically assess how multiple drivers collectively shape coastal erosion in Bạc Liêu. While further research is needed to validate outcomes and refine the quantitative understanding of each driver's contribution, it provides new insights into the relative influence of drivers and spatial variations. By building on these findings, future research can deepen the knowledge of local erosion dynamics and support the development of integrated solutions that protect both the communities and ecosystems of Bạc Liêu.

References

[1] *[Singapore, Malaysia, Cambodia, Vietnam] China Sea - Southern Portion - Western Sheet. Compiled from the latest Surveys, 1881. with corrections to 1953.* URL: https://www.raremaps.com/gallery/detail/42027/singapore-malaysia-cambodia-vietnam-china-sea-southe-british-admiralty.

[2] Daniel M. Alongi. "The Impact of Climate Change on Mangrove Forests". In: *Current Climate Change Reports* 1.1 (Jan. 2015), pp. 30–39. DOI: 10.1007/s40641-015-0002-x. URL: https://doi.org/10.1007/s40641-015-0002-x.

[3] Edward J. Anthony et al. "Linking rapid erosion of the Mekong River delta to human activities". In: *Scientific Reports* 5.1 (Oct. 2015). DOI: 10.1038/srep14745. URL: https://doi.org/10.1038/srep14745.

[4] Manon Besset et al. "Mangroves and shoreline erosion in the Mekong River delta, Viet Nam". In: *Estuarine Coastal and Shelf Science* 226 (Oct. 2019), p. 106263. DOI: 10.1016/j.ecss.2019.106263. URL: https://doi.org/10.1016/j.ecss.2019.106263.

[5] David Biggs. "Canals in the Mekong Delta: A Historical Overview from 200 C.E. to the Present". In: Apr. 2005. ISBN: 9780471478447. DOI: 10.1002/047147844X.wh18.

[6] NRRC Booij, Roeland C Ris, and Leo H Holthuijsen. "A third-generation wave model for coastal regions: 1. Model description and validation". In: *Journal of geophysical research: Oceans* 104.C4 (1999), pp. 7649–7666.

[7] Judith Bosboom. *Coastal dynamics*. TU Delft, Jan. 2021.

[8] Jean-Paul Bravard, Marc Goichot, and Stéphane Gaillot. "Geography of Sand and Gravel Mining in the Lower Mekong River". In: *EchoGéo* 26 (Dec. 2013). DOI: 10.4000/echogeo.13659. URL: https://doi.org/10.4000/echogeo.13659.

[9] Linh Hong Nhat Bui and Long Ta Bui. "Modelling bank erosion dependence on natural and anthropogenic factors — case study of Ganh Hao estuary, Bac Lieu - Ca Mau, Vietnam". In: *Environmental Technology and Innovation* 19 (June 2020), p. 100975. DOI: 10.1016/j.eti.2020.100975. URL: https://doi.org/10.1016/j.eti.2020.100975.

[10] Ian C Campbell. "Biodiversity of the Mekong delta". In: *The Mekong Delta System: Interdisciplinary Analyses of a River Delta*. Springer, 2012, pp. 293–313.

[11] Yining Chen et al. "Differential sediment trapping abilities of mangrove and saltmarsh vegetation in a subtropical estuary". In: *Geomorphology* 318 (June 2018), pp. 270–282. DOI: 10.1016/j.geomorph.2018.06.018. URL: https://doi.org/10.1016/j.geomorph.2018.06.018.

[12] Stephen E. Darby et al. "Fluvial sediment supply to a mega-delta reduced by shifting tropical-cyclone activity". In: *Nature* 539.7628 (Oct. 2016), pp. 276–279. DOI: 10.1038/nature19809. URL: https://doi.org/10.1038/nature19809.

[13] Richard A. Davis and Miles O. Hayes. "What is a wave-dominated coast?" In: *Marine Geology* 60.1-4 (Aug. 1984), pp. 313–329. DOI: 10.1016/0025-3227(84)90155-5. URL: https://doi.org/10.1016/0025-3227(84)90155-5.

[14] ECMWF. *ERA5 monthly averaged data on single levels from 1940 to present*. URL: https://cds.climate.copernicus.eu/cdsapp#!/dataset/reanalysis-era5-single-levels-monthly-means?tab=overview.

[15] Laura E Erban, Steven M Gorelick, and Howard A Zebker. "Groundwater extraction, land subsidence, and sea-level rise in the Mekong Delta, Vietnam". In: *Environmental Research Letters* 9.8 (Aug. 2014), p. 084010. DOI: 10.1088/1748-9326/9/8/084010. URL: https://doi.org/10.1088/1748-9326/9/8/084010.

[16] pla Erftemeijer et al. *Increasing coastal resilience through mangrove affoIncreasing coastal resilience through mangrove afforestation in the Mekong Delta: International Examples and Lessons LearntRestation in the Mekong Delta: International Examples and Lessons Learnt*. Tech. rep. Dec. 2021.

[17] Jason P. Ericson et al. "Effective sea-level rise and deltas: Causes of change and human dimension implications". In: *Global and Planetary Change* 50.1-2 (Jan. 2006), pp. 63–82. DOI: 10.1016/j.gloplacha.2005.07.004. URL: https://doi.org/10.1016/j.gloplacha.2005.07.004.

[18] Carl Friedrichs. "Tidal flat morphodynamics: A synthesis". In: *ResearchGate* (Jan. 2011). URL: https://www.researchgate.net/publication/285298496_Tidal_flat_morphodynamics_A_synthesis.

[19] Eric Gilman, Joanna Ellison, and Richard Coleman. "Assessment of Mangrove Response to Projected Relative Sea-Level Rise And Recent Historical Reconstruction of Shoreline Position". In: *Environmental Monitoring and Assessment* 124.1-3 (Dec. 2006), pp. 105–130. DOI: 10.1007/s10661-006-9212-y. URL: https://doi.org/10.1007/s10661-006-9212-y.

[20] Leo H. Holthuijsen. *Waves in Oceanic and Coastal Waters*. Technische Universiteit Delft, Jan. 2007. DOI: 10.1017/cbo9780511618536. URL: https://doi.org/10.1017/cbo9780511618536.

[21] Erik Martijn Horstman et al. "Deposition gradients across mangrove fringes". In: *Coastal dynamics* (2017), pp. 911–922. URL: https://ris.utwente.nl/ws/files/29526104/Horstman_et_al_2017_CD.pdf.

[22] Chuanjiang Huang and Fangli Qiao. "Sea level rise projection in the South China Sea from CMIP5 models". In: *Acta Oceanologica Sinica* 34 (2015), pp. 31–41.

[23] *Hydropower*. 2019. URL: https://www.mrcmekong.org/hydropower/.

[24] Hu Jian-Yu et al. "Tidal features in the China Seas and their adjacent sea areas as derived from TOPEX/POSEIDON altimeter data". In: *Chinese Journal of Oceanology and Limnology* 19.4 (Dec. 2001), pp. 293–305. DOI: 10.1007/bf02850732. URL: https://doi.org/10.1007/bf02850732.

[25] Olivier M. Joffre et al. "What drives the adoption of integrated shrimp mangrove aquaculture in Vietnam?" In: *Ocean & Coastal Management* 114 (2015), pp. 53–63. ISSN: 0964-5691. DOI: https://doi.org/10.1016/j.ocecoaman.2015.06.015. URL: https://www.sciencedirect.com/science/article/pii/S0964569115001684.

[26] Ernie Amira Kamil, Husna Takaijudin, and Ahmad Mustafa Hashim. "Mangroves as coastal bioshield: a review of mangroves performance in wave attenuation". In: *Civil Engineering Journal* 7.11 (2021), pp. 1964–1981.

[27] Claudia Kuenzer et al. "Flood mapping and flood dynamics of the Mekong Delta: ENVISAT-ASAR-WSM based time series analyses". In: *Remote Sensing* 5.2 (2013), pp. 687–715.

[28] Say-Chong Lee and Ashish J. Mehta. "Problems in Characterizing Dynamics of Mud Shore Profiles". In: *Journal of Hydraulic Engineering* 123.4 (Apr. 1997), pp. 351–361. DOI: 10.1061/(asce)0733-9429(1997)123:4(351. URL: https://doi.org/10.1061/(asce)0733-9429(1997)123:4(351).

[29] R. Li et al. "Regional trends in early-monsoon rainfall over Vietnam and CCSM4 attribution". In: *Climate Dynamics* 52.1-2 (Apr. 2019), pp. 363–372. DOI: 10.1007/s00382-018-4198-z. URL: https://doi.org/10.1007/s00382-018-4198-z.

[30] J. Paul Liu et al. "A seismic study of the Mekong subaqueous delta: Proximal versus distal sediment accumulation". In: *Continental Shelf Research* 147 (July 2017), pp. 197–212. DOI: 10.1016/j.csr.2017.07.009. URL: https://doi.org/10.1016/j.csr.2017.07.009.

[31] J.P. Liu et al. "Fate of sediments delivered to the sea by Asian large rivers: Long-distance transport and formation of remote alongshore clinothems". In: *The Sedimentary Record* 7.4 (Dec. 2009), pp. 4–9. DOI: 10.2110/sedred.2009.4.4. URL: https://doi.org/10.2110/sedred.2009.4.4.

[32] Arjen Luijendijk et al. "The State of the World's Beaches". In: *Scientific Reports* 8.1 (Apr. 2018). DOI: 10.1038/s41598-018-24630-6. URL: https://doi.org/10.1038/s41598-018-24630-6.

[33] Phuoc Vo-Luong and Stanislaw Massel. "Energy dissipation in non-uniform mangrove forests of arbitrary depth". In: *Journal of Marine Systems* 74.1-2 (2008), pp. 603–622.

[34] *Mangrove Living Lab*. URL: https://www.tudelft.nl/global/research/education-entrepreneurship/navigating-the-future-building-resilient-deltas-in-vietnam/mangrove-living-lab.

[35] Patrick Marchesiello et al. “Erosion of the coastal Mekong delta: Assessing natural against man induced processes”. In: *Continental Shelf Research* 181 (May 2019), pp. 72–89. DOI: 10.1016/j.csr.2019.05.004. URL: https://doi.org/10.1016/j.csr.2019.05.004.

[36] Yoshihiro Mazda and Eric Wolanski. “Hydrodynamics and modeling of water flow in mangrove areas”. In: *Coastal wetlands: An integrated ecosystem approach* 8 (2009), pp. 231–262.

[37] AL McIvor et al. “Mangroves as a sustainable coastal defence”. In: *7th International Conference on Asian and Pacific Coasts (APAC). The Nature Conservancy, University of Cambridge, and Wetlands International, Bali, Indonesia, September*. 2013, pp. 24–26.

[38] Fernando J Mendez and Inigo J Losada. “An empirical model to estimate the propagation of random breaking and nonbreaking waves over vegetation fields”. In: *Coastal Engineering* 51.2 (2004), pp. 103–118.

[39] P S J Minderhoud et al. “Impacts of 25 years of groundwater extraction on subsidence in the Mekong delta, Vietnam”. In: *Environmental Research Letters* 12.6 (June 2017), p. 064006. DOI: 10.1088/1748-9326/aa7146. URL: https://dx.doi.org/10.1088/1748-9326/aa7146.

[40] P.S.J. Minderhoud et al. “The relation between land use and subsidence in the Vietnamese Mekong delta”. In: *Science of The Total Environment* 634 (2018), pp. 715–726. ISSN: 0048-9697. DOI: https://doi.org/10.1016/j.scitotenv.2018.03.372. URL: https://www.sciencedirect.com/science/article/pii/S004896971831132X.

[41] PSJ Minderhoud et al. “Mekong delta much lower than previously assumed in sea-level rise impact assessments”. In: *Nature communications* 10.1 (2019), p. 3847.

[42] Van Lap Nguyen, Thi Kim Oanh Ta, and Masaaki Tateishi. “Late Holocene depositional environments and coastal evolution of the Mekong River Delta, Southern Vietnam”. In: *Journal of Asian Earth Sciences* 18.4 (Aug. 2000), pp. 427–439. DOI: 10.1016/s1367-9120(99)00076-0. URL: https://doi.org/10.1016/s1367-9120(99)00076-0.

[43] General Statistics Office. *Statistical Yearbook of 2022*. 2022. URL: https://www.gso.gov.vn/en/data-and-statistics/2023/06/statistical-yearbook-of-2022/.

[44] Hanh T.H. Pham and Long Ta Bui. “Mechanism of erosion zone formation based on hydrodynamic factor analysis in the Mekong Delta coast, Vietnam”. In: *Environmental Technology and Innovation* 30 (Mar. 2023), p. 103094. DOI: 10.1016/j.eti.2023.103094. URL: https://doi.org/10.1016/j.eti.2023.103094.

[45] t v Pham et al. “Agro-ecological dynamics in the coastal areas of the Vietnamese Mekong Delta in the context of climate change (A case study in Bac Lieu Province)”. In: *Can Tho University Journal of Science* 1 (Nov. 2015), pp. 81–88. DOI: 10.22144/ctu.jen.2015.027.

[46] H M Phan. *Coastal and seasonal hydrodynamics and morphodynamics of the Mekong Delta*. 2020. DOI: 10.4233/uuid:2bcb33bf-5b73-4873-9168-08b1e7a2836f.

[47] Hung Manh Phan et al. “Tidal wave propagation along The Mekong deltaic coast”. In: *Estuarine Coastal and Shelf Science* 220 (Feb. 2019), pp. 73–98. DOI: 10.1016/j.ecss.2019.01.026. URL: https://www.sciencedirect.com/science/article/pii/S0272771418303512.

[48] Linh K. Phan, Jaap S.M. Van Thiel De Vries, and Marcel J.F. Stive. “Coastal Mangrove Squeeze in the Mekong Delta”. In: *Journal of Coastal Research* 300 (Oct. 2014), pp. 233–243. DOI: 10.2112/jcoastres-d-14-00049.1. URL: https://doi.org/10.2112/jcoastres-d-14-00049.1.

[49] M H Phan and M J F Stive. “Managing mangroves and coastal land cover in the Mekong Delta”. In: *Ocean & Coastal Management* 219 (Mar. 2022). URL: https://doi.org/10.1016/j.ocecoaman.2021.106013.

[50] Bac Lieu Portal. *Statistical Year Book*. 2016. URL: https://baclieu.gov.vn/web/portalenglish/-/social-and-economic-conditio-1.

[51] H. Postma. “Transport and accumulation of suspended matter in the Dutch Wadden Sea”. In: *Netherlands Journal of Sea Research* 1.1-2 (Apr. 1961), pp. 148–190. DOI: 10.1016/0077-7579(61)90004-7. URL: https://doi.org/10.1016/0077-7579(61)90004-7.

[52] N. Saintilan et al. “Thresholds of mangrove survival under rapid sea level rise”. In: *Science* 368.6495 (June 2020), pp. 1118–1121. DOI: 10.1126/science.aba2656. URL: https://doi.org/10.1126/science.aba2656.

[53] Thomas Stocker. *Climate change 2013 : the physical science basis : Working Group I contribution to the Fifth Assessment Report of the Intergovernmental Panel on Climate Change*. Jan. 2013. URL: http://ci.nii.ac.jp/ncid/BB15229414.

[54] Thi Kim Oanh Ta et al. *Holocene Delta Evolution and Depositional Models of the Mekong River Delta, Southern Vietnam*. River Deltas-Concepts, Models, and Examples, Jan. 2005, pp. 453–466. DOI: 10.2110/pec.05.83.0453. URL: https://doi.org/10.2110/pec.05.83.0453.

[55] Thi Kim Oanh Ta et al. “Sediment facies and Late Holocene progradation of the Mekong River Delta in Bentre Province, southern Vietnam: an example of evolution from a tide-dominated to a tide- and wave-dominated delta”. In: *Sedimentary Geology* 152.3-4 (Oct. 2002), pp. 313–325. DOI: 10.1016/s0037-0738(02)00098-2. URL: https://doi.org/10.1016/s0037-0738(02)00098-2.

[56] Toru Tamura et al. “Long-term sediment decline causes ongoing shrinkage of the Mekong megadelta, Vietnam”. In: *Scientific Reports* 10.1 (May 2020). DOI: 10.1038/s41598-020-64630-z. URL: https://doi.org/10.1038/s41598-020-64630-z.

[57] Vo Quoc Thanh et al. “A numerical investigation on the suspended sediment dynamics and sediment budget in the Mekong Delta”. In: *Continental Shelf Research* (Jan. 2025), p. 105427. DOI: 10.1016/j.csr.2025.105427. URL: https://doi.org/10.1016/j.csr.2025.105427.

[58] Vo Khac Tri. “Hydrology and Hydraulic Infrastructure Systems in the Mekong Delta, Vietnam”. In: *The Mekong Delta System: Interdisciplinary Analyses of a River Delta*. Ed. by Fabrice G. Renaud and Claudia Kuenzer. Dordrecht: Springer Netherlands, 2012, pp. 49–81. ISBN: 978-94-007-3962-8. DOI: 10.1007/978-94-007-3962-8_3. URL: https://doi.org/10.1007/978-94-007-3962-8_3.

[59] Daniel Unverricht et al. “Modern sedimentation and morphology of the subaqueous Mekong Delta, Southern Vietnam”. In: *Global and Planetary Change* 110 (Jan. 2013), pp. 223–235. DOI: 10.1016/j.gloplacha.2012.12.009. URL: https://doi.org/10.1016/j.gloplacha.2012.12.009.

[60] Celine E. J. Van Bijsterveldt et al. “Subsidence reveals potential impacts of future sea level rise on inhabited mangrove coasts”. In: *Nature Sustainability* 6.12 (Oct. 2023), pp. 1565–1577. DOI: 10.1038/s41893-023-01226-1. URL: https://doi.org/10.1038/s41893-023-01226-1.

[61] M. Van Der Wegen, J. A. Roelvink, and B. E. Jaffe. “Morphodynamic Resilience of Intertidal Mudflats on a Seasonal Time Scale”. In: *Journal of Geophysical Research Oceans* 124.11 (Nov. 2019), pp. 8290–8308. DOI: 10.1029/2019jc015492. URL: https://doi.org/10.1029/2019jc015492.

[62] Nguyen Van Manh et al. “Future sediment dynamics in the Mekong Delta floodplains: Impacts of hydropower development, climate change and sea level rise”. In: *Global and Planetary Change* 127 (Jan. 2015), pp. 22–33. DOI: 10.1016/j.gloplacha.2015.01.001. URL: https://www.sciencedirect.com/science/article/pii/S0921818115000168?casa_token=iBpuQGymu8MAAAAA:L_jE1aMHnqt_risK4w2EHzfVr8EoeToZjVU3dZilt9OSr83qvxyhDXSAOBbfZy0C1XHvdm3UPCo.

[63] Frank Wagner, Vuong Bui Tran, and Fabrice G. Renaud. *Groundwater Resources in the Mekong Delta: Availability, Utilization and Risks*. Jan. 2012, pp. 201–220. DOI: 10.1007/978-94-007-3962-8\{_}7. URL: https://doi.org/10.1007/978-94-007-3962-8_7.

[64] J.P. Walsh et al. “Clinoform mechanics in the Gulf of Papua, New Guinea”. In: *Continental Shelf Research* 24.19 (Oct. 2004), pp. 2487–2510. DOI: 10.1016/j.csr.2004.07.019. URL: https://doi.org/10.1016/j.csr.2004.07.019.

[65] J C Winterwerp et al. *A sustainable solution for massive coastal erosion in Central Java*. Tech. rep. Feb. 2014. URL: https://cms.deltares.nl/assets/common/downloads/Deltares-WI-2014-Sustainable-solution-massive-erosion-Central-Java.pdf.

[66] J. C. Winterwerp et al. “Defining Eco-Morphodynamic Requirements for Rehabilitating Eroding Mangrove-Mud Coasts”. In: *Wetlands* 33.3 (Mar. 2013), pp. 515–526. DOI: 10.1007/s13157-013-0409-x. URL: https://doi.org/10.1007/s13157-013-0409-x.

[67] Johan C. Winterwerp, William G. Borst, and Mindert B. De Vries. “Pilot Study on the Erosion and Rehabilitation of a Mangrove Mud Coast”. In: *Journal of Coastal Research* 212 (Mar. 2005), pp. 223–230. DOI: 10.2112/03-832a.1. URL: https://doi.org/10.2112/03-832a.1.

[68] Zehua Zhong and Zhan Hu. “The Impact of Reclamation on Tidal Flat Morphological Equilibrium”. In: *Frontiers in Marine Science* 8 (Nov. 2021). DOI: 10.3389/fmars.2021.769077. URL: https://doi.org/10.3389/fmars.2021.769077.

A

Recent vs historic bathymetry

This chapter presents a recent and historic bathymetry map

A.1. Recent bathymetry

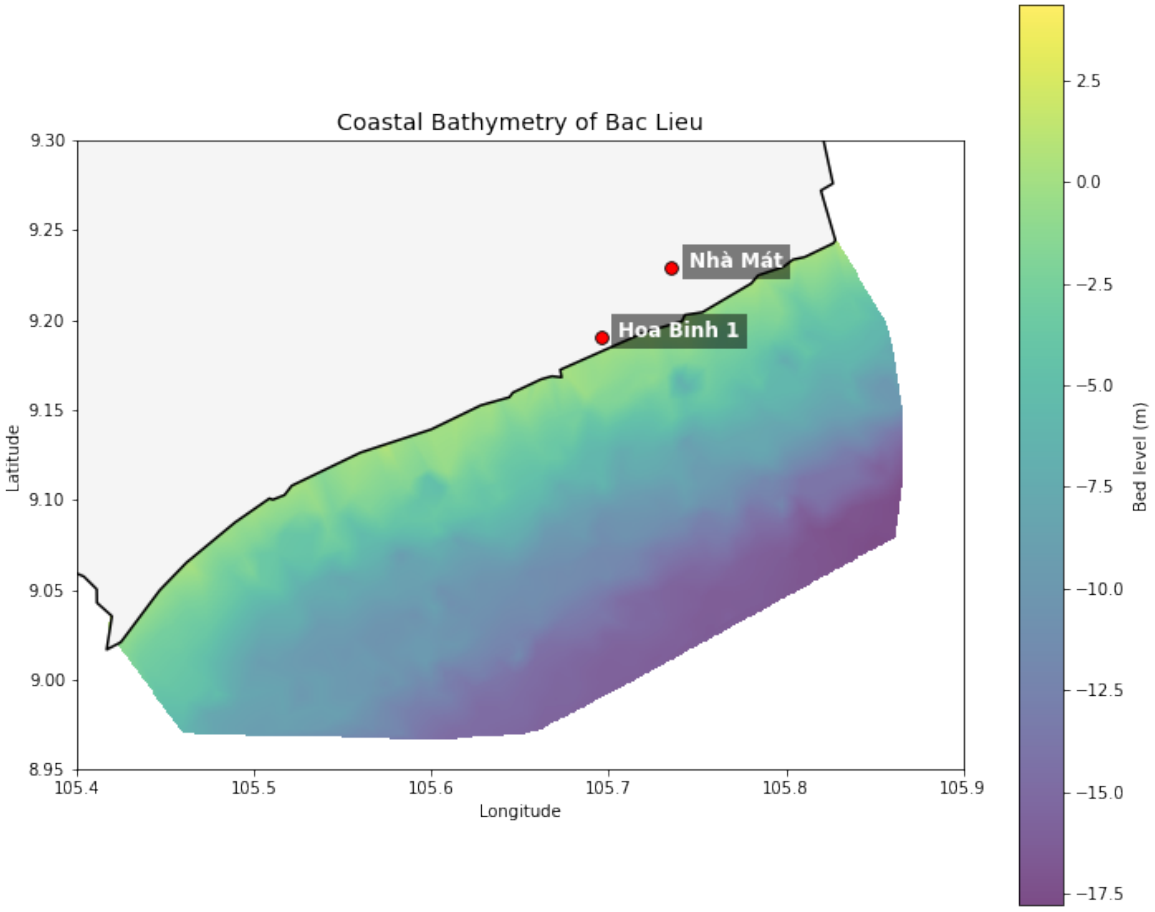

Figure A.1: Coastal bathymetry of Bạc Liêu relative to MSL. The data was provided by SIWRP in 2023 and is linearly interpolated between data points.

A.2. Historic bathymetry

Figure A.2 shows a section of a admiralty map from 1881. The map shows a water depth of $3fathom$ relative to low water at a location $20km$ from the present day coast.

$3ftm = 5.5m$
$MLW - 5.5m = MSL - 6.5m$

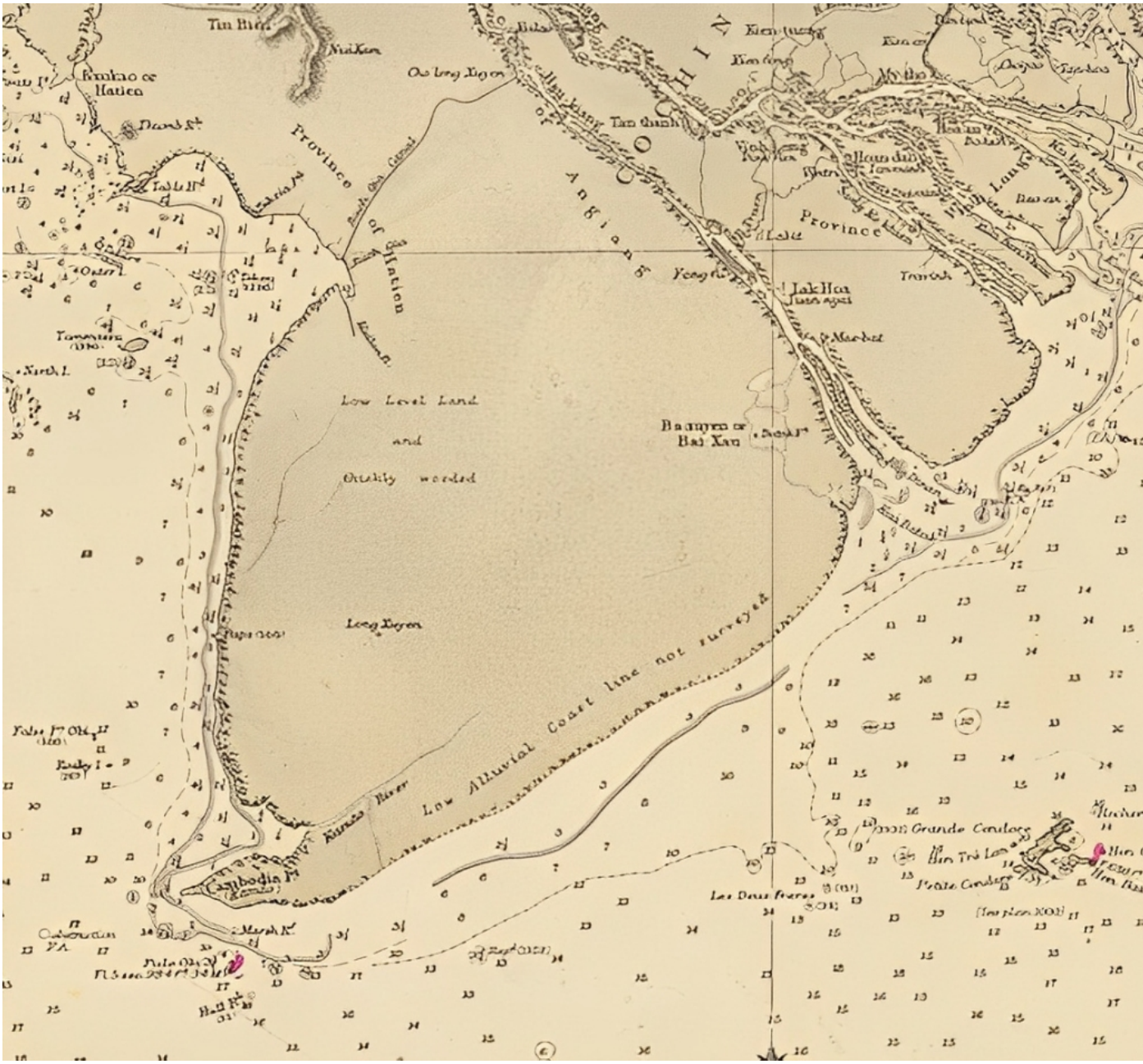

Figure A.2: Coastal bathymetry of Bạc Liêu in 1881 in fathoms relative to low water [1]

B

Model set up

This chapter discusses the model set up and used parameters.

B.1. Initial bed profile

The initial bed profile consists of a combination of two measurements. A cross-shore bathymetry measurement inside the fishponds and natural mangrove area (transect 23-66, Living Lab 2023) and a cross-section from a bathymetry map of the Bạc Liêu coast (SIWRP, n.d.). The locations are given in Figure B.1. Figure B.2 shows the resulting cross-section, which is artificially extended at the seaward side with a slope of approximately 0.0001

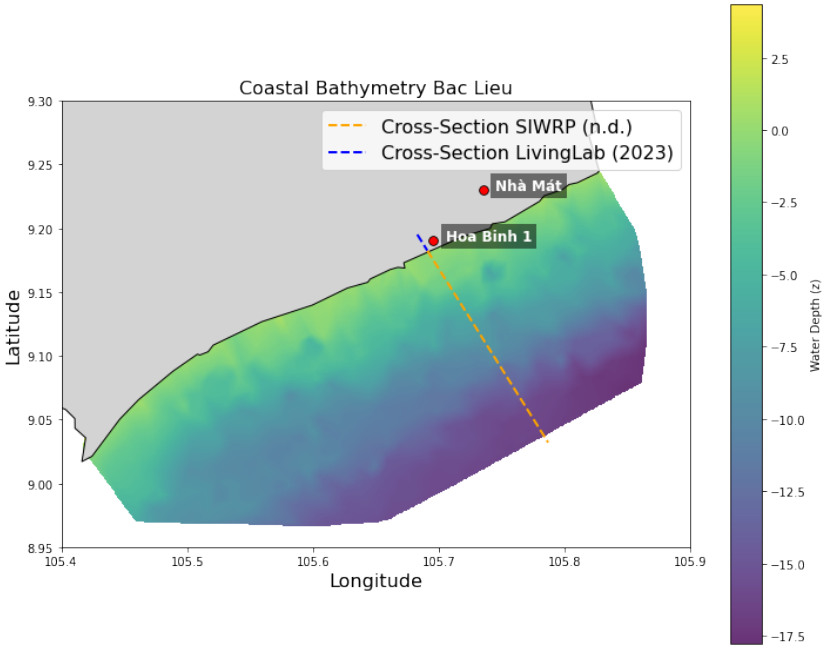

Figure B.1: Location of the cross-sections taken for the initial bed profile

As this report focuses on the erosion of the coastline and mangroves, a zoomed in version of the cross-section profile will be used for sediment transport simulations. This zoomed in profile consists of elevation levels of the concrete dike at the land side, the fishponds, the earthen dike, a channel, the natural mangrove forest, a cliff and the bathymetry of up to $2.4km$ off shore (Figure B.3).

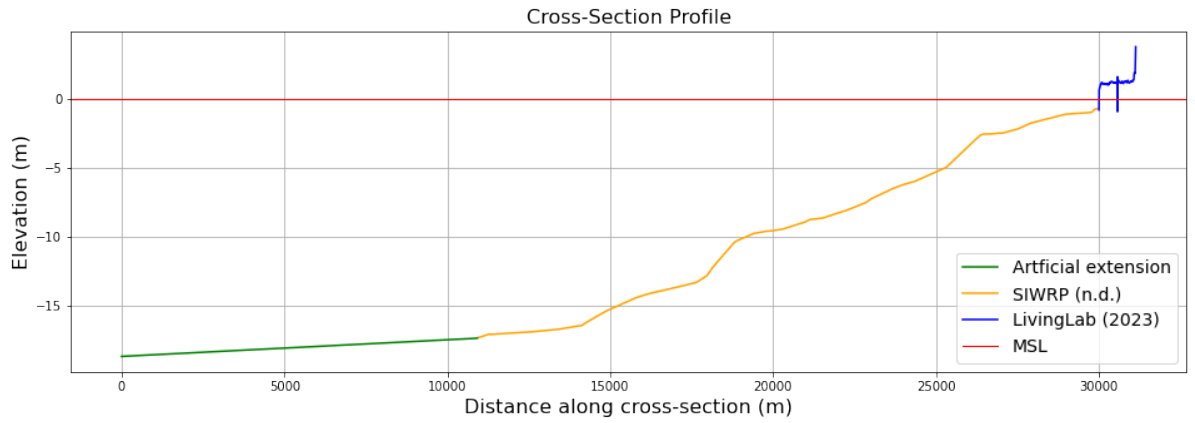

Figure B.2: Resulting large scale cross-section of the Bạc Liêu coast.

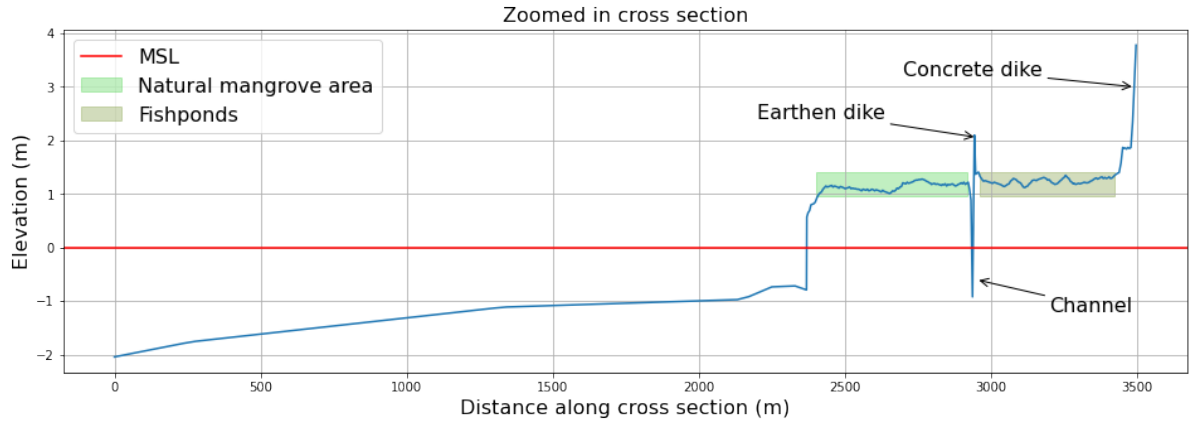

Figure B.3: Zoomed in cross-section of the Bạc Liêu coast, indicating different zones of the profile.

B.2. Hydrodynamics

B.2.1. Wave transformation

The waves in the model are represented by two parameters: The root mean squared wave height (H_{rms}) and the peak period (T_p). Using a 20 year time series from the Copernicus satellite program [14] average values for H_{rms} and T_p are obtained for both the dry season (November till April) and wet season (May till October) at a location $31km$ offshore. As the domain of the model is only $3.5km$, the transformation of the waves first needs to be calculated over a larger domain (Figure B.2). For this, a simplified Mflat model is used.

First, the average significant wave height H_s and peak period are obtained by analyzing the Copernicus dataset. As Mflat takes H_{rms} as input, H_s needs to be converted by:

$$H_{rms} = \frac{H_s}{\sqrt{2}} \tag{B.1}$$

[20]

The results are shown in Figure B.4 and in Table B.1.

	$T_p(s)$	$H_s(m)$	$H_{rms}(m)$
Dry season	4.35	0.8	0.57
Wet season	3.83	0.56	0.40

Table B.1: Input values for large wave transformation model

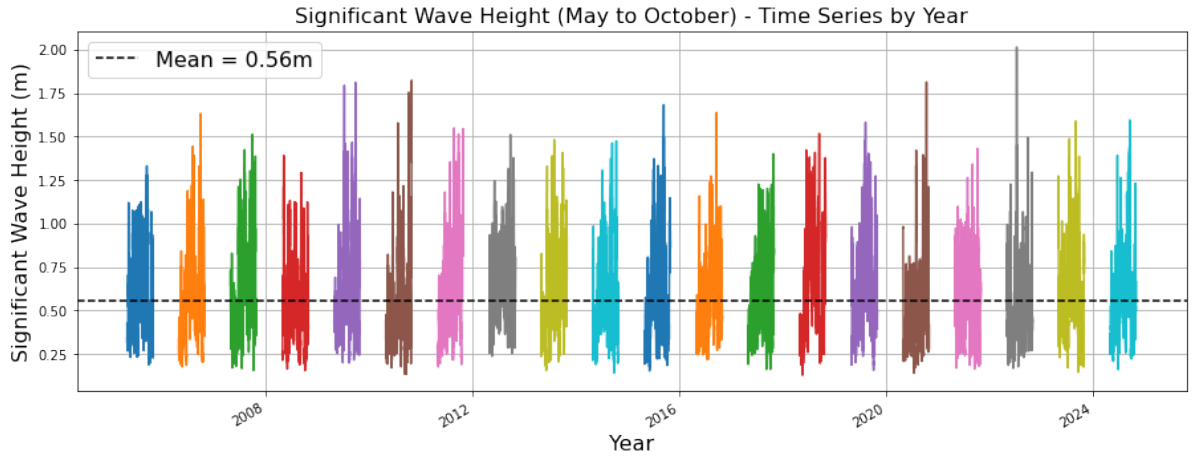

(a)

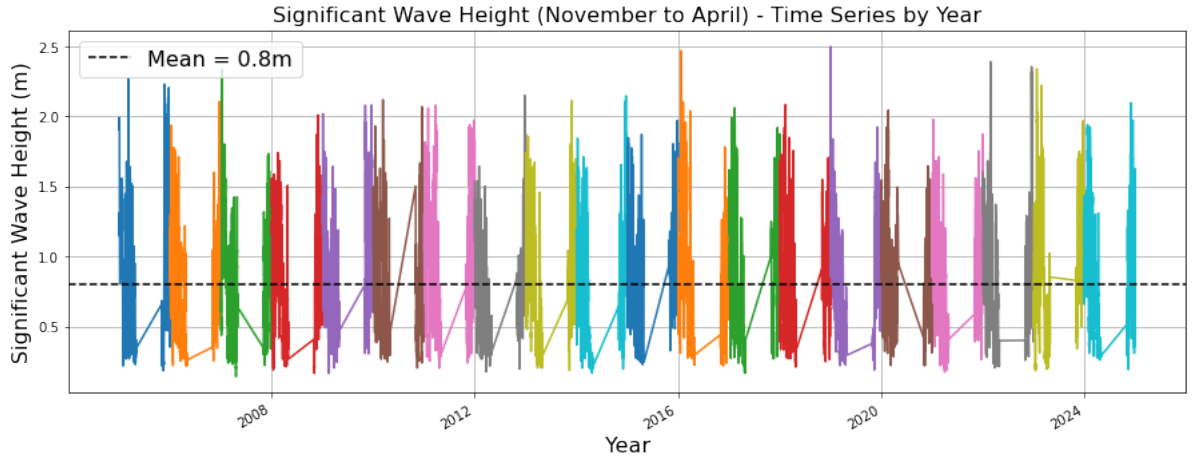

(b)

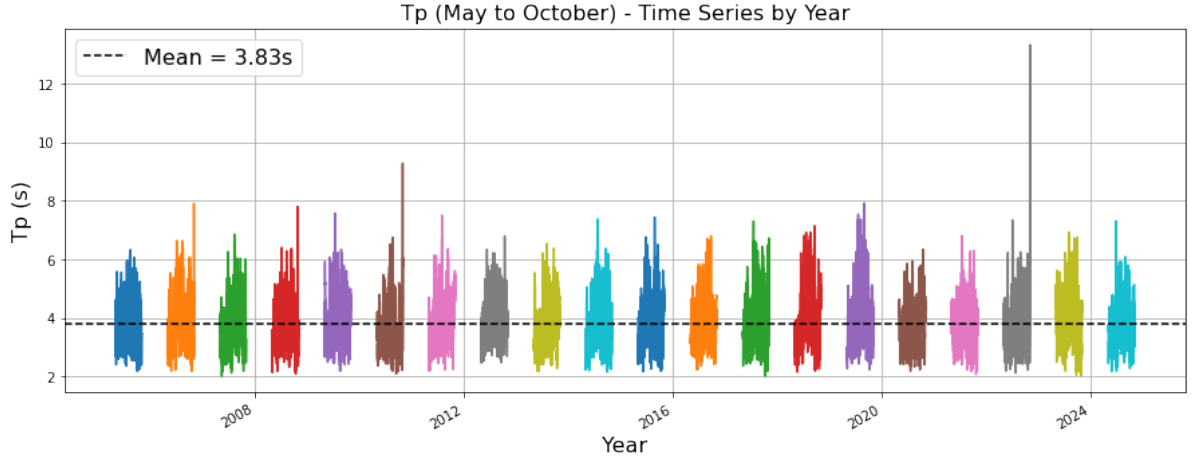

(c)

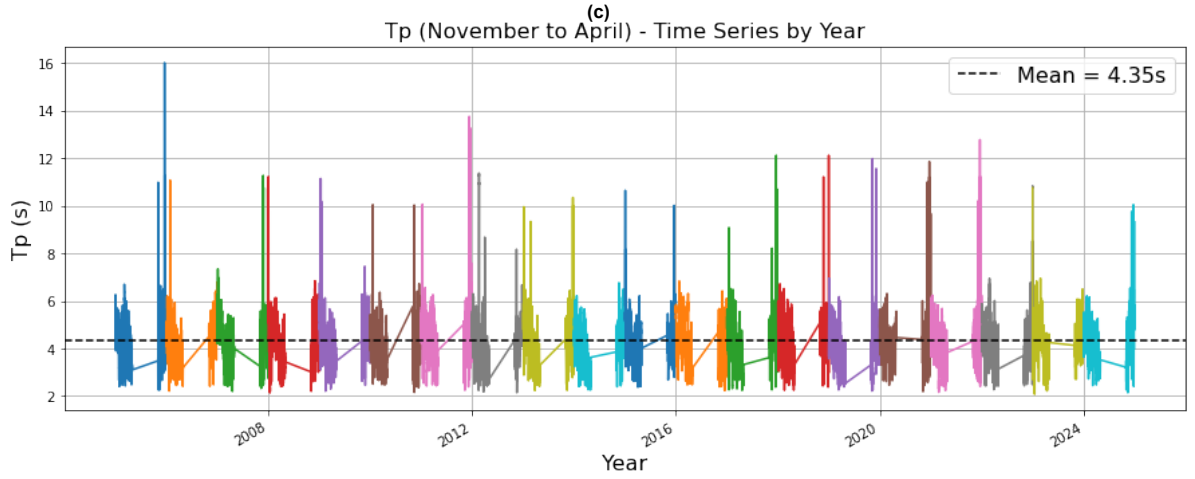

(d)

Figure B.4: 20 years of significant wave heights (a,b) and peak periods (c,d) in both the dry (a,c) and wet (b,d) seasons [14].

Next, Mflat calculates the wave height profiles over the cross-section. The small model starts at $x = 27.6km$. The results are shown in Figure B.5 and Table B.2.

	$H_{rms}(m)$ at $x = 27.6km$
Dry season	0.30
Wet season	0.23

Table B.2: Output of wave transformation model

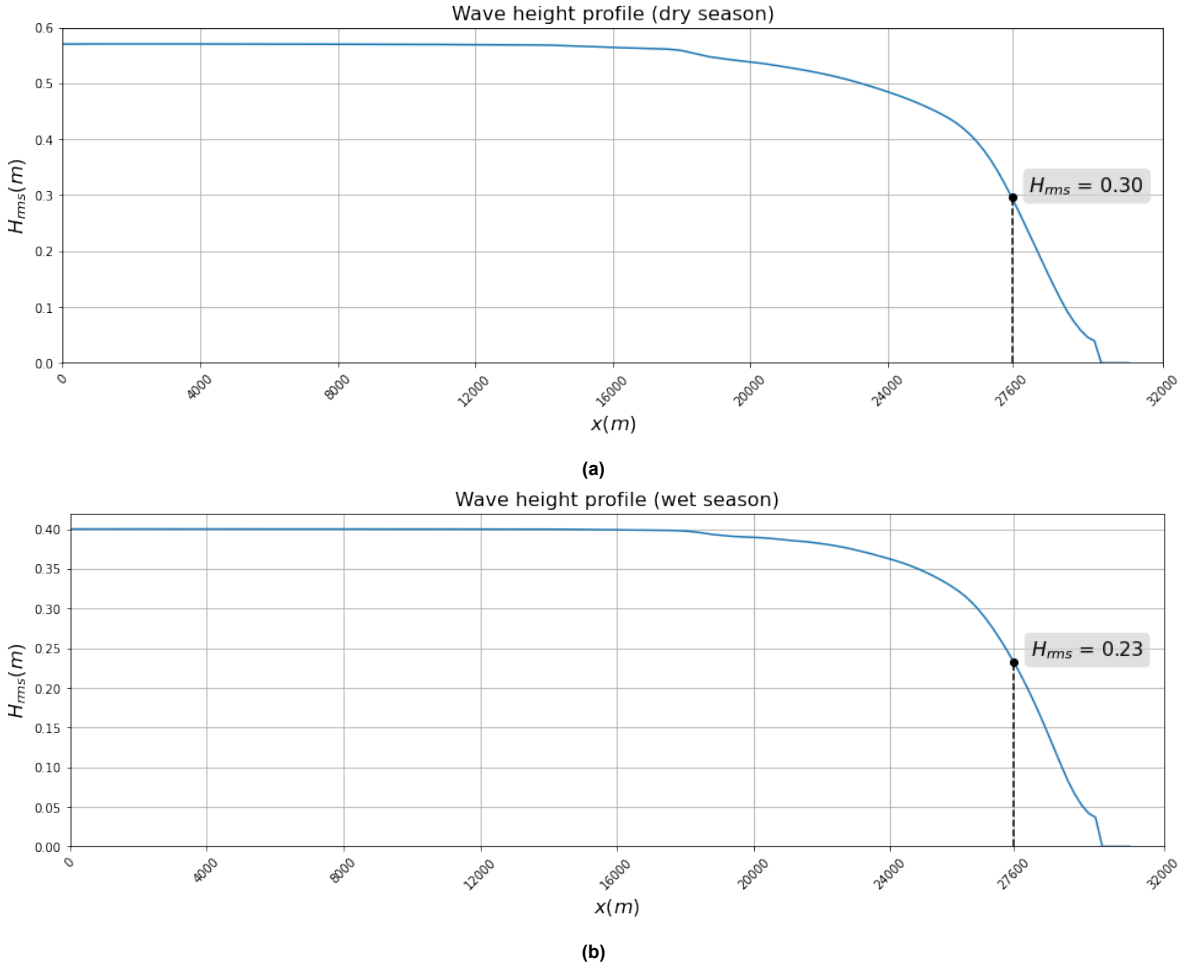

(a)

(b)

Figure B.5: Transformed H_{rms} in the dry (a) and wet (b) season

B.2.2. Wind

Using a 11 year time series from Copernicus satellite program [14] wind speeds and directions are calculated for both the dry and wet season. The results are plotted in the wind roses in Figure B.6. Average values are shown in Table B.3

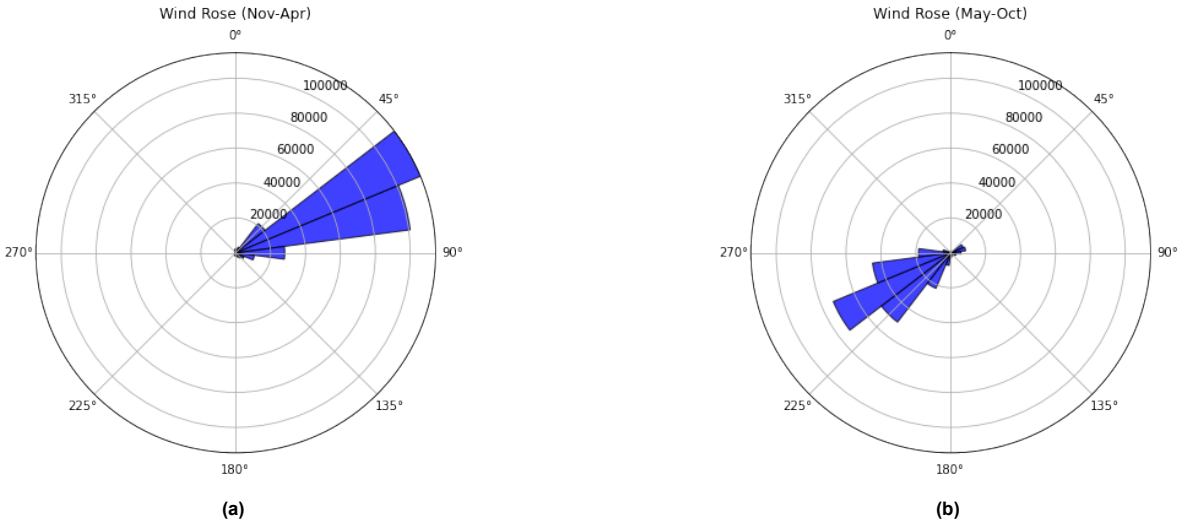

Figure B.6: Wind roses of the dry (a) and wet (b) season. Counted by wind direction, weighted by wind speeds.

	Average wind speed (m/s)	Average direction (°)
Dry season	5.67	77.95
Wet season	3.82	241.87

Table B.3: Average values for wind speed and direction in the dry and wet season.

However, since Mflat is a cross-shore model, the cross-shore component of the wind speeds need to be calculated. The coast of Bạc Liêu is shifted $70°$ from North, leading to a cross-shore direction at $160°$. The cross-shore wind component (U_{cross}) is given by:

$$U_{\text{cross}} = U\cos(\theta_{\text{wind}} - \theta_{\text{cross}}) \tag{B.2}$$

where:

U = the average wind speed

θ_{wind} = the average wind direction

θ_{cross} = the cross-shore direction $(160°)$

This leads to cross-shore wind speeds of:

Dry season: $0.78m/s$

Wet season: $0.54m/s$

Mflat calculates the wind driven energy (S_w) by:

$$S_w = \frac{c_g \rho u_{10}^2}{\left[8a^2 b\left(\frac{16gE}{a^2\rho u_{10}^4}\right)^{\frac{1}{2b}-1}\right]} \tag{B.3}$$

Where:

c_g = Group velocity of the waves

ρ = Air density

u_{10} = Wind speed

E = Wave energy

g = Gravity

a, b = Coefficients

Since the calculated cross-shore wind speed components are small compared to the real wind speed (factor 0.14), and the formula shows that wind energy scales with u^2 and u^4, the effect to the wind driven energy is even smaller (factor 0.02 and 0.0004). Therefore, it is assumed that the calculated cross-shore wind components will have a minimal effect on the wave height and sediment transport, and can therefore be neglected.

B.3. Calibration

In order to use Mflat as a tool to model the effects of different erosion drivers, the model needs to accurately represent current real world morphological phenomena. However, sediment data is lacking and different other physical parameters, that influence the model's outcome, are not known. Therefore, the model must be calibrated using a phenomenological approach, as limited quantitative validation data is available. This means that calibration is done by reproducing qualitatively observed behaviors rather than by minimizing numerical errors against measurements.

As described in appendix B.1, the bathymetry of the model is based on the profile of cross-section transect 23-66. Therefore the aim is to simulate morphodynamic behavior similar to the behavior observed at this location. Appendix E shows that between 2004 and 2022, the mangrove fringe at transect 23-66 has been horizontally retreating with an average rate of $16.67m/year$. This report assumes that the system has not reached equilibrium yet, and that this erosion rate stays constant over time. Additionally, it is assumed that the mangroves will stay at the same elevation. Lastly, subsection 2.3.6 showed how the foreshore can change from a convex-up to a more concave-up profile and therefore, it is expected that the foreshore will erode.

The goal of the calibration is to achieve plausible model behavior in line with the expected morphodynamic phenomena. The approach is iterative, combining trial-and-error with conceptual understanding of different parameters.

B.3.1. Calibration parameters

An overview of calibration parameters and their initial values is given in Table B.4 and are conceptually explained below.

Parameter (unit)	Initial value
Fall velocity (m/s)	0.0005
Critical shear stress (Pa)	0.25
Erosion factor ($kg/m^2/s$)	0.00005
Maximum slope (-)	0.01
Wave friction factor	Equation B.6
Diffusion coefficient	6
Vegetation critical shear stress adjustment parameter	0
Water level correction factor (m)	0

Table B.4: Overview of calibration parameters and their initial values before tuning.

Fall velocity

The fall velocity is the velocity of a sediment particle sinking to the bottom. It determines sediment deposition rate in a grid cell by:

$$D = cw \tag{B.4}$$

Where:

D = The sediment deposition rate (g/m^2s)

c = The sediment concentration (g/m^3)

w = The fall velocity (m/s)

Therefore, a higher fall velocity results in faster settling of suspended sediment, limiting lateral transport and favoring vertical accretion, leading to steeper and higher profiles.

Critical shear stress

The critical shear stress is the stress required to initiate motion of a settled particle. It determines erosion rates in a grid cell by:

$$E = \begin{cases} M\left(\tau_{\text{tot}} - \tau_{e,\text{cr}}\right) & \text{for } \tau_{\text{tot}} \geq \tau_{e,\text{cr}} \\ 0 & \text{for } \tau_{\text{tot}} < \tau_{e,\text{cr}} \end{cases} \tag{B.5}$$

Where:

E = erosion rate (g/m^2s)

M = erosion factor ($kg/m^2/s$)

τ_{tot} = total shear stress (Pa)

$\tau_{e,cr}$ = critical shear stress for erosion (Pa)

Therefore, a higher critical shear stress leads to a profile that is harder to erode, leading to higher and steeper profiles.

Erosion factor

The erosion factor determines how fast sediment is eroded once the bed shear stress exceeds the critical threshold. It determines erosion rates with equation B.5. A higher erosion factor leads to more erosion and therefore to lower and less steep profiles.

Maximum slope

The maximum slope is a threshold parameter that prevents steep slopes. Each timestep a filter mimics avalanching steep slopes until the threshold is met. This factor is important for the purpose of this research since cliffs at the mangrove fringe are observed. It is assumed that this cliff can only move horizontally and approximately keeps it original slope. The value of the maximum slope controls the rate of this artificial avalanching, thereby influencing the horizontal erosion rate of the cliff.

Wave friction factor

The wave friction factor (f_w) determines the amount of wave energy dissipated by friction and is calculated in Mflat with:

$$f_w = e^{5.213(kb/A)^{0.194} - 5.977} \tag{B.6}$$

Where:

kb = physical roughness length scale (m)

A = wave excursion (m)

f_w is used to determine wave dissipation due to bed friction with:

$$D_f = \rho f_w |u_{rms}|^3 \tag{B.7}$$

Where:

ρ = water density (kg/m^3)

f_w = wave friction factor (-)

u_{rms} = root-mean-squared orbital velocity (m/s)

Therefore, a higher f_w leads to more wave dissipation, causing lower waves to reach the shore, leading to less erosion.

Vegetation critical shear stress adjustment parameter

The vegetation critical shear stress adjustment parameter (K_c) is a parameter that is used to locally adjust the critical shear stress for area's where mangroves are growing. This parameter is needed to mimic the capabilities of mangroves to trap sediment and make the soil less erodible. It locally increases the critical shear stress with:

$$\tau_{crit} = \tau_{crit} + (1 + K_c W_{bg}/W_{bg,max}) \tag{B.8}$$

Where:

- W_{bg} = below ground biomass (kg)
- $W_{bg,max}$ = below ground biomass of a matured tree (kg)

Therefore, a higher value for K_{veg} leads to a higher locally increased critical shear stress.

B.3.2. Calibration process

The calibration process is divided into three phases. First, the initial exploration phase, where many parameters were changed to understand their role and the sensitivity of the model. Next, the second phase where more focused adjustments were made. And lastly, the third phase, where final refinements were made. This subsection summarizes the calibration processes, highlighting the crucial steps made to obtain the final model configurations.

Initial exploration

The initial exploration phase was mainly focused on understanding the role of the sediment parameters: critical shear stress, fall velocity and the erosion parameter. To isolate the effect of a parameter, only one parameter was changed for every run. The effects of the parameters became clear and matched the expected outcomes based on the conceptual descriptions from subsection B.3.1. It also became clear that changing the sediment parameters have a bigger effect on the profile's elevation than the slope.

However, the first runs were still far from realistic, implying problems that can not be fixed by tweaking sediment parameters and call for more fundamental changes to the model. Figure B.7 shows that the model does not show any of the required phenomena: The foreshore is (partially) accreting, the cliff at the mangrove fringe smooths out and the fishponds have accreted vertically.

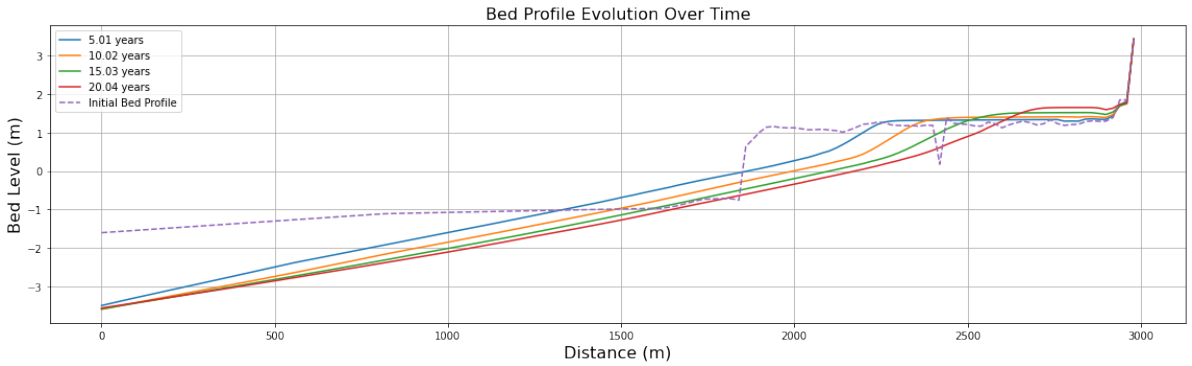

Figure B.7: Bed profile evolution of initial model

Increasing maximum slope

In the initial runs, the cliff at the mangrove fringe smooths out. This is due to the initial very small maximum slope (0.001). An iterative process was used to test maximum slope values between 0.002 and 0.2. Low values continued to show cliff smoothing, whereas high values stopped horizontal erosion almost entirely. A maximum slope of 0.05 preserved the original cliff shape reasonably well, while still showing horizontal erosion. Figure B.8 shows the updated profile. In addition to increasing the maximum slope, sediment parameters were also adjusted to reduce profile steepness. The diffusion coefficient was set to $5m/s$ to improve numerical stability.

Although the profile shows improvements compared to figure B.7, the heightened elevation level in the mangrove forest, horizontal erosion rates and foreshore are still not as expected.

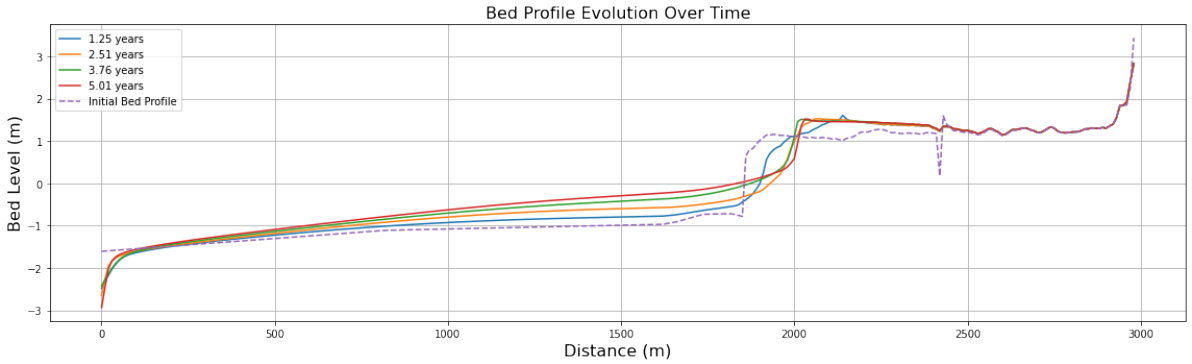

Figure B.8: Bed profile evolution with adjusted sediment parameters, maximum slope of 0.05 and diffusion coefficient of $5m/s$

Derivation of A_0

Figure B.8 shows that the model overestimates sediment deposition in the mangrove zone, indicating that high water levels may be exaggerated. Comparing the models water level input (Figure B.10a) with observed water levels near the coast of Bạc Liêu (Figure B.10b) confirms this and shows that high water peaks in the model reach up to $MSL + 2.2m$, while the real world data shows maximum water levels at $MSL + 1.5m$. This difference is likely caused by a mismatch in the phase reference between the tidal constituent derivation method and MFlat's internal handling of the phase. To correct for this, a factor $A_0 = 0.7m$ is introduced. This vertical offset reduces all modeled water levels, aligning peak levels with observed values. Figure B.10c shows that Mflat now uses water level peaks at roughly the same level as the observed water levels. The trade-off is that low and mean water levels are also reduced, this leads to an underestimation of inundation in certain tidal periods.

Figure B.9 shows the resulting bed profile after applying the water level correction. Unrealistic sedimentation in the natural mangrove forest no longer occurs, indicating improved vertical water level representation. However, the figure also shows that horizontal erosion at the cliff has stopped. This is likely due to the reduced water levels decreasing the inundation duration and frequency at the cliff toe, thereby limiting the periods during which waves can erode the cliff. Additionally, the lower water depth causes increased wave energy dissipation offshore, resulting in smaller waves reaching the cliff, causing a reduction in wave induced shear stress.

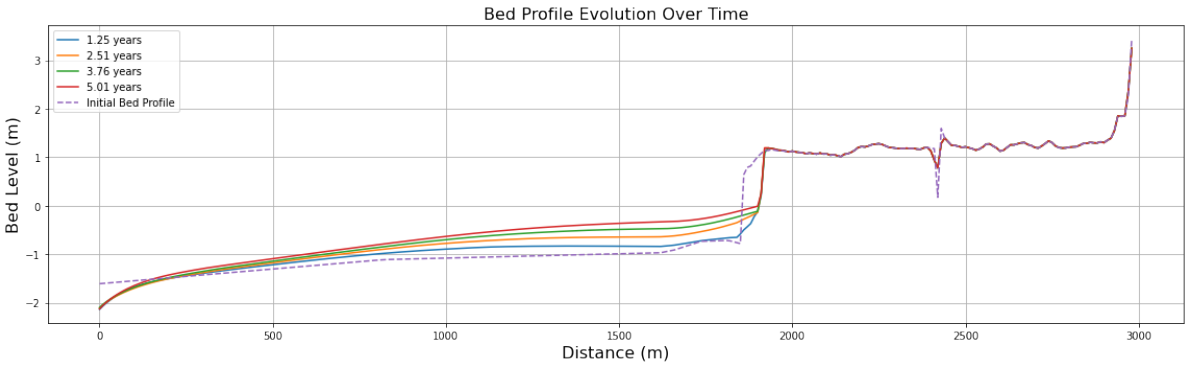

Figure B.9: Bed profile evolution with $A_0 = 0.7m$

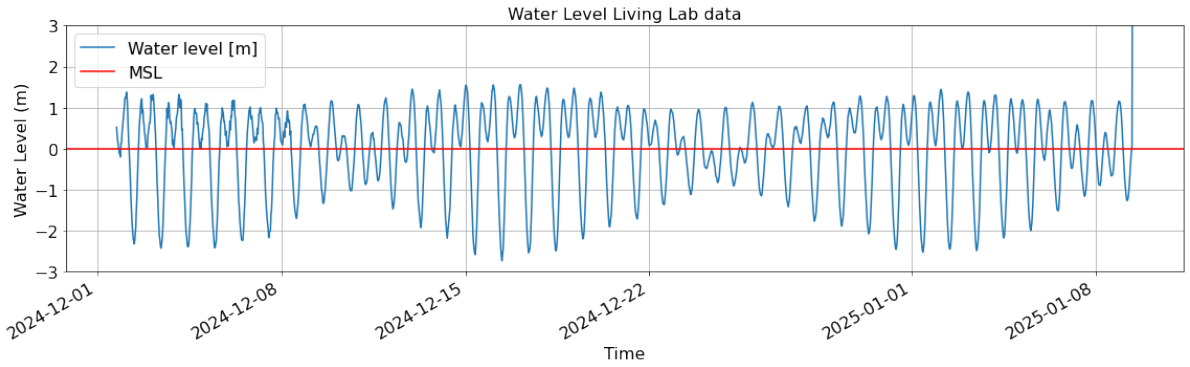

(a) Observed water level

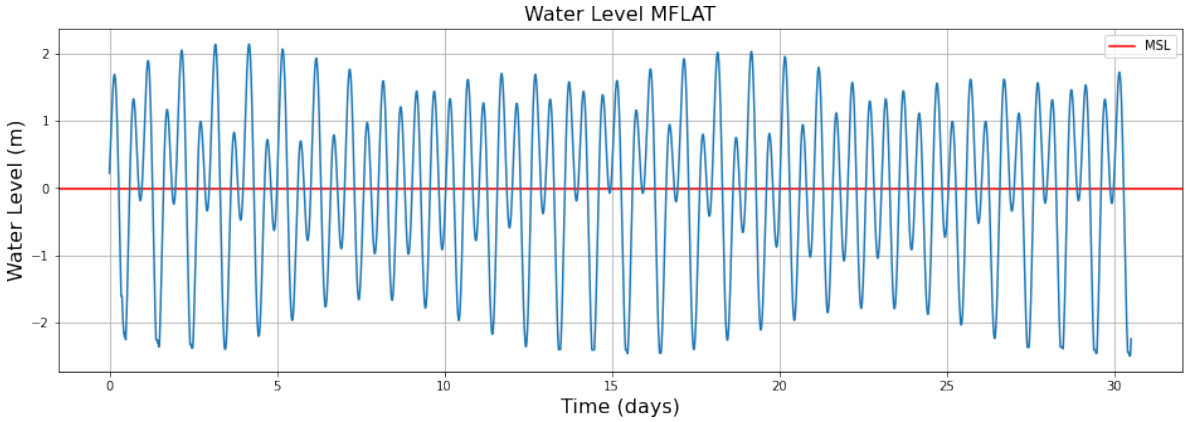

(b) Water level input in MFlat based on tidal constituents without A_0

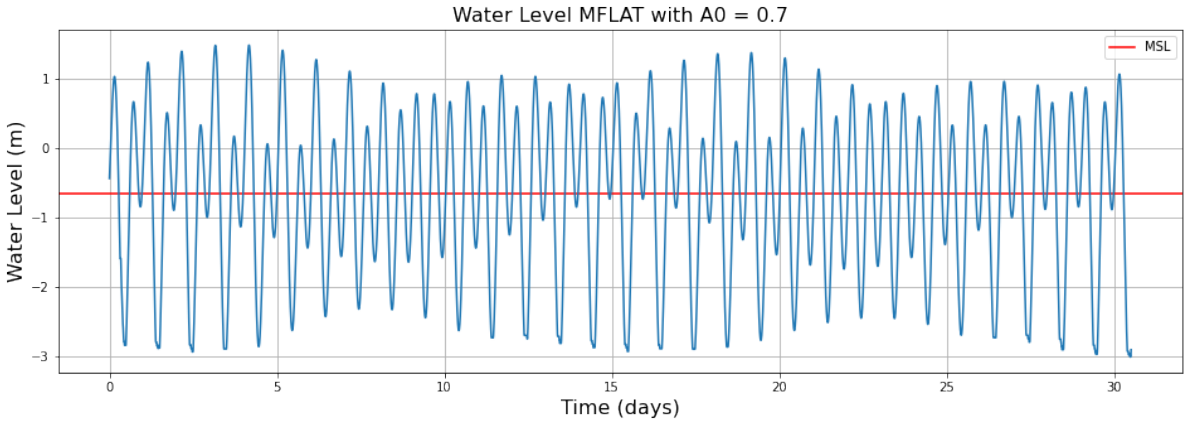

(c) Water level input in MFlat based on tidal constituents corrected with $A_0 = 0.7$

Figure B.10: Comparison between observed water levels (a) and input water levels for MFlat, before (b) and after (c) introducing A_0

Fixing f_w

Mflat calculates wave dissipation using a wave friction parameter (equation B.7). However, due to the lower water level, this dissipation gets overestimated, leading to less erosion at the cliff. To address this, the dynamic formulation (equation B.6) was replaced with a fixed value. An iterative calibration was performed, testing values between 0.008 and 0.08. A value of 0.01 was found to produce the most realistic balance between wave energy dissipation and nearshore erosion. Figure B.11 shows the resulting bed profile evolution.

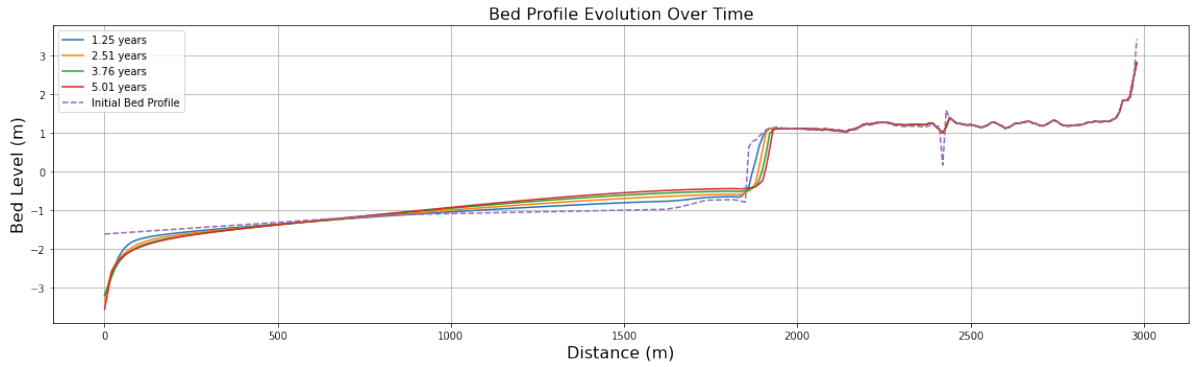

Figure B.11: Bed profile evolution with $f_w = 0.01$

Final sediment parameter refinements

The profile of Figure B.11 shows relatively good behavior, with a retreating cliff, stable elevation levels in the mangrove forest and a foreshore slope close to the original. However, final refinements in the sediment parameters are needed to make the model as accurate as possible. The foreshore still shows accretion and the foot of the cliff is too high. At the same time, the profile now shows an average horizontal erosion rate of only $7m/year$.

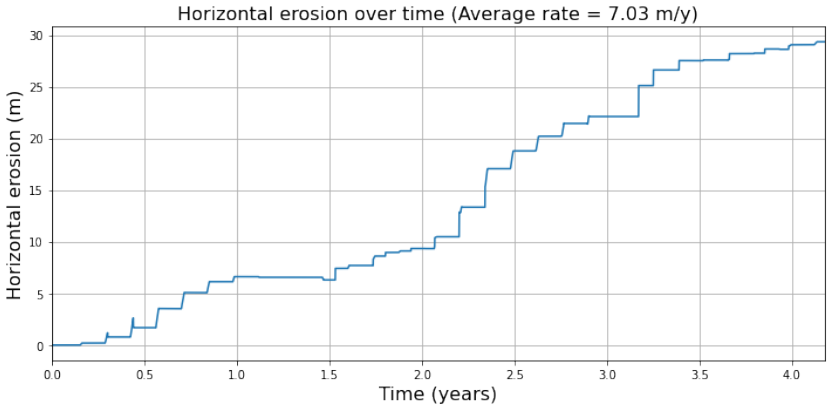

Figure B.12: Erosion rates of cliff front (at z = 1m) before final refinements

Sediment parameters at this point are:

- Fall velocity = $0.0001m/s$
- Critical shear stress = $0.25Pa$
- Erosion parameter = $0.0005kg/m^2/s$

According to the insights from subsection B.3.1, a lower profile can be obtained by reducing the critical shear stress and fall velocity or increasing the erosion parameter. These actions should also increase the horizontal erosion rate. The fall velocity already has a low value from previous calibrations, therefore the final refinements will focus on the critical shear stress and the erosion parameter.

An iterative calibration was performed, testing values between $0.15Pa$ and $0.25Pa$ for the critical shear stress and values between $0.0005kg/m^2/s$ and $0.001kg/m^2/s$ for the erosion parameter. A critical shear stress value of $0.20Pa$ and an erosion parameter value of $0.0007kg/m^2/s$ were found to keep the elevation of the foot of the cliff, while showing erosion on the foreshore. However, with these configurations, the horizontal erosion rate is too high (Figure B.13).

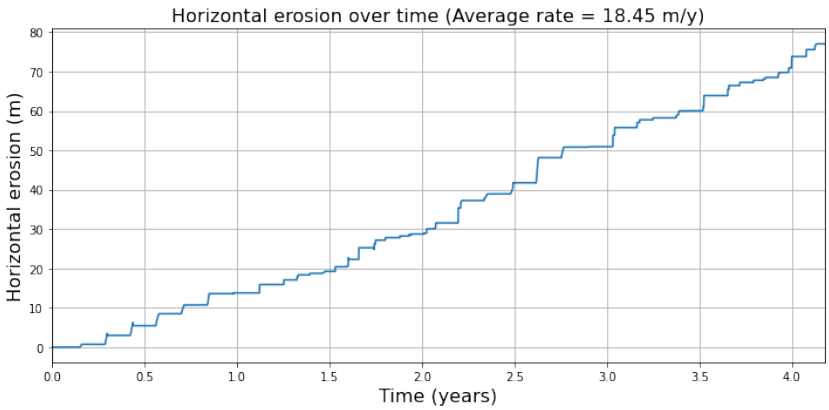

Figure B.13: Erosion rate of mangrove fringe with final sediment parameter configurations

Introducing K_c

To lower the horizontal erosion rate, the last step is to introduce the vegetation critical shear stress adjustment parameter (K_c). This locally increases the critical shear stress where the mangroves are growing, slowing down the erosion, while keeping the foreshore at the same level.

After an iterative process, a K_c value of 0.9 was found to accurately adjust the critical shear stress in order to get an erosion rate of $16.71 m/year$. This is considered close enough to the observed erosion rate of $16.67 m/year$. The final profile and horizontal erosion are shown Figure B.14 and Figure B.15, respectively.

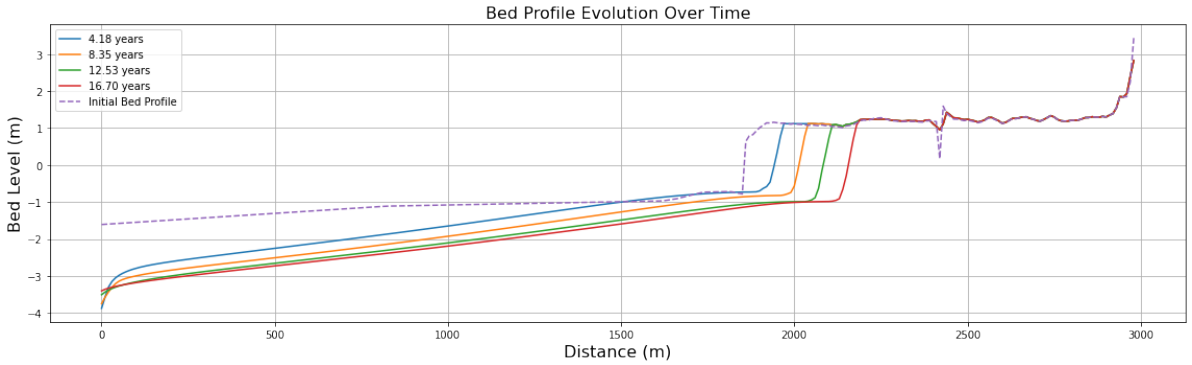

Figure B.14: Bed profile evolution of final model

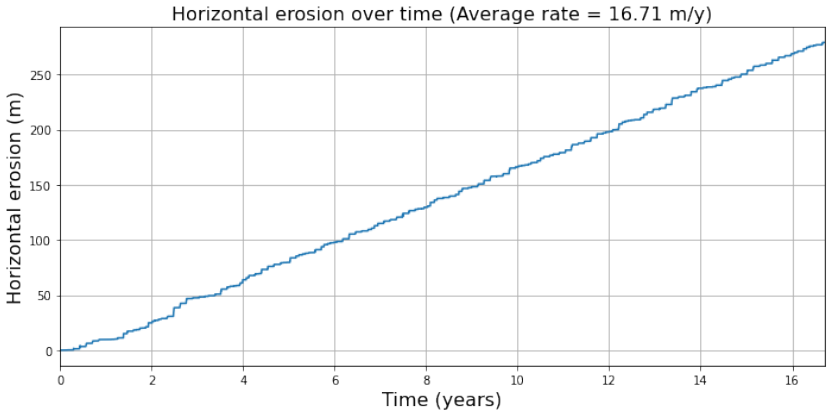

Figure B.15: Erosion rate of mangrove fringe of final model

Final remarks on calibration

The goal of the calibration was to obtain a model that exhibits observed or expected phenomena at transect 23-66. This was done by tweaking sediment parameters and the numerical diffusion coefficient, fixing the wave friction coefficient (f_w) and introducing parameters A_0 and K_c. The final model showed expected behavior with a vertically stable and horizontally retreating mangrove zone, and a foreshore that erodes.

However, it must be noted that the foreshore erosion can not be validated with real world data and is likely over exaggerated due to the introduction of A_0, fixing f_w and tuning the sediment parameters to more erosive values. Additionally, the phenomenological approach of the calibration process leads to uncertainty in the quantitative validity of the models results. Therefore, the model can only be used to qualitatively analyze the differences between different scenario simulations and not be used for more detailed, quantitative predictions. Other implications on the results are discussed in chapter 5.

B.4. Model parameters

Table B.5: Mflat input table

Type	Parameters (unit)	Value	Source
Wave data	RMS wave height dry season (m)	0.30	Copernicus Satellite data [14] and wave transformation (Appendix B.2.1)
	RMS wave height wet season (m)	0.23	
	Peak period dry season (s)	4.35	
	Peak period wet season (s)	3.83	
Tidal constituents	Amplitude M2 (m)	1.08	Phan et al. (2019) [47], Hu et al. (2001) [24]
	Phase M2 ($^\circ$)	118	
	Amplitude N2 (m)	0.07	
	Phase N2 ($^\circ$)	65	
	Amplitude S2 (m)	0.39	
	Phase S2 ($^\circ$)	177	
	Amplitude K2 (m)	0.05	
	Phase K2 ($^\circ$)	180	
	Amplitude K1 (m)	0.67	
	Phase K1 ($^\circ$)	3	
	Amplitude O1 (m)	0.45	
	Phase O1 ($^\circ$)	310	
	Amplitude P1 (m)	0.16	
	Phase P1 ($^\circ$)	340	
	Amplitude Sa (m)	0.16	
	Phase Sa ($^\circ$)	280	
	Correction A0 (m)	0.7	
Sediment characteristics	Fall velocity (m/s)	0.0001	Calibration (Appendix B.3
	Critical shear stress (Pa)	0.2	
	Erosion factor ($kg/m^2/s$)	0.00007	
	Chézy factor ($m^{1/2}/s$)	60	
	Suspended sediment concentration (-)	0.5	
Mangrove characteristics	Plant density ($/m^2$)	0.625	Living Lab (2023)
	Average diameter (m)	0.07	
	Height (m)	7	
Model parameters	$dx(m)$	10	Calibration (Appendix B.3
	$dt(s)$	5	
	Diffusion coefficient (unit)	5	
	Morphological factor	50	
	Maximum slope	0.05	
	$f_w(-)$	0.01	
	$K_c(-)$	0.9	

C

Scenario set up

C.1. Extended mangrove forest without dikes

To simulate the absence of dikes and fishpond dams, the small profile from Figure B.3 is adjusted. The high elevation levels from the dikes are removed, and the profile is extended in landward direction for $500m$ with the same slope as the original profile and a random offset. The foreshore and hydrodynamics are kept constant.

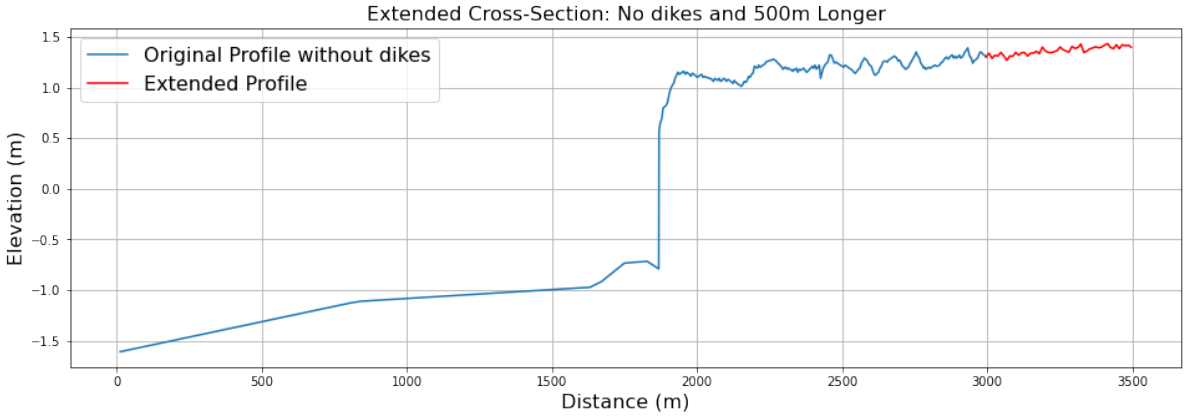

Figure C.1: Transect 23-66 adjusted. The dike and fishpond dam are removed and profile is extended with $500m$

C.2. Historic wave transformation

To simulate how the system behaved with the historic foreshore and associated the current profile is simulated with wave heights associated a historic bed levels. The British admiralty map (Appendix A.2), shows that the historic profile was less deep than the current profile. However, the maps low resolution and uncertainties in the location of the shoreline don't allow for an exact profile recreation. Therefore, to model the effect of a historic, less eroded foreshore, the entire foreshore is elevated with $1.9m$ and wave transformation is redone. Figure C.2 shows the used profile, Figure C.3 shows the resulting wave heights.

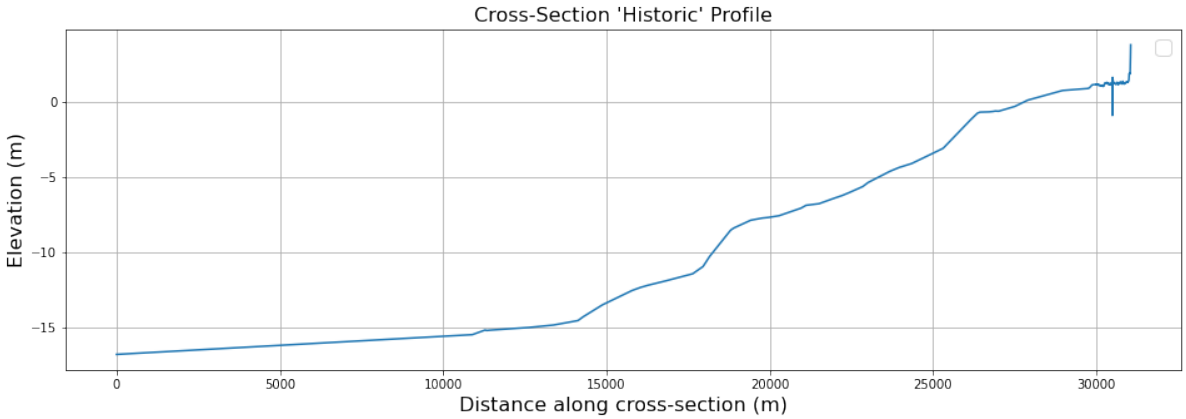

Figure C.2: Representation of the historic foreshore used for the new wave transformation.

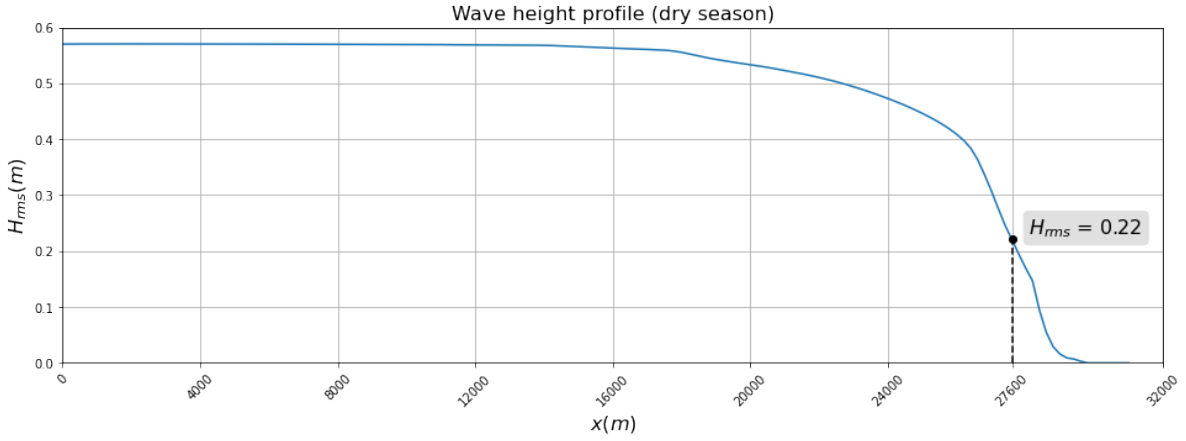

(a)

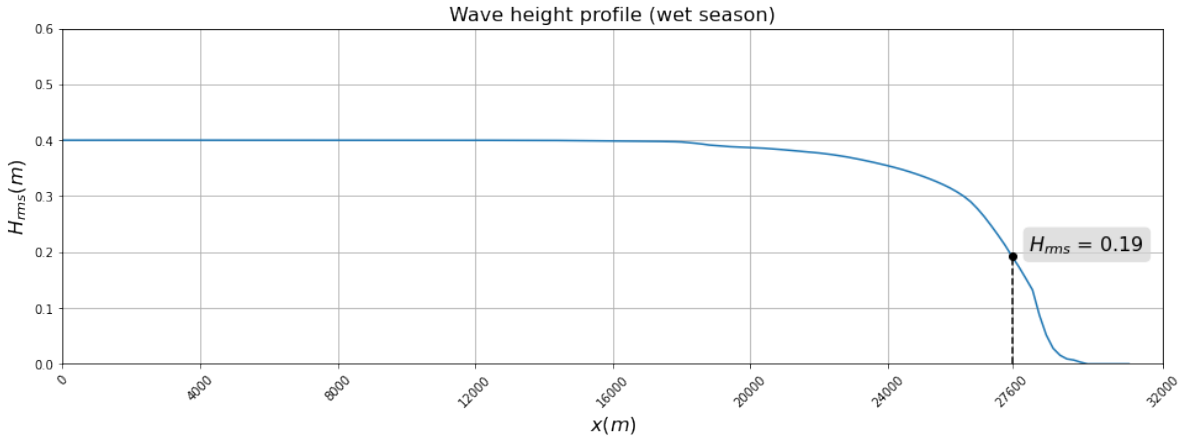

(b)

Figure C.3: Transformed H_{rms} in the dry (a) and wet (b) season on the historic foreshore

D

Cross section results

This chapter discusses the incomplete transects made during field campaigns in 2023 and 2024. The locations of all transects are shown in Figure 3.1. The results of the complete transects (23-45 and 23-66) are discussed in section 4.1.

D.1. Results

D.1.1. Transect 23-22

Transect 23-22 (Figure D.1) is located in an area without fishponds. It starts at the concrete dike and extends towards the seaward edge of the natural mangrove forest. Only a small strip of natural mangroves is left, which approximately lies at MHW. Since no reference measurements were taken behind the dike, it is not possible to draw conclusions about relative contributions of subsidence and sediment deposition in this area.

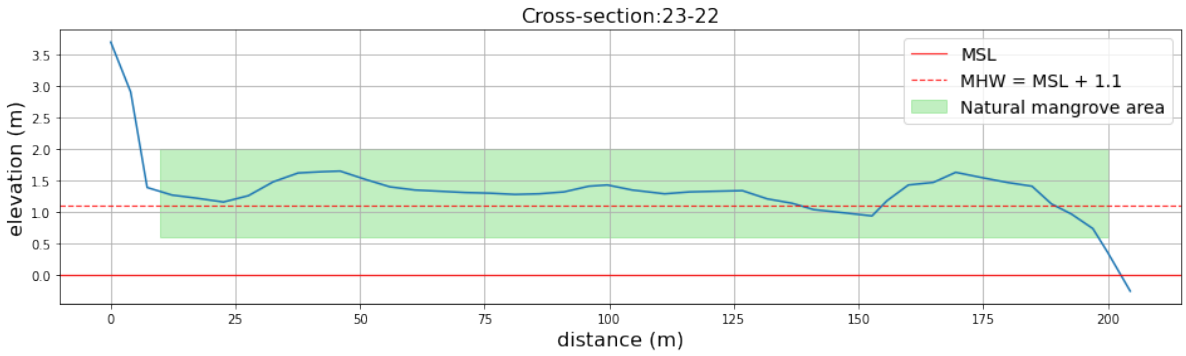

Figure D.1: Cross section of transect 23-22

D.1.2. Transect 23-34

Transect 23-34 (Figure D.2) is located in an area without fishponds. It starts at the concrete dike and extends towards the end of the natural mangrove forest. The location is eroding but still has a relatively wide strip of natural mangroves, which approximately lie at MHW. Since no reference measurements were taken behind the dike, it is not possible to draw conclusions about relative contributions of subsidence and sediment deposition in this area.

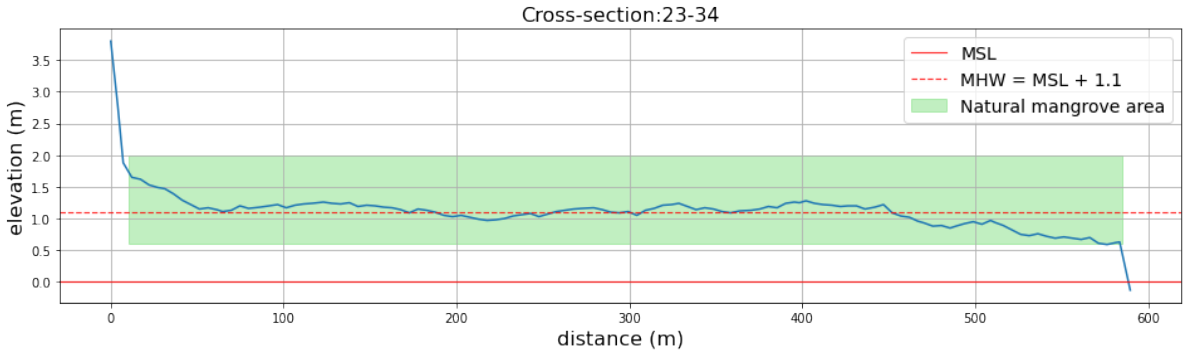

Figure D.2: Cross section of transect 23-34

D.1.3. Transect 23-44

Transect 23-44 (Figure D.3) is located in an area with fishponds. The cross section starts at the earthen dike and extends towards the end of the natural mangrove forest. The location is eroding but still has a relatively wide strip of natural mangroves. The mangroves lie approximately at MHW, but elevation levels are fluctuating more than in previous transects. Since no reference measurements were taken behind the dike, it is not possible to draw conclusions about relative contributions of subsidence and sediment deposition in this area.

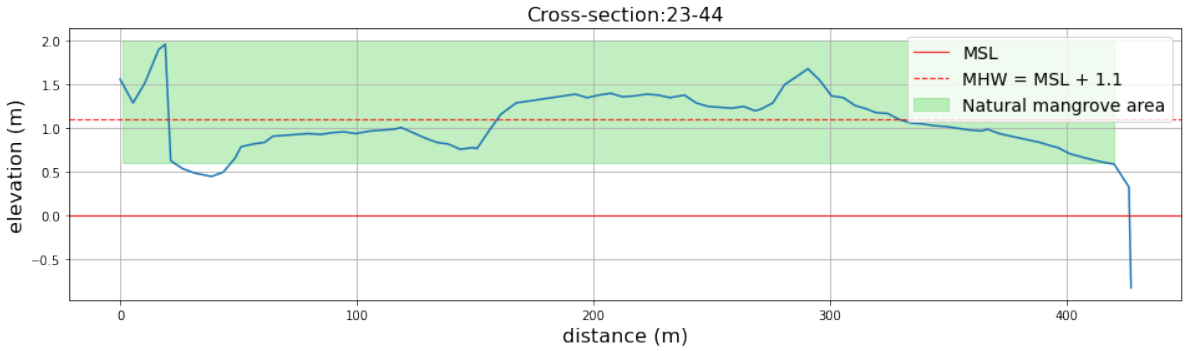

Figure D.3: Cross section of transect 23-44

D.1.4. Transect 24-0

Transect 24-0 (Figure D.4) is measured at approximately the same location as transect 23-34. However, unlike transect 23-34, it neither starts at the dike nor ends at the edge of the natural mangrove forest. The figure shows that mangroves are positioned at MHW, similar to transect 23-34.

Since the two transects are made approximately one year apart, they could have been useful to monitor the change of the coast and potentially indicate subsidence. However, due to the unknown exact location of transect 24-0 relative to transect 23-34, and the use of a larger interval (20–30 m instead of 5–10 m), such comparisons are not possible.

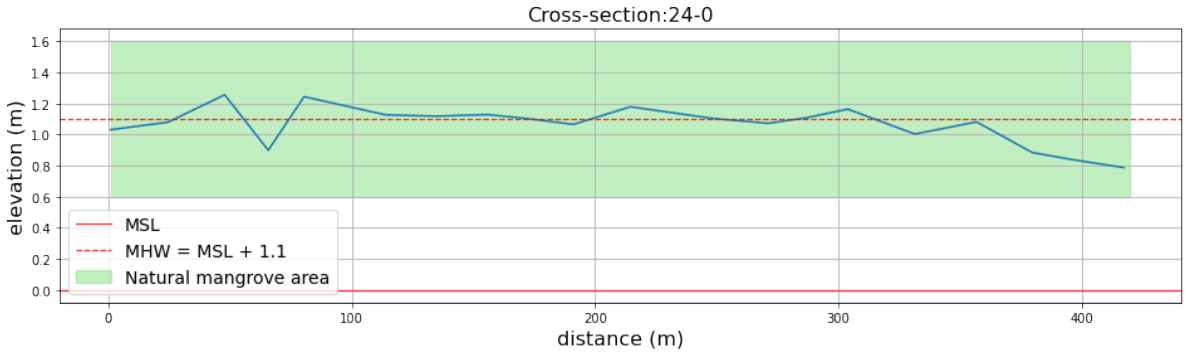

Figure D.4: Cross section of transect 24-0

D.1.5. Transect 24-1

Transect 24-1 (Figure D.5) is conducted at approximately the same location as transect 23-66. It starts at the concrete dike, but stops at the earthen dike and doesn't include the natural mangrove forest.

A comparison with transect 23-66 shows that elevation levels inside the fishpond area are a few decimeters higher in 2024 than they were one year earlier, while the crest of the concrete dike stays at roughly the same level. This implies vertical accretion, which is assumed to be impossible in the fishpond area, especially at the observed rates. Also, the observed peak at $x = 450m$ can not be explained. This suggests that measuring errors or wrong references were made. Inside the fishponds there is an elevated path. It is likely possible that measurements were done at the height of this path, instead of the ground where the mangroves are growing.

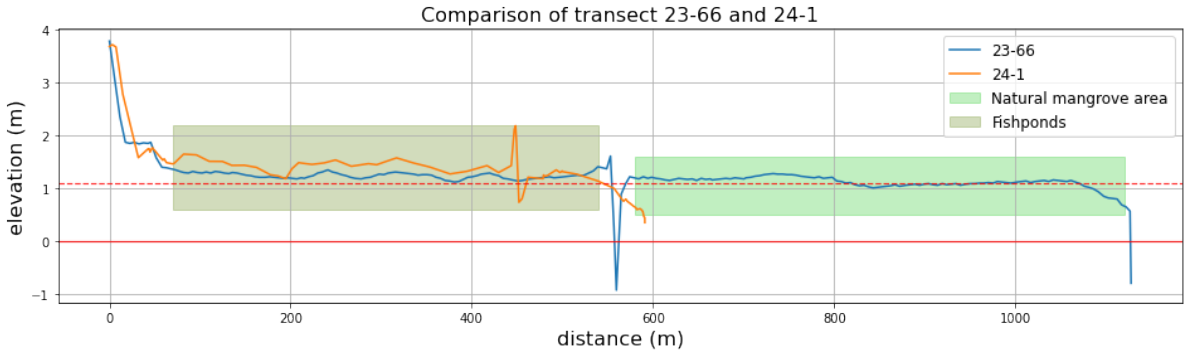

Figure D.5: Cross section of transect 24-1 and 23-66

D.1.6. Transect 24-2

Transect 24-2 (Figure D.6) is located at the Hòa Bình 1 windmill farm. The cross section starts at the concrete dike, through the visitor center of the windmill farm, through the fishponds, over the earthen dike, to the edge of the natural mangrove forest. The figure shows that the area disconnected from the sediment transport system lies more than $1.5m$ above MHW and the natural mangroves. The visitor center of the wind farm has high economic value (restaurant, coffee shop, new buildings). Therefore it is likely possible that the whole visitor area is artificially elevated to reduce flood risk. Also, an elevated path is going through the fishponds. It is likely possible that measurements were done at the height of this path, instead of the ground were the mangroves are growing.

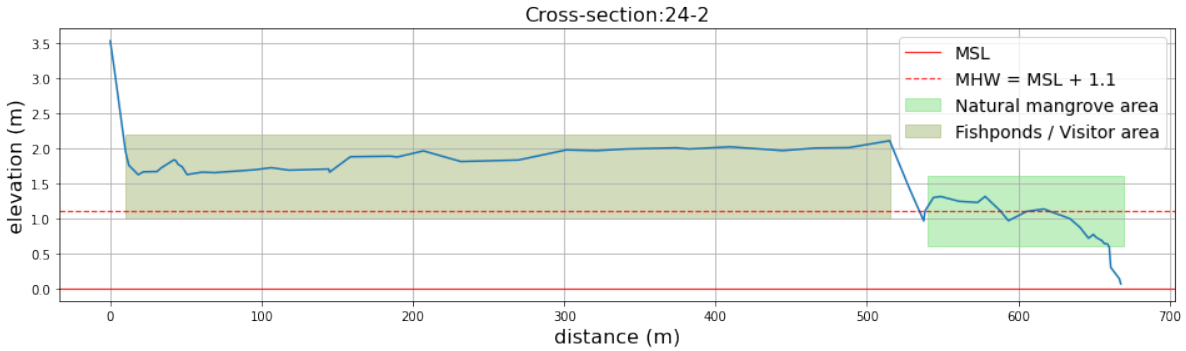

Figure D.6: Cross section of transect 24-2

D.1.7. Transect 24-3

Transect 24-3 (Figure D.5) is conducted at approximately the same location as transect 23-45. The figure shows that elevation levels inside the fishpond area are a up to one meter higher in 2024 than one year earlier, while the crest of the concrete dike stays at roughly the same level. This, again, suggests that measurements were done at one of the elevated paths through the fishponds instead of the ground were the mangroves are growing, making a proper comparison impossible.

For the natural mangrove area, GPS data shows that a different route through the mangroves was chosen in 2024 compared to 2023. This could explain the longer natural mangrove forest in 2024 compared to 2023. The 2024 transect also shows a higher elevation than in 2023. Since the same route was not taken, it is impossible to determine whether this is due to vertical accretion of the region or an original spatial variation in elevation levels.

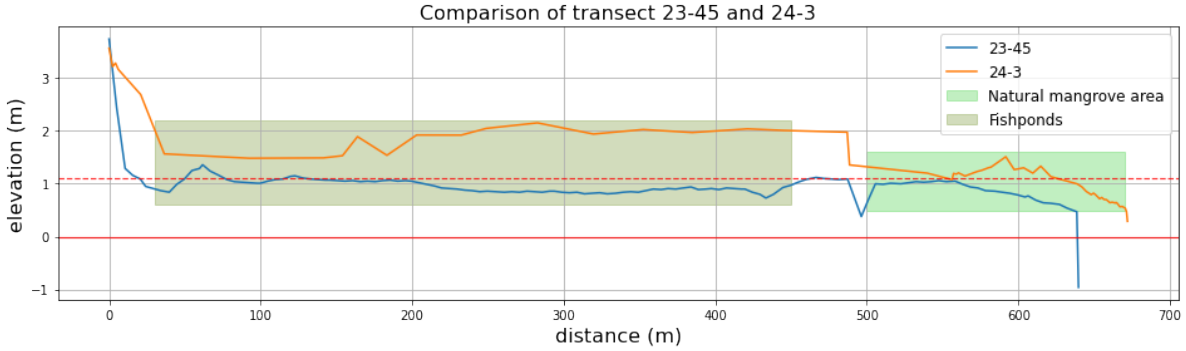

Figure D.7: Cross section of transect 24-3 and 23-45

D.2. Conclusion

From the nine transects made in 2023 and 2024, seven were considered to be incomplete or not useful to analyze the relative contribution of subsidence and sediment deposition rates. To make this analysis, it is crucial to have reference measurements from an area which is disconnected from the sediment transport system. This reference measurement is lacking in transect 23-22, 23-34, 23-44 and 24-0.

Additionally, when comparing transects from different years at the same location, it is important that the way the data is collected, as well as the exact location, is correct and constant. The fishponds at transect 24-1, 24-2 and 24-3, seem to be at unrealistic elevation levels, especially when comparing them to one year earlier.

E

Historic coastline evolution

This chapter presents the historic coastline evolution of transects 23-45 and 23-66.

E.1. Transect 23-45

(a) Coastline position in 1986

(b) Coastline position in 2004

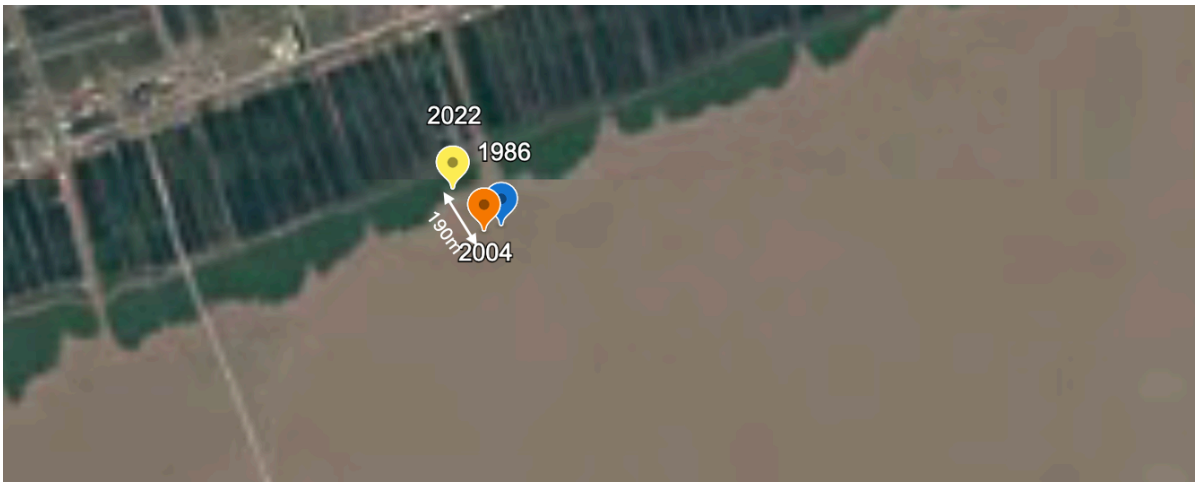

(c) Coastline position in 2022

E.2. Transect 23-66

(a) Coastline position in 1986

(b) Coastline position in 2004

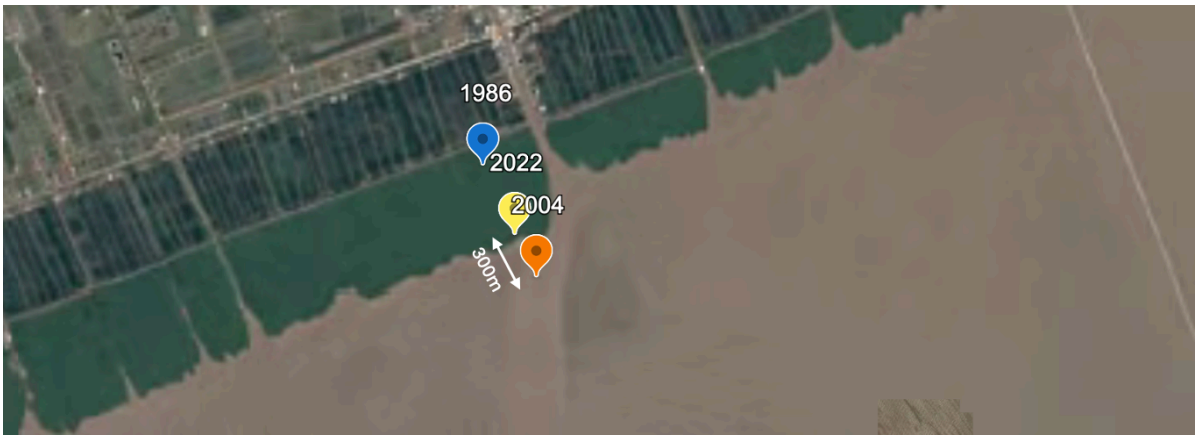

(c) Coastline position in 2004

Bed profile evolution with combined drivers

F.1. No dikes + subsidence

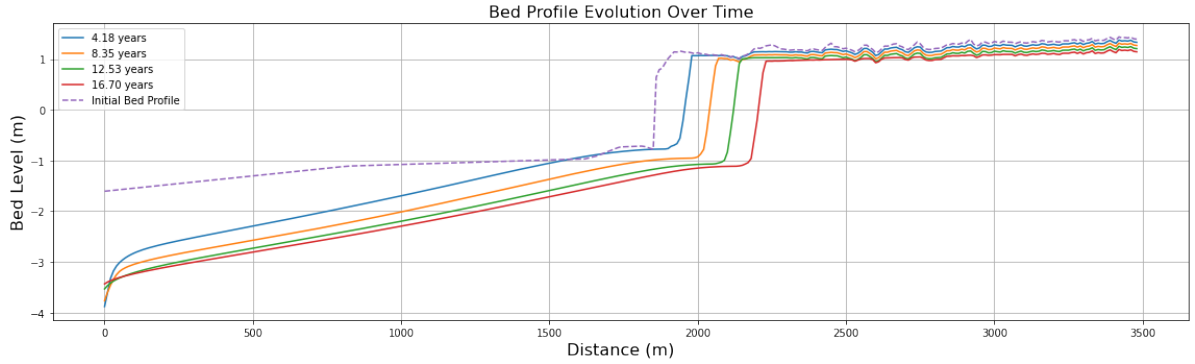

Figure F.1

F.2. No dikes + increased SSC

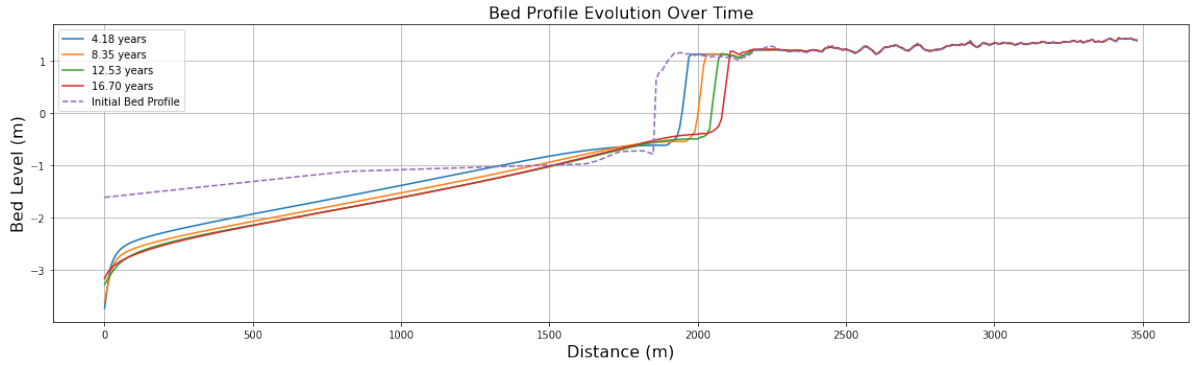

Figure F.2

F.3. No dikes + historic wave heights

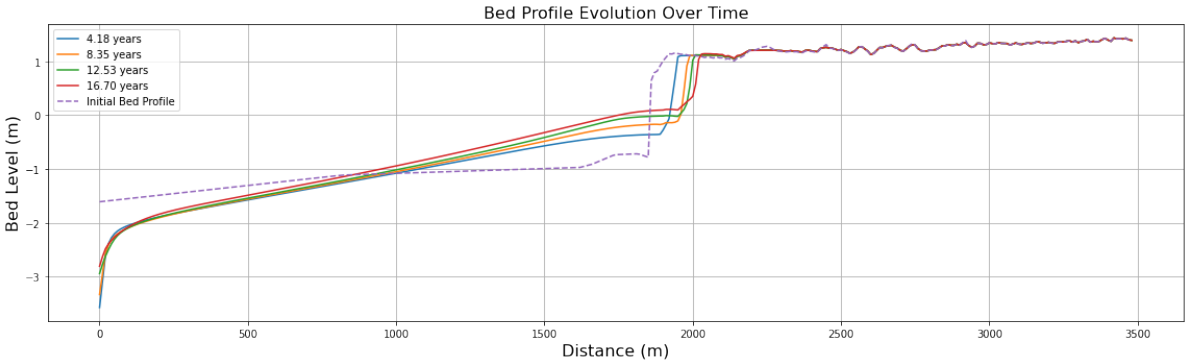

Figure F.3

F.4. Subsidence + increased SSC

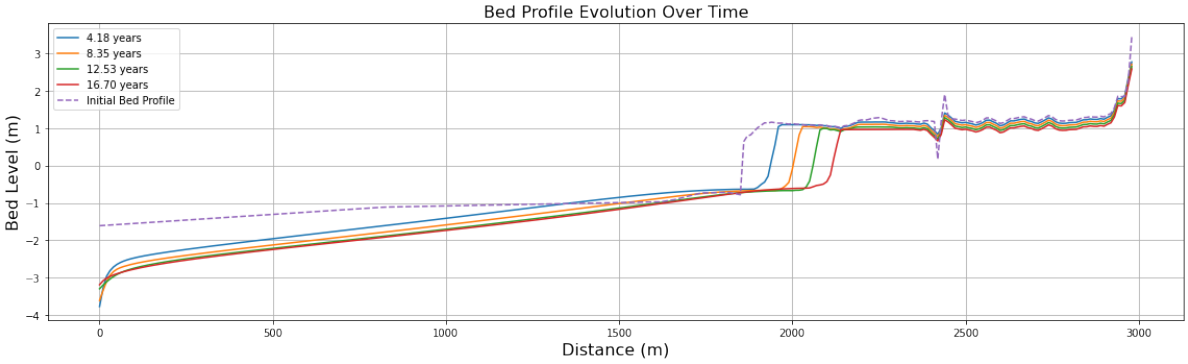

Figure F.4

F.5. Subsidence + historic wave heights

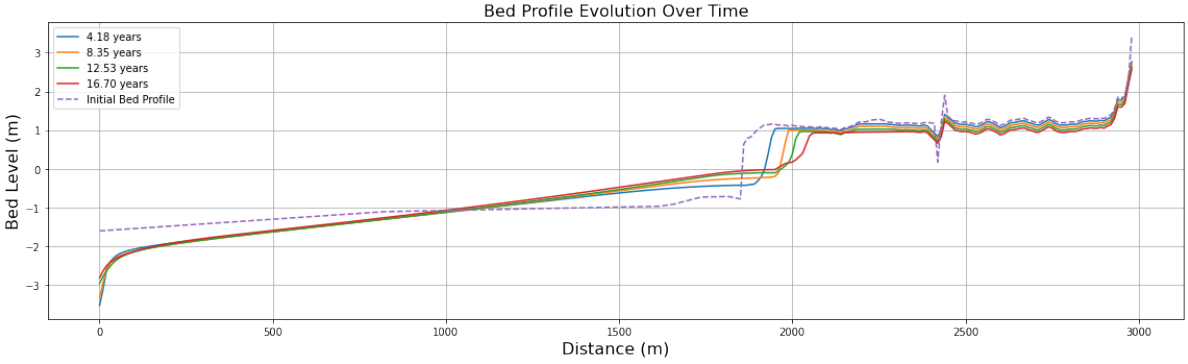

Figure F.5

F.6. Historic wave heights + increased SSC

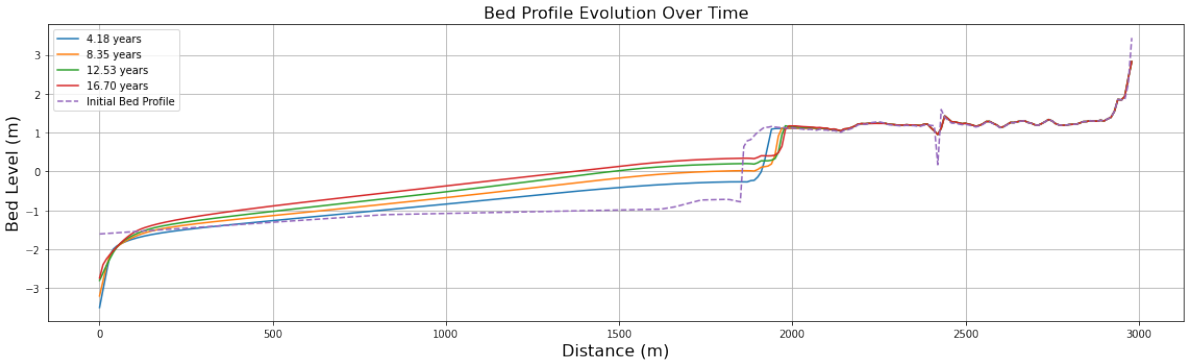

Figure F.6

F.7. No dikes + subsidence + increased SSC

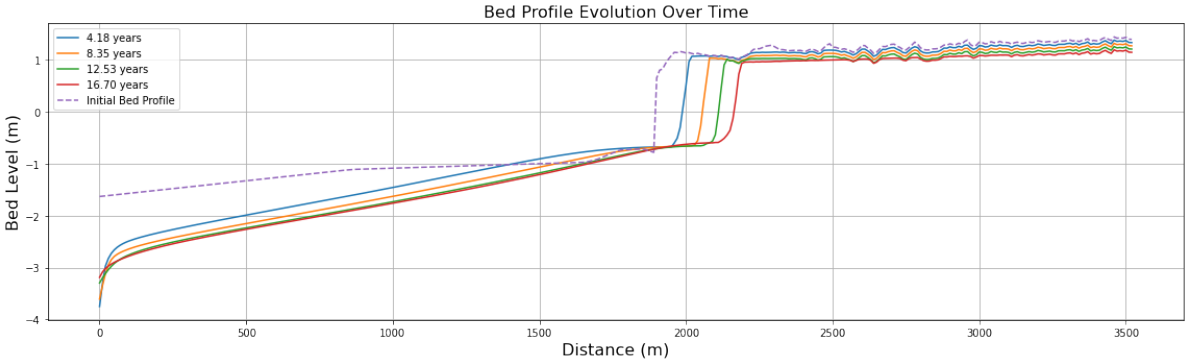

Figure F.7

F.8. No dikes + subsidence + historic wave heights

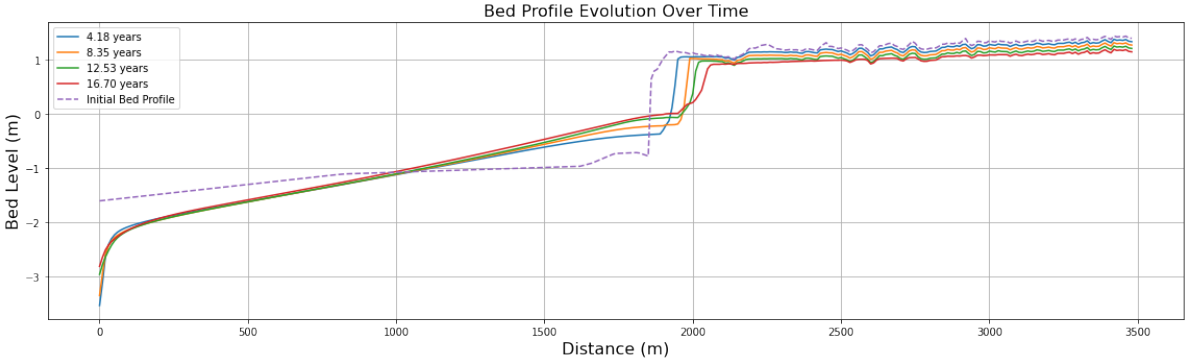

Figure F.8

F.9. No dikes + historic wave heights + increased SSC

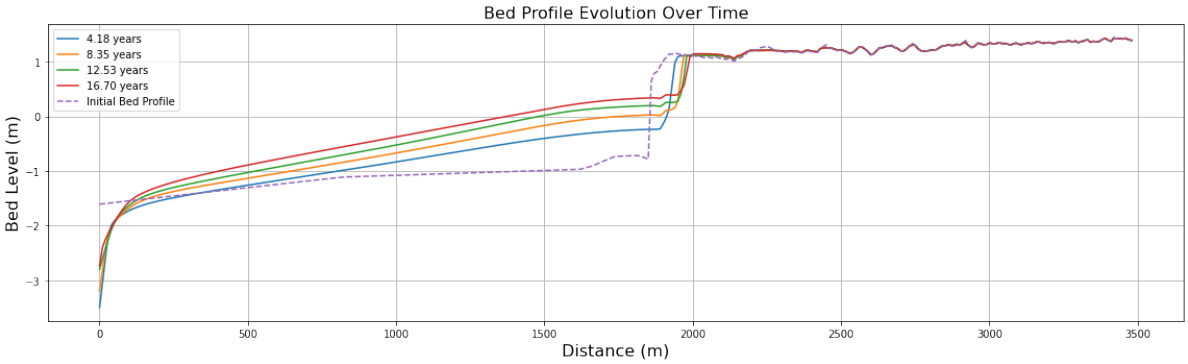

Figure F.9

F.10. Subsidence + historic wave heights + increased SSC

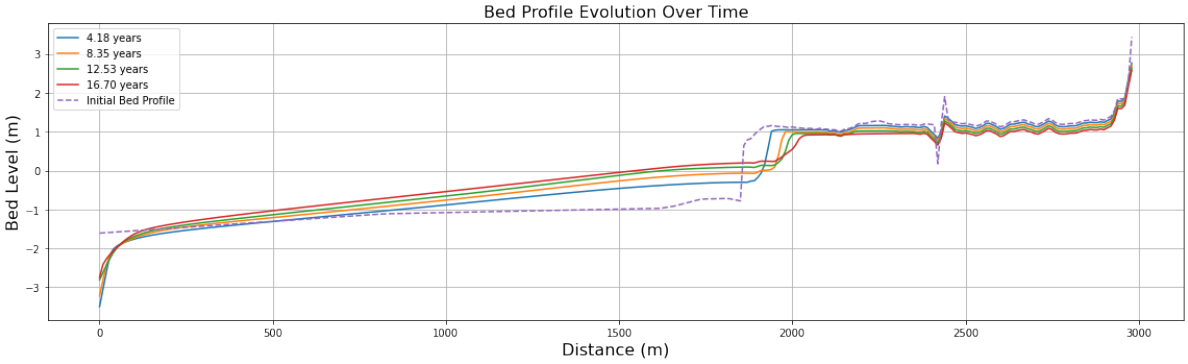

Figure F.10

F.11. No dikes + Subsidence + historic wave heights + increased SSC

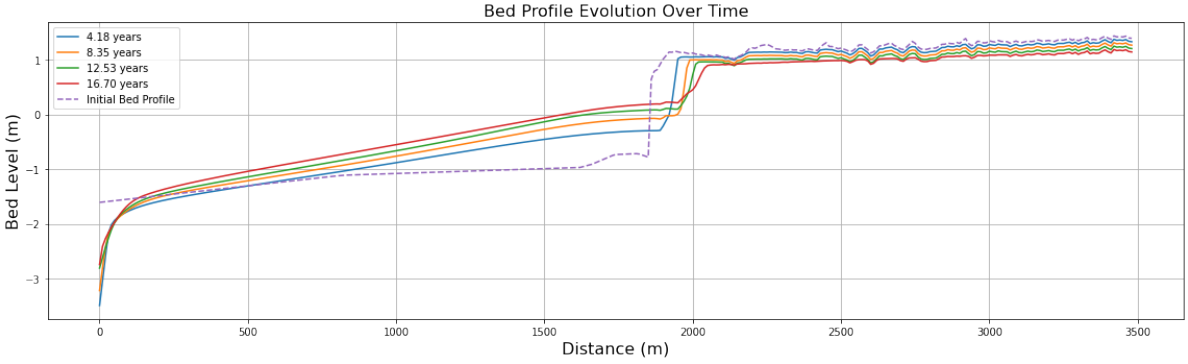

Figure F.11